A SIMULATION STUDY
OF THREE-DIMENSIONAL MAGNETIC RECONNECTION

By

ZHI-WEI MA

RECOMMENDED:

J. R. Kan

G. E. Shaw

R. W. Smith

J. G. Hawkins

L. C. Lee, Chairman, Advisory Committee

Head, Physics Department

APPROVED:

Dean, College of Natural Sciences

Dean, Graduate School

August 3, 1994

Date

A SIMULATION STUDY
OF THREE-DIMENSIONAL MAGNETIC RECONNECTION

A

THESIS

Presented to the Faculty of the University of Alaska

in Partial Fulfillment of the Requirements

for the Degree of

DOCTOR OF PHILOSOPHY

By

Zhi-Wei Ma, B.S., M.S.

Fairbanks, Alaska

August 1994

ABSTRACT

The magnetic reconnection process plays an important role in the interaction between the solar wind and the magnetosphere. It leads to the transfer of energy from the solar wind into the magnetosphere. In this thesis, we study three-dimensional (3D) aspects of magnetic reconnection based on magnetohydrodynamic (MHD) simulations.

First, we examine the magnetic field topology of magnetic flux ropes formed in multiple X line reconnection (MXR). It is found that the magnetic field topology depends on the relative extent and location of the two neighboring X lines. Magnetic flux ropes with either smooth or frayed ends are obtained in our simulations. For magnetic flux ropes with smooth ends, a major amount of magnetic flux is connected at each end to only one side of magnetopause.

Second, the evolution of the core magnetic field in the magnetic flux tube is studied for various magnetic reconnection processes. We find that the 3D cases always lead to a larger enhancement of core field than the corresponding 2D cases since plasma can be squeezed out of the flux tube in the third direction. The MXR process gives rise to a larger increase of the core field than the single X line reconnection process. The core magnetic field can be enhanced to three times the ambient magnetic field strength in the 3D MXR process.

Finally, we examine the generation and propagation of Alfven waves and field-aligned currents in the 3D reconnection process. For cases with a zero guide field, it is found that a large portion of the field-aligned currents ($\sim$ 40%) is located in the closed field line region. Both the pressure gradient term and inertia term contribute to the generation of field-aligned currents. For cases with nonzero guide field, one sense of field-aligned currents is dominant due to the presence of the initial field-aligned current. In these cases, the inertia term makes a major contribution to the redistribution of field-aligned currents. The influence of the initial guide field on the longitudinal shift of the current reversal site is found to be consistent with observations.

TABLE OF CONTENTS

	Page
Abstract	iii
Table of Contents	iv
List of Figures	vi
List of Tables	x
Acknowledgments	xi
1. **Introduction**	1
1.1 Magnetic reconnection	1
1.1.1 "Frozen-in" concept	1
1.1.2 Definitions of 2D magnetic reconnection	4
1.1.3 Definitions of 3D magnetic reconnection	6
1.2 The basic properties associated with magnetic reconnection	7
1.3 Magnetic reconnection models	8
1.3.1 2D theoretical models	8
1.3.2 Dungey's open magnetospheric model	8
1.4 Satellite observations at the dayside magnetopause	9
1.5 Theoretical FTE models	12
1.5.1 Patchy and intermittent reconnection model	12
1.5.2 MXR model	14
1.5.3 Bursty SXR model	16
1.6 Observations in the polar ionosphere	16
1.7 Objectives and outline of the thesis	19
2. **Topology of magnetic flux ropes formed by multiple X line reconnection.**	23
2.1 Introduction	23
2.2 Field line topology of magnetic flux ropes	26
2.3 Simulation model	32
2.4 Simulation results	36
2.4.1 MSP to MSP connection	37
2.4.2 Other magnetic connections	42
2.5 Formation of fossil FTEs and the low-Latitude boundary layer	45
2.6 Discussion and conclusion	48

3. Enhancements of core magnetic field in different reconnection processes 50

3.1 Introduction 50

3.2 Simulation model 52

3.3 Simulation results 55

3.3.1 Two-dimensional MXR and SXR processes 55

3.3.2 Three-dimensional MXR and patchy reconnection processes 61

3.4 Summary and discussion 70

4. Generation of field-aligned currents and Alfven waves by magnetic reconnection 76

4.1 Introduction 76

4.2 Simulation model 80

4.3 Simulation results: $B_y = 0$ case 82

4.4 Simulation results: $B_y \neq 0$ cases 93

4.5 Discussion and summary 103

5. Discussion and summary 106

References 111

LIST OF FIGURES

		Page
Fig. 1.1	Schematic illustration of magnetic reconnection process in a current sheet. The separatrices are shown by the heavy lines.	5
Fig. 1.2	Configuration of magnetic field lines in Dungey's open magnetospheric model.	10
Fig. 1.3	Data from ISEE 1, for a one-hour period on 29 November, 1977, showing 3 magnetosheath FTEs (*Paschmann et al.*, 1982).	13
Fig. 1.4	Magnetic flux rope in the patchy reconnection model. Magnetosheath field lines, slanted arrows, have connected with magnetospheric field lines, vertical arrows, possibly off the lower edge of the figure. The connected flux tube moves in the direction of the large arrow (*Russell and Elphic*, 1978).	15
Fig. 1.5	Multiple X line reconnection model (a) a perspective view of the open magnetic flux tube and the regular open field lines as a result of multiple X line reconnection at the dayside magnetopause, and (b) the projection of flux tubes in the noon-midnight meridian plane (*Lee and Fu*, 1985).	17
Fig. 1.6	A schematic drawing of the bursty single X line reconnection model (*Scholer*, 1988).	18
Fig. 1.7	(a) Time distribution between successive PMAF intervals observed in the dayside aurora oval *Fasel et al.* [1993a] and (b) distribution of inter-FTE intervals taken from *Lockwood and wild* [1993] .	20
Fig. 2.1	Magnetic field lines in a frayed magnetic rope formed in the 3D MXR reconnection. Solid (dashed) lines indicate sections of field lines on the magnetosphere (magnetosheath) side (*Fu et al.*, 1990).	27
Fig. 2.2	Six possible patterns of the field line topology of the magnetic flux rope. The heavy bars denote the reconnection *X* lines. The solid (dashed) lines indicate field lines on the magnetosheath (magnetospheric) side.	28
Fig. 2.3	Simplified reconnection geometry for two *X* lines (thick plotted lines) in a projection onto the *y*-*z* plane. The chosen geometry refers to the sketch in Figure 2.2*a*.	30

Fig. 2.4	Illustration of the geometry of the initial configuration for the three-dimensional MHD simulations. The shaded area represents the current layer in the system. The orientations of magnetic fields are indicated on the boundary surfaces.	35
Fig. 2.5	Perspective view of magnetic field lines in a magnetic flux ropes with an MSP-MSP connection formed in the 3D MXR reconnection.	39
Fig. 2.6	Illustration of the magnetic topology in a cross section of the flux rope bounded by thick solid lines for the configuration shown in Figure 2.5. The sign +, $*$, $\bullet$, and Δ stand for MSP-MSP IMF-IMF, IMF-MSP, MSP-IMF connections.	40
Fig. 2.7	(a) The plasma flow pattern in the plane $x = 0$ and (b) the x integrated value of the FACs obtained at $t = 100$.	41
Fig. 2.8	Perspective view of magnetic field lines with (a) an IMF-MSP connection, (b) an IMF-IMF connection, (c) an MSP-IMF connection, and (d) a complex mixed connection.	43
Fig. 2.9	The detailed magnetic field topologies in the plane $x = 0$. The boundaries of magnetic flux ropes are indicated by thick solid lines. The sign +, $*$, $\bullet$, and Δ stand for MSP-MSP IMF-IMF, IMF-MSP, MSP-IMF connections.	44
Fig. 2.10	Perspective sketch of a flux rope on closed geomagnetic field lines.	47
Fig. 3.1	Schematic drawing of the initial configuration. Curve (a) is the constant B_y case, and curve (b) is the force-free state.	53
Fig. 3.2	Contours of magnetic field lines (left), contours of the B_y component (middle), and the plasma flow pattern (right) for the two-dimensional multiple X line reconnection (MXR) simulation with initial force-free configuration (case 1) at $t = 150$.	58
Fig. 3.3	Contours of magnetic field lines (left), contours of the B_y component (middle), and the plasma flow pattern (right) for 2D single X line reconnection (SXR) simulation with initial force-free configuration (case 2) at $t = 180$.	60
Fig. 3.4	The maximum value of B_y as a function of time obtained in different reconnection processes. Solid and dashed lines represent results from 2D MXR and SXR simulations, respectively, for (a) the initial force-free configuration (cases 1 and 2) and (b) the initial constant B_y profile (cases 7 and 8).	62

Fig. 3.5	The magnetic field (left) and plasma flow pattern (right) in the $y = 0$ plane at $t = 210$ for case 3, which corresponds to 3D MXR with $X_L = 20$.	64
Fig. 3.6	The total force (F) and the thermal pressure gradient force ($\mathbf{F_p}$) along the flux rope axis at $t = 210$ for case 3.	66
Fig. 3.7	(a) The plasma flow pattern in the $x = 0$ plane and (b) the distribution of the B_y component in the $y = 0$ plane at $t = 210$ for case 3.	67
Fig. 3.8	Schematic illustration of the core magnetic field and the tube-aligned flow in the magnetic flux tube. The magnetic tension force associated with the helical fields leads to the radially inward pinch of the rope as well as the enhancement of B_y and plasma pressure in the flux rope. The enhanced plasma pressure results in the outward tube-aligned flow.	68
Fig. 3.9	The magnetic field (left), plasma flow pattern (middle), and contours of B_y (right) in the $y = 0$ plane at $t = 210$ for case 4, which corresponds to the 3D patchy reconnection with $X_L = 20$.	69
Fig. 3.10	The maximum value of the B_y component obtained at $t = 200$ as a function of X line length X_L.	71
Fig. 3.11	The maximum value of the B_y component as a function of time for (a) MXR with $X_L = 10$, 30, and 50 and the 2D case and (b) patchy reconnection with $X_L = 10$ and 20.	72
Fig. 4.1	The distribution and flow directions of large-scale field-aligned currents in invariant latitude-MLT coordinates [Iijima and Potemra, 1976b].	78
Fig. 4.2	Perspective view of leading bulge structure formed in the 3D magnetic reconnection. The arrows indicate plasma flow directions.	84
Fig. 4.3	Contours of field-aligned currents ($J_{\|\|}$) at $t = 180$ in the plane (a) $x = -1.5$ and (b) $y = 10$. Solid (dashed) lines stand for positive (negative) values. The thick solid lines indicate the boundary of the open and closed field line region.	85
Fig. 4.4	(a) Contours of FAC ($J_{\|\|}$), (b) contours of parallel vorticity ($\Omega_{\|\|}$), and (c) topology of magnetic field lines in the plane $z = 70$ obtained at $t = 180$. Solid (dashed) lines stand for positive (negative) values. The thick solid lines indicate the boundary of the open and closed field line region.	87

Fig. 4.5	A schematic illustration of the evolution of the pertubations of the magnetic field and plasma flow associated with Alfven waves.	91
Fig. 4.6	Scatter plot of field-aligned current ($J_{\|\|}$) and parallel vorticity ($\Omega_{\|\|}$) in the plane $z = 70$ obtained at $t = 180$.	92
Fig. 4.7	Contour plots of (a) the inertia term, (b) the pressure term, and (c) the divergence of field-aligned currents in the plane $x = 1.5$ at $t = 180$.	94
Fig. 4.8	Perspective view of magnetic flux rope-like structure formed in the 3D magnetic reconnection.	96
Fig. 4.9	(a) Contours of FAC ($J_{\|\|}$), (b) contours of parallel vorticity ($\Omega_{\|\|}$), and (c) topology of magnetic field lines in the plane $z = 70$ obtained at $t = 240$. Solid (dashed) lines stand for positive (negative) values. The thick solid lines indicate the boundary of the open and closed field line region.	97
Fig. 4.10	Contours of field-aligned currents associated with Alfven waves propagating (a) antiparallel and (b) parallel to the ambient magnetic field.	99
Fig. 4.11	Contour plots of (a) the inertia term, (b) the pressure term, and (c) the divergence of field-aligned currents in the plane $x = 1.5$ at $t = 240$.	101
Fig. 4.12	The maximum magnitudes of field-aligned currents in the plane $z = 70$ at $t = 180$ as a function of the initial value of B_y.	102
Fig. 4.13	A schematic drawing of the global view of magnetic field and the resulting pattern of field-aligned currents due to magnetic reconnection.	104

LIST OF TABLES

Page

Table 3.1 Physical parameters and results for 12 simulation cases. 56

ACKNOWLEDGMENTS

I would deeply like to appreciate Professor L. C. Lee, my thesis adviser, for introducing me to the study of space physics and showing me how to discover and solve problems during my graduate study. His constant encouragement, advice, and valuable help made the completion of the thesis possible. I have been extremely fortunate to have this opportunity to study this field under his guidance.

In the preparation of this thesis, my committee members, Profs. J. Hawkins, J. Kan, G. Shaw, and R. Smith, reviewed each draft patiently and gave many helpful suggestions for improving the thesis. I want to express my thanks to them all.

I also wish to thank Dr. A. Otto for very helpful dscussions and comments. Many of my fellow students at the Geophysical Institute have offerred me their generous help. I am grateful to them.

This work was supported by a grant from the Department of Energy, the National Aeronautics and Space Administration, and the National Science Foundation to the University of Alaska. The computing work was supported by the San Diego Supercomputing Center, the Pittsburgh Supercomputing center, and the Arctic Region Supercomputing Center.

I gratefully extend my thanks to Professor X. M. Qiu, who was my Master thesis adviser at the Southwestern Institute of Physics in China. He introduced me to the study of space plasma.

Finally, I would like to thank my wife Junmei Hou and other family members for their continuous support, love, and encouragement. Without them, the thesis would not have been completed.

CHAPTER 1

Introduction

Magnetic field line reconnection, first proposed by Giovanelli [1947], is now widely believed to be an important process in cosmic plasmas, particularly in the solar corona and the magnetosphere. Two important features of the magnetic reconnection process are (a) the release and conversion of huge amounts of energy stored in the magnetic field into plasma kinetic energy in a very short period of time and (b) a change of magnetic field topology. Hoyle [1949] and Dungey [1961] applied the idea to geomagnetic phenomena, remarkably concerning the interaction between the interplanetary magnetic fields (IMFs) and the geomagnetic fields. On the other hand, Giovanelli's original reconnection idea was further developed and refined by a number of authors [Sweet, 1958; Parker, 1957; Petschek, 1964; Sonnerup, 1970; Yeh and Axford, 1970; Priest and Forbes, 1986; and Priest and Lee, 1991]. The present theories of magnetic reconnection are based on their works.

1.1 Magnetic reconnection

1.1.1 "Frozen-in" concept

In order to understand the phenomenon of magnetic reconnection, it is important to understand the "frozen-in" concept, i.e., fluid elements which are at one time connected

by a common magnetic field line remain so thereafter. We start with the magnetic induction equation for a conducting fluid. Faraday's law has the form

$$\frac{\partial \mathbf{B}}{\partial t} = -\nabla \times \mathbf{E}, \tag{1.1}$$

where $\mathbf{B}$ is the magnetic field and $\mathbf{E}$ the electric field. For a fluid with infinite conductivity, Ohm's law becomes

$$\mathbf{E} = -\mathbf{v} \times \mathbf{B}, \tag{1.2}$$

where $\mathbf{v}$ is the fluid velocity. Inserting Equation (1.2) into Equation (1.1), we have

$$\frac{\partial \mathbf{B}}{\partial t} = \nabla \times (\mathbf{v} \times \mathbf{B}). \tag{1.3}$$

Since $\nabla \cdot \mathbf{B} = 0$, Equation (1.3) has the same form as:

$$\frac{\partial \mathbf{\Omega}}{\partial t} = \nabla \times (\mathbf{v} \times \mathbf{\Omega}) \tag{1.4}$$

for vorticity transport in an inviscid fluid, where $\mathbf{\Omega} = \nabla \times \mathbf{v}$ is the vorticity. According to the Kelvin-Helmholtz theorem, the flux of vorticity through a closed loop moving with the fluid is conserved, which implies that a vortex tube moves with the fluid while its strength remains constant. We assume that the cross-section of the vortex tube approaches zero so that the vortex tube becomes a vortex line. Thus we can regard a vortex line as being "frozen" to the fluid. The same conclusions also hold for magnetic field in the perfect conducting fluid. The elements of fluid which are connected by a single magnetic field line at one time remain connected at subsequent times.

For real plasmas found in space or in the laboratory, the conductivity σ is finite. Hence the Ohm's law is modified as

$$\mathbf{J} = \sigma(\mathbf{E} + \mathbf{v} \times \mathbf{B}), \tag{1.5}$$

where $\mathbf{J}$ is the electric current. Using Amperes law $\mu_0 \mathbf{J} = \nabla \times \mathbf{B}$ with μ_0 the permeability in free space, the flux transport equation has the new form:

$$\frac{\partial \mathbf{B}}{\partial t} = \nabla \times (\mathbf{v} \times \mathbf{B}) + \frac{\eta}{\mu_0} \nabla^2 \mathbf{B}, \tag{1.6}$$

where the resistivity $\eta = 1/\sigma$ has been assumed constant for convenience. The ratio of the first (magnetic convection) term to the second (magnetic diffusion) term on the right hand side of Eq.(1.6) is approximately equal to a dimensionless quantity known as the magnetic Reynolds number $R_m = \mu_0 V_A L/\eta$, where V_A and L are the Alfven speed and length scale of the system, respectively. For a large magnetic Reynolds number, the magnetic field convection is dominant, which implies that magnetic field lines diffuse slowly relative to the fluid and the frozen-in condition approximately holds. If there exists a region in which L is small (e.g., a current sheet with magnetic field reversal), the magnetic Reynolds number becomes smaller, and the magnetic field diffusion term becomes comparable to the magnetic convection term so that the frozen-in condition is violated in this local region.

Fig. 1.1 shows the magnetic reconnection process in a localized region. Two regions with different magnetic field orientation are separated by a one-dimensional current sheet indicated by the dashed line. The shaded area is the localized diffusive region where the magnetic field diffusion is important. The labels (a, a', b and b') represent the fluid elements that are initially located in the two different regions. When the magnetic field line defined by fluid elements a and a' and the oppositely-directed

field line defined by fluid elements b and b' approach each other and pass through the diffusion region where the frozen-in condition is violated, the connection between a and a' and between b and b' will be broken and the new reconnected field lines defined by fluid elements a and b and by fluid elements a' and b' convect away due to the magnetic field tension force.

1.1.2 Definitions of 2D magnetic reconnection

From the topological point of view, Vasyliunas [1975] defines "magnetic field line reconnection or merging" as "the process whereby plasma flows across a surface that separates regions containing topologically different magnetic field lines." In this picture, two separatrix branches intersect along a line known as the "X line" or "separator" (see Figure 1.1b) [Vasyliunas, 1984; Sonnerup, 1984]. An alternative definition is that reconnection is the process associated with a non-zero electric field component along all or part of the magnetic X line or separator, which implies a localized violation of the frozen-in condition [Baum and Bratenahl, 1980; and Vasyliunas, 1984]. Other authors [e.g., Cowley, 1976; Sonnerup, 1984] pointed out that the electric field component parallel to the separator is a more appropriate definition than the flow across the separatrix. Using the plasma fluid element concept, Axford [1984] suggested that the localized violation of the frozen-in condition leads to change the magnetic field connection. In the two-dimensional (2D) case, those three definitions listed above are equivalent.

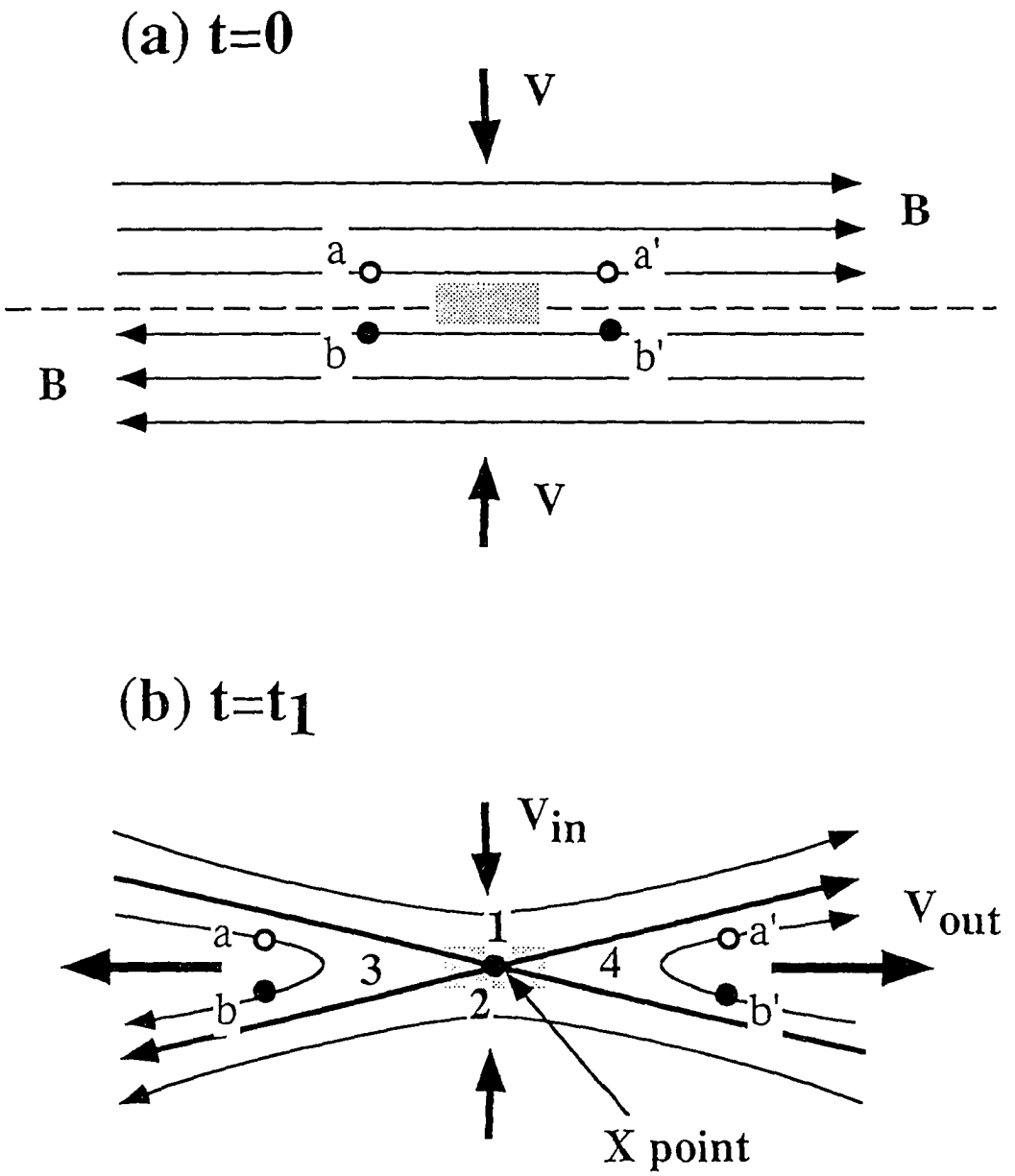

Figure 1.1 Schematic illustration of magnetic reconnection process in a current sheet. The separatrices are shown by the heavy lines.

1.1.3 Definitions of 3D magnetic reconnection

Although these concepts of magnetic reconnection have been notably successful in understanding the magnetic reconnection process in 2D geometries, it is difficult to generalize the first two definitions by Vasyliunas [1975,1984] and Baum and Bratenahl [1980] to 3D magnetic field configurations. The reason is that the properties of the X line or separator and separatrix do not exist in the general 3D situations. An arbitrarily small perturbation of the magnetic field will cause the disappearance of the X line in 3D cases. In 2D cases such arbitrary small field perturbation can only shift but not remove the X line. Hence, the X line is structurally unstable in the three-dimensional case. This has been illustrated by the 3D simulations of the multiple X line reconnection by Fu et al. [1990]. It was found that the flux rope formed in the simulation has "frayed ends" and a rather complex magnetic topology. But no such problem arises regarding the last definition by Axford [1984]. Schindler et al. [1988] proposed a new definition of the magnetic reconnection called "general magnetic reconnection" according to Axford's definition. General magnetic reconnection is defined as the "breakdown of magnetic connection due to a localized nonidealness." There is a simple criterion for magnetic reconnection to hold: it is necessary and sufficient for magnetic reconnection that

$$\mathbf{B} \times \nabla \times (\mathbf{E} + \mathbf{v} \times \mathbf{B}) \neq 0 \tag{1.7}$$

in a localized region. This property was proven by Hesse and Schindler [1988]. Another definition of the magnetic reconnection is that there is some kind of singular behavior of magnetic field lines [Greene 1988], which indicates that isolated magnetic neutral points can allow magnetic reconnection process to take place.

1.2 The basic properties associated with magnetic reconnection

We have briefly described the concept and the various definitions of the magnetic reconnection. We now discuss the properties associated with magnetic reconnection, e.g., the energy conversion and topology change. For simplification, we only consider a 2D case as shown in Figure 1.1. According to the topology of magnetic field lines, there are only two regions separated by a one-dimensional current sheet, which is denoted by a dashed line before the onset of magnetic reconnection ($t = 0$) in Figure 1.1a. In this magnetic field configuration, there is a certain amount of free magnetic energy to be converted by magnetic reconnection. After the onset of magnetic reconnection, the magnetic field lines nearest to the current sheet are cut in the diffusion region and reconnected to form two new field lines as shown in Figure 1.1b. In this magnetic field configuration, there are essentially four regions which consist of topologically different magnetic fields. Regions 1 and 2 consist of unreconnected magnetic fields and are referred to as inflow regions. Regions 3 and 4 consist of reconnected magnetic field lines and referred to as the outflow regions. The reconnected magnetic field lines in Region 3 and 4 are highly bent and the strong magnetic tension force accelerates plasma to high speed as it moves away from the diffusion region. Consequently, a certain amount of energy stored in the upstream magnetic field is converted to the downstream plasma kinetic or thermal energy. The change of magnetic field topology leads to a direct coupling between the magnetic fields and plasmas on the two sides of the current sheet. In three-dimensions, the topology of the magnetic field is more complicated and it may be impossible to distinguish the four regions. Nevertheless, the basic features (e.g., energy conversion from magnetic field to plasma and the coupling between the two sides of the current sheet) are always observed in the magnetic reconnection process.

1.3 Magnetic reconnection models

1.3.1 2D theoretical models

Theoretical steady-state models of magnetic reconnection were successfully developed by Parker [1957], Sweet [1958], Petschek [1964], Sonnerup [1970], and Yeh and Axford [1970] during the early epoch of the study of magnetic reconnection. Vasyliunas [1975] pointed out that the above 2D models are fundamentally consistent, representing different aspects of the reconnection process. Priest and Forbes [1986] found that the magnetic reconnection configuration is very sensitive to the conditions imposed at the inflow and outflow boundaries. They obtained a unified family of linear models for the incompressible, steady-state magnetic reconnection process. Recently, Priest and Lee [1991] proposed a new theory for the nonlinear fast steady-state magnetic reconnection process. This model includes highly curved magnetic field lines in the inflow region, which differs from that in the classical model of Petschek, and a separatrix jet of plasma ejected from the central diffusion region along the magnetic separatrix.

1.3.2 Dungey's open magnetospheric model

The concept of magnetic reconnection was first applied to the Earth's magnetosphere to explain the geomagnetic storms and auroral activities by Dungey [1961]. He pointed out that the interplanetary magnetic field (IMF) and the geomagnetic field connect at the dayside magnetopause as well as in the nightside magnetotail when the IMF has a southward B_z component. Figure 1.2 shows the configuration of magnetic reconnection in Dungey's open magnetosphere model. Based on the topological properties,

there are three classes of field lines: (1) closed field lines that connect to the earth in both directions, (2) open field lines that connect the earth at one end and to the distant IMF at the other, and (3) IMF lines that do not connect to the earth at all. Magnetic reconnection between the IMF and the magnetospheric fields takes place when the solar wind with a southward IMF impinges on the dayside magnetopause. The reconnected or open magnetospheric fields convect to the nightside magnetotail with the solar wind flow. The pile-up of the magnetic flux in the magnetotail triggers the magnetic reconnection at a certain location which forms new closed magnetospheric fields and IMFs. The newly reconnected magnetospheric fields return to the dayside magnetopause to form a quasi-steady process. Associated with this process, the transfer of mass, momentum, and energy from the solar wind plasma to the magnetosphere produces the geomagnetic storms and auroral activities. Since Dungey's first open magnetosphere model, dayside reconnection has been considered as playing an important role in the coupling between the solar wind and the Earth's magnetosphere [Vasyliunas, 1975; Sonnerup, 1979; Cowley, 1982; Haerendel and Paschmann, 1982; Lundin, 1988].

1.4 Satellite observations at the dayside magnetopause

Based on ISEE satellite observations of isolated but large scale disturbances of the magnetic field, plasma and energetic particle environment at and near the dayside magnetopause, Russell and Elphic [1978] suggested that impulsive reconnection takes place. They termed such disturbances as flux transfer events (FTEs) in which magnetic flux is transferred from the solar wind into the earth's magnetosphere. Earlier, Haerendel et al. [1978], using HEOS 2 magnetometer and plasma data, found localized and transient events which are termed "flux erosion events". FTEs and flux erosion

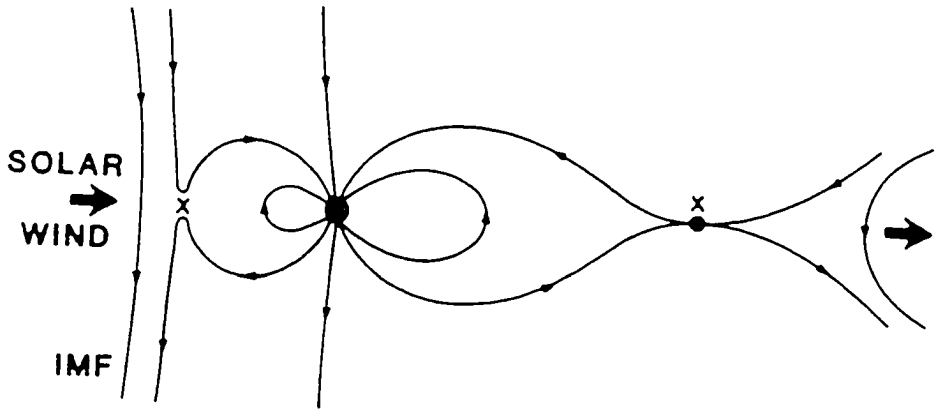

Figure 1.2 Configuration of magnetic field lines in Dungey's open magnetospheric model.

events are identified as the same physical process by Rijnbeek and Cowley [1984]. These events indicate that the dayside magnetic reconnection is an intermittent and sporadic process rather than a steady process as suggested by Dungey [1961]. Figure 1.3 shows an example of magnetosheath FTEs observed on Nov. 29, 1977 by ISEE 1 and 2 [Paschmann et al. 1982]. The total plasma density N_P; the partial densities N_P and N_E of energetic ions between 8 and 40 keV (solid line) and electrons between 1.7 and 20 keV (dotted line); the plasma flow velocity v_P (km s^{-1}) are plotted in the top three panels, while the magnetic field components in the L, M, and N boundary normal coordinates and the total magnetic field strength (B) are shown in the bottom four panels. The L, M, and N boundary normal coordinates were first introduced by Russell and Elphic [1978]. In this coordinate system, N points along the magnetopause normal, M is directed perpendicular to both N and the geocentric solar magnetospheric (GSM) Z axis, and L completes the right-handed system. The origin of the GSM coordinates is at the center of the earth, with X pointing sunward, Z northward and in the plane determined by X and the earth's magnetic dipole, and Y duskward and completing the right-handed orthogonal system.

Figure 1.3 shows three magnetosheath FTEs lablled by 1, 2, and 3. The basic signature of FTEs is a bipolar variation of normal magnetic field component B_N. Many authors [e.g., Russell and Elphic, 1978, 1979; Daly et al., 1981, 1984; Scholer et al., 1981, 1982; Sonnerup et al., 1981, 1987; Berchem and Russell, 1982, 1984; Paschmann et al. 1982, 1986; Rijnbeek et al., 1982, 1984, 1987; Saunders et al., 1984; Farrugia et al., 1987, 1988; Klumpar et al., 1990; Gosling et al., 1990; Elphic, 1990] have further examined plasma and magnetic field signatures associated with FTEs and identified a large number of different properties for these events. These bipolar signatures in B_N during FTEs are often accompanied by an increase in the magnetic field strength when

the magnetosheath magnetic field is strongly southward. The bipolar B_N component variation tends to be $+/-$ (termed 'direct') in the north of the magnetic equator, while the opposite sense $-/+$ ('reverse') is found in the south. This implies that FTEs originate as pairs near the equator and convect away to north and south. Moreover, the magnitude of the B_M component is usually seen to maximize at the center of the B_N signature, indicating core magnetic field enhancement of the magnetic flux tube. Energetic magnetospheric particles flow along the local magnetic field in FTEs, away from the earth, while the bulk properties of the FTE plasma are a mixture of tenuous, hot magnetospheric plasma, and the dense, cold magnetosheath plasma. The bulk flow velocity in FTEs is sometimes above the local magnetosheath speed. Usually, FTEs with a duration about 2 minutes are observed to repeat approximately every 10 minutes.

1.5 Theoretical FTE models

A number of theoretical models have been proposed to explain the intermittent and spatial nature of the dayside magnetic reconnection process associated with FTEs.

1.5.1 Patchy and intermittent reconnection model

Russell and Elphic [1978] suggested a patchy and intermittent model for the dayside reconnection. They envisaged an FTE as the passage of elbow-shaped magnetic flux tubes, which connect the IMF with the magnetospheric field (see Figure 1.4). The scenario of the patchy and intermittent model can explain most of the observed features of FTEs, e.g., the proper sense of the B_N bipolar signature, energetic particle escape and the mixture of the plasma between the magnetosheath and magnetosphere. Due to the weak twist of the magnetic field in this model (see Song and Lysak [1989]), it is

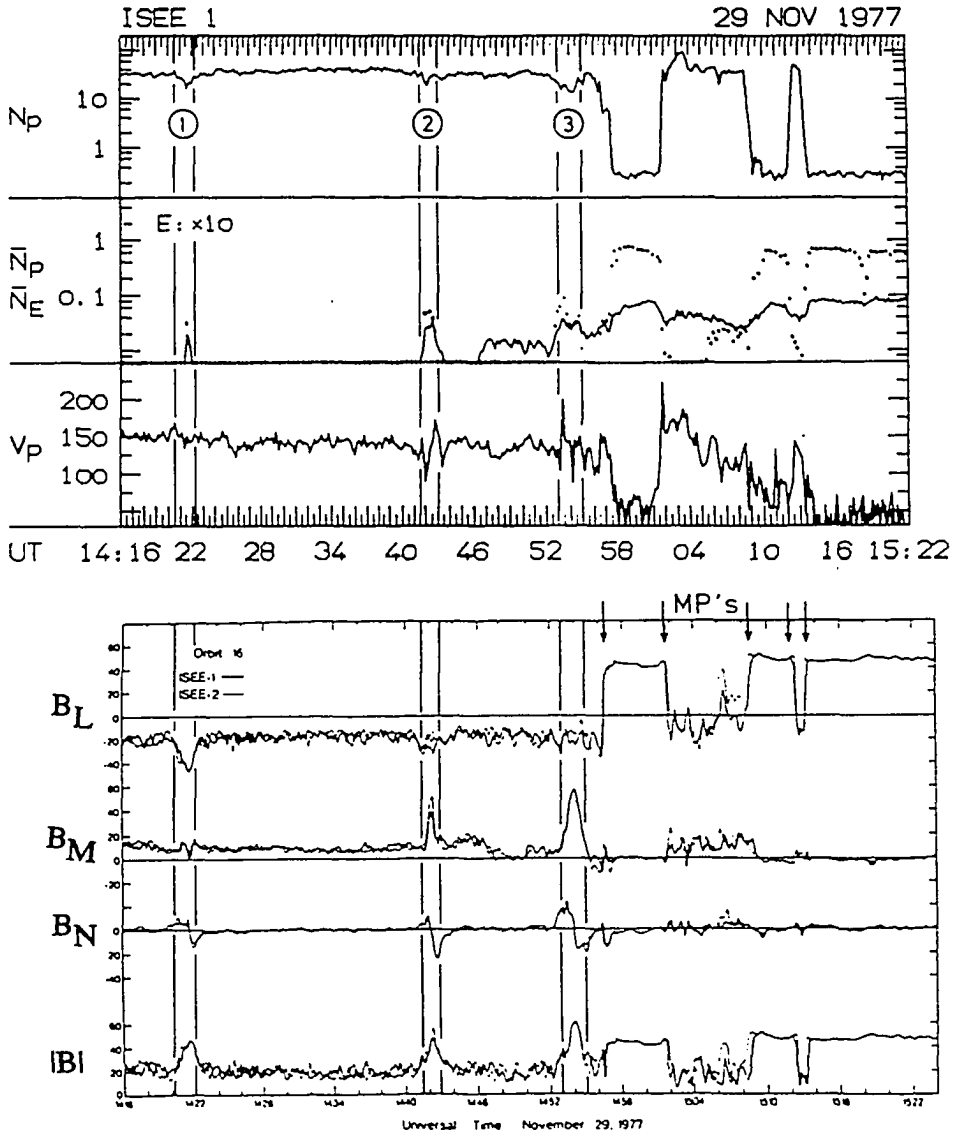

Figure 1.3 Data from ISEE 1, for a one-hour period on 29 November, 1977, showing 3 magnetosheath FTEs (*Paschmann et al.*, 1982).

difficult to explain the strong enhancement of the total pressure or core magnetic field that is frequently observed in the flux tube. Kan [1988] proposed a theory of patchy and intermittent reconnections based on 3D tearing mode instability of the magnetopause current sheet. The nature of the 3D tearing is localized reconnection sites and the limited timescale due to the fluctuation of the solar wind. The 3D tearing reconnection provides a mechanism for patchy reconnection. The multiple layer reconnection proposed by Galeev et al. [1986] was used to explain the occurrence of patchy reconnection. In this model, the magnetic surfaces in the dayside magnetopause can be destroyed by the growth and overlapping of magnetic islands. The random walk of the magnetic field lines between the destroyed magnetic surfaces leads to magnetic percolation or connection between the two sides of the magnetopause. The saturation of the magnetic islands due to coupling between the drift tearing mode and ion sound waves halts the percolation process and produces the intermittent nature.

1.5.2 MXR model

Lee and Fu [1985] proposed an alternative model for creating FTEs at the magnetopause. They pointed out that multiple X line reconnection (MXR) can produce magnetic islands at the magnetopause current sheet. If the magnetosheath and magnetospheric fields are not exactly antiparallel, the islands will contain a field component along the island axis, which implies that the magnetic islands are magnetic flux ropes in the 3D case [Figure 1.5]. As the islands grow to some certain size and are eventually convected away from the subsolar region, the process repeats, which is demonstrated by the numerical simulations [Fu and Lee, 1985, 1986; Lee and Fu, 1986; Ding et al.,

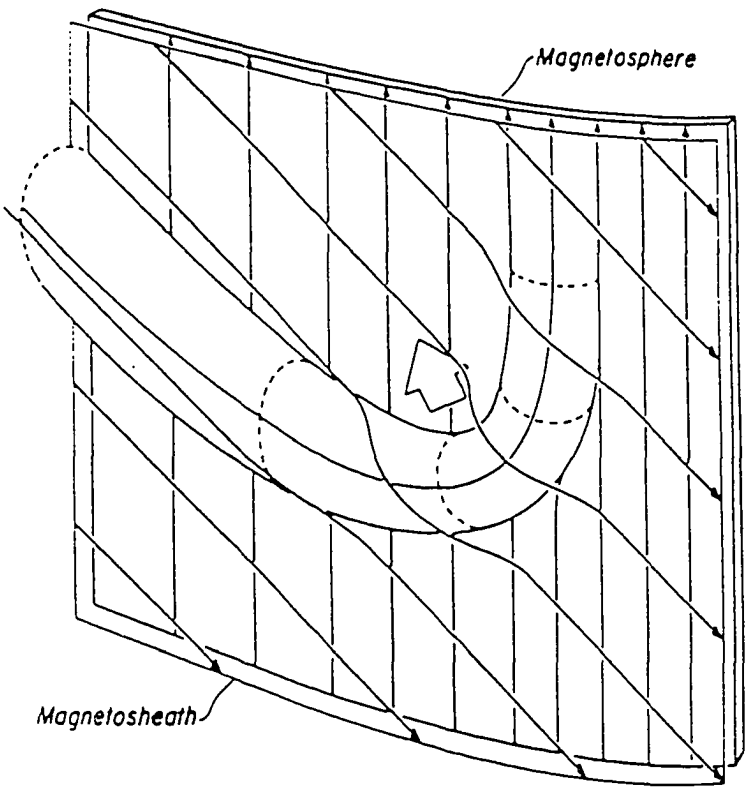

Figure 1.4 Magnetic flux rope in the patchy reconnection model. Magnetosheath field lines, slanted arrows, have connected with magnetospheric field lines, vertical arrows, possibly off the lower edge of the figure. The connected flux tube moves in the direction of the large arrow (*Russell and Elphic*, 1978).

al., 1988]. The MXR model can explain the properties of the magnetic field signatures, plasma acceleration and energetic particle anisotropy.

1.5.3 Bursty SXR model

Further, *Scholer* [1988a] and *Southwood et al.* [1988] suggested that FTE signatures are produced by bursty reconnection at a single X line which extends over a large longitudinal segment of the dayside magnetopause [Figure 1.6], based on the time-dependent Petschek-type reconnection discussed by Semenov et al. [1984] and Biernat et al. [1987]. Near the reconnection site the magnetic field and plasma have established the inflow and outflow characteristics of the steady-state Petschek reconnection, while far away from the reconnection site the initial magnetopause current sheet is unperturbed. Hence, in the single X line reconnection (SXR), magnetic field lines are open field lines, a loop-like structure is produced, and no magnetic flux ropes are formed.

1.6 Observations in the polar ionosphere

According to the theoretical FTE models discussed above, the magnetic flux reconnected at the dayside magnetopause is pulled tailward, which produces some signatures in the polar ionosphere. The FTE flux tube contains the field-aligned currents and Alfven waves due to the twist of the magnetic field. The Alfven waves carrying FACs propagate away from the dayside magnetosphere to the ionosphere, which results in perturbations of the local magnetic fields. Furthermore, the upward FAC will accelerate the electrons to high energies, leading to auroral brightening. It is widely believed that the field-aligned current associated with the FTE flux tube plays an important role in the

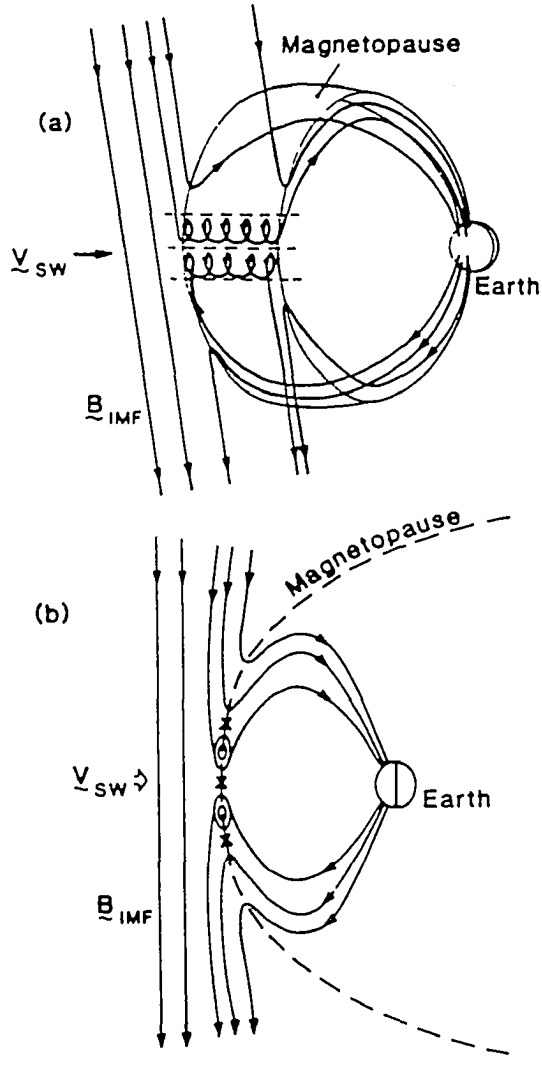

Figure 1.5 Multiple X line reconnection model (a) a perspective view of the open magnetic flux tube and the regular open field lines as a result of multiple X line reconnection at the dayside magnetopause, and (b) the projection of flux tubes in the noon-midnight meridian plane (*Lee and Fu*, 1985).

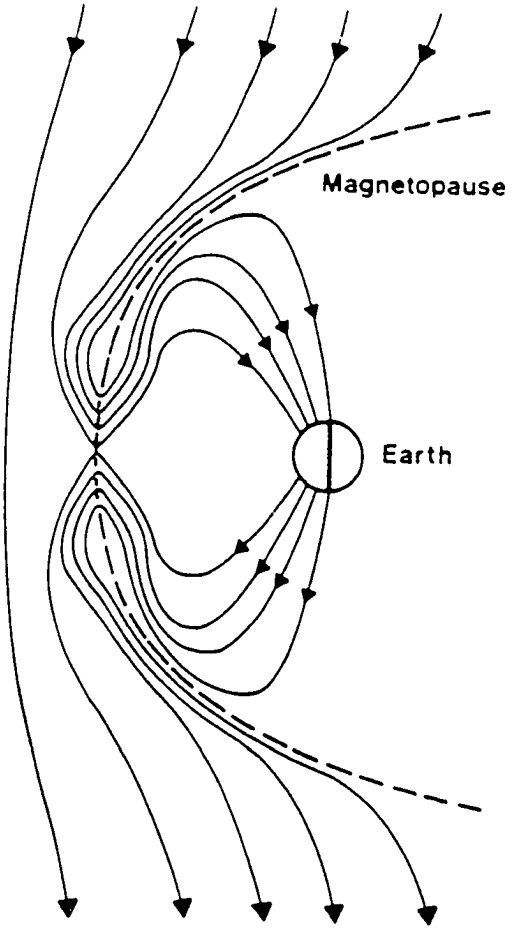

Figure 1.6 A schematic drawing of the bursty single X line reconnection model (*Scholer*, 1988).

coupling between FTEs in the dayside magnetopause and the dayside auroral arcs in the ionosphere.

After the discovery of FTEs, many researchers have been attracted to study the ionospheric effects of FTEs. Poleward-moving auroral forms (PMAFs) observed by ground-based optical instruments are possible high-latitude ionospheric signatures of FTEs [e.g., Sandholt et al., 1986; Mende et al., 1990; Lockwood, 1991; Fasel et al., 1992, 1993a]. After the initial brightening, the PMAF moves away from the dayside auroral oval into the polar cap, which may relate to the tailward convection of the reconnected magnetic flux. Recently, Fasel et al. [1992, 1993a] found that most PMAFs have multiple brightenings as they drift into the polar cap. The time between successive brightenings is typically 1.5-2 minutes. In addition, Fasel et al. [1993a] further studied the time distribution between successive PMAF intervals and found that there appears to be a good correlation between the time distribution for the PMAFs seen in the dayside aurora oval as shown in Figure 1.7a and for FTEs observed at the magnetopause in Figure 1.7a, which are produced by Lockwood and Wild [1993]. More recently, Fasel et al. [1993b] suggested that the patchy multiple X-line reconnection (PMXR) may explain the formation, motion, and brightening history of poleward-moving auroral forms.

1.7 Objectives and outline of the thesis

The observations of magnetic FTEs [Russell and Elphic, 1978] and accelerated plasma flow [Sonnerup, 1981; Paschmann et al., 1986; Gosling, 1990], as well as ground based observations [Lanzerotti et al., 1991; Lockwood and Smith, 1989; Fasel et al., 1993a], provide substantial evidence that magnetic reconnection is an important physical process at the dayside magnetopause during periods of sufficient magnetic shear across

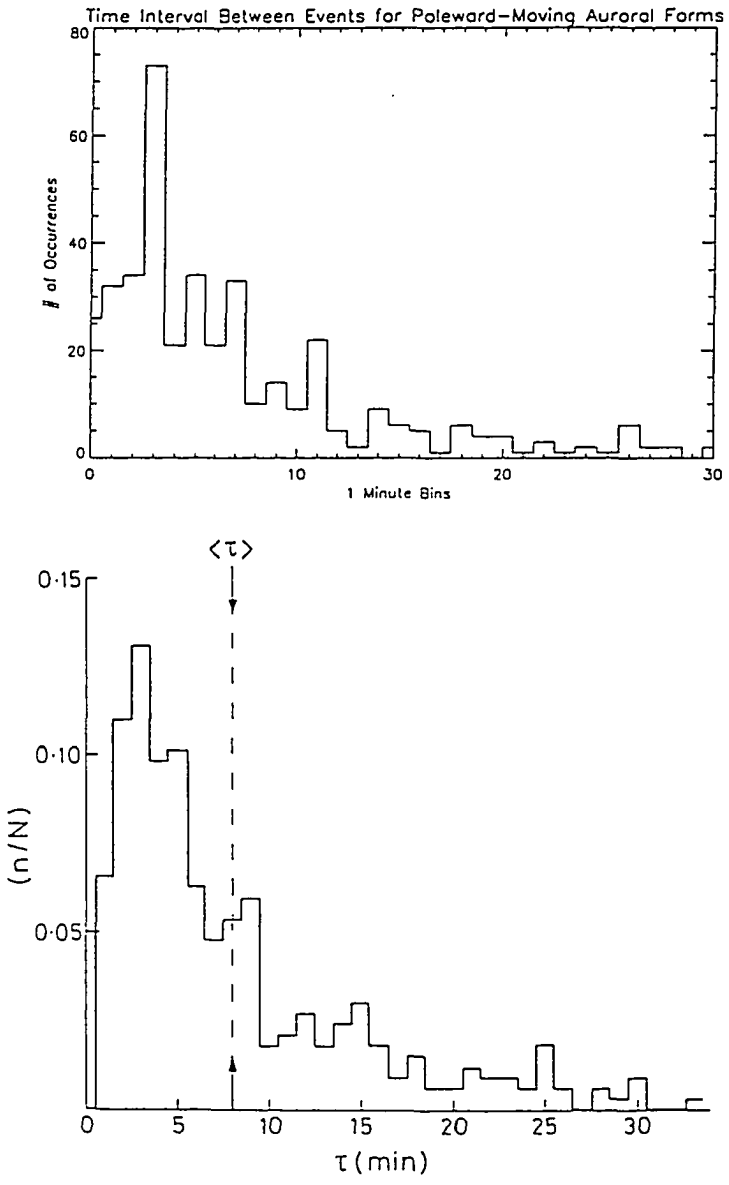

Figure 1.7 (a) Time distribution between successive PMAF intervals observed in the dayside aurora oval *Fasel et al.* [1993a] and (b) distribution of inter-FTE intervals taken from *Lockwood and wild* [1993]

the magnetopause. Dayside reconnection has been modeled by numerical simulations on a global scale and in a local approximation (i.e., on small scales compared to the overall size of the dayside magnetopause). While the global approach is important for the interaction of various parts of the magnetosphere (Sato, et al., 1986; Ogino et al., 1989; Fedder et al., 1991), local simulations provide better resolution for processes which involve small length scales. A number of models discussed above for dayside reconnection have been suggested to explain the observations of FTEs in a local approach. In addition, conservation of magnetic helicity is an important constraint for the change of magnetic topology [Wright and Berger, 1989; Song and Lysak, 1989]. Magnetic reconnection at the dayside magnetopause is a 3D process due to the finite size of the dayside magnetopause. Thus, it is important to examine the properties of the associated processes: (1) the magnetic topology, (2) the core magnetic field enhancement, and (3) the generation and evolution of field-aligned currents during the reconnection process through the 3D simulation.

In Chapter 2, we will illustrate that the magnetic flux in the flux rope formed in the 3D MXR process may show certain preferable magnetic connections under certain condition. We also develop a 3D compressible MHD code to study the dynamics and topological aspects of MXR. The results will be applied to explain the new observations of fossil FTEs (see discussion on p.24) and the formation of the low-latitude boundary layer.

FTEs often show a significant increase of the magnetic field strength at the center of the events [e.g., Paschmann et al., 1982]. In most cases, the major contribution of this increase is due to an amplification of the M component of the magnetic field in boundary normal coordinates. Similar magnetic field observations have been reported for structures in or near the plasma sheet of the magnetotail at about $20R_E$ [Elphic et

al., 1986]. The scale size of these magnetotail structures was estimated to roughly 3 - 5 R_E. In chapter 3, 2D and 3D simulations SXR, MXR, and patchy reconnection are presented to examine and compare the amplification of the magnetic field in the center of the developing flux tubes.

Field-aligned currents play an important role in the coupling of the magnetosphere to the polar ionosphere [Iijima and Potemra, 1976; Iijima et al., 1978; Akasofu, 1984]. Previous studies of the generation of field-aligned currents by 3D reconnection have assumed magnetotail-like configurations in which the magnetic fields are nearly anti-parallel [Birn and Hones, 1981; Sato et al., 1984; Hesse and Birn, 1991; Scholer and Otto, 1991]. In Chapter 4, we will study the generation of the Alfven waves and field-aligned currents associated with magnetic reconnection at the dayside magnetopause. In this study, the influence of the B_y component of the IMF on the generation of the field-aligned currents is considered.

The discussion and summary are given in Chapter 5.

CHAPTER 2

Topology of magnetic flux ropes formed by multiple X line reconnection.

2.1 Introduction

As mentioned Chapter 1, magnetic field topology associated with magnetic reconnection is an important topic. Three-dimensional magnetic reconnection is qualitatively different from the two-dimensional process [*Greene*, 1988; *Schindler et al.*, 1988; *Hesse and Schindler*, 1988; *Fu et al.*, 1990; *Otto*, 1991, Lee et al., 1993]. In two-dimensions, there are well-defined boundaries or separatrices to separate the regions with different magnetic field topology and plasma properties. The two separatrices intersect to form an X point. The magnetic reconnection can be defined as plasma flow across the separatrix. But X points and separatrices, often regarded as central properties of two-dimensional reconnection [*Vasyliunas*, 1975], have been shown to be structurally unstable in three dimensions [*Schindler et al.*, 1988], i.e., a small three-dimensional perturbation can lead to the disappearance of these structural elements.

Lee and Fu [1985] proposed an MXR model to explain the observational signatures associated with FTEs as shown in Figure 1.5. At the same time, they also pointed out that two ends of the magnetic flux rope formed by MXR reconnection can be connected to both the IMFs or the geomagnetic fields. *Fu et al.* [1990] carried out three-dimensional simulations of multiple *X* line reconnection. However, they found that the flux rope formed in the simulation has "frayed ends," i.e., field lines in the flux rope demonstrate all possible connections (entering from the magnetosphere or

magnetosheath and leaving the rope into either of these regions) and thus reveals a rather complex magnetic topology. Thus, it is impossible to determine the separatrix according to magnetic field topology. Separatrices and X lines are no longer present in three-dimensional reconnections. Lee et al. [1993] proposed a mechanism to produce the well-defined topology in the magnetic flux rope associated with MXR reconnection. Furthermore, they pointed out that the combination of local patchy reconnection and multiple X line reconnection can produce various magnetic configurations at the dayside magnetopause. From the topological point of view, they explained the formation of the low-latitude boundary layer and the fossil FTEs reported by Klumpar and Fuselier [1990]. The evolution of the magnetic helicity associated with magnetic reconnection has been examined by Wright and Berger [1989] and Song and Lysak [1989].

Since the early FTE observations, the observational methods have been extended to include additional data on plasma electrons, energetic ions and plasma ion composition. Using such data from the AMPTE/CCE satellite, *Klumpar and Fuselier* [1990], and *Klumpar et al.* [1990] claimed that they identified a new type of FTEs, which are observed in the magnetosphere. A detailed examination of the plasma signatures for a number of events [*Klumpar and Fuselier* 1990] has revealed that (1) the electron distribution in the central region of the events is remarkably similar to the low-latitude boundary layer (LLBL) distribution, (2) the boundary region is composed of hot trapped electrons and cold bidirectionally streaming electron beams, and (3) magnetospheric plasma is detected immediately outside the events. The measured magnetic field exhibits the bipolar signature of the normal magnetic field component. However, some properties which have been reported previously for the magnetospheric FTEs, such as, the presence of LLBL-like plasma outside of FTEs and strong ion flows, are not present for this new class of FTEs. The observed particle features for these events indicate that

magnetosheath plasma is trapped on closed field lines earthward of the magnetopause and that reconnection has ceased for these structures. The presence of the observed bipolar B_N signatures indicates that the magnetic field lines in these FTE flux tubes are twisted and have an azimuthal component. If these signatures indeed originate from closed field line regions earthward of the LLBL, most of the models which have been proposed for FTE formation ought to be revisited for this class of FTEs. Since it seems that reconnection has ceased for these structures, we will call them "fossil" FTEs.

A number of different explanations for the observation of these flux transfer events are discussed in the literature. *Sibeck* [1990, 1992] explained these events by a magnetopause motion and transient entries into a layered structure of the low-latitude boundary layer. Kan and Klumpar [1993] suggested that the re-reconnection associated with multiple patchy reconnection is also a possible process for the formation of boundary layer plasma on closed magnetospheric field lines [*Kan*, 1988; *Nishida*, 1989]. As a result of reconnection, solar wind plasma may enter the magnetosphere along open reconnected field lines. However, because of the multitude of reconnection patches, two reconnected flux tubes can be hooked with each other, leading to re-reconnection. Magnetosheath plasma on some flux tubes might eventually be found on closed magnetospheric field lines as a result of re-reconnection.

In this chapter we will illustrate that, for appropriate conditions, the magnetic flux in such flux ropes may show certain preferable magnetic connections. The formation of fossil FTEs as well as the LLBL can also be explained by multiple X line reconnection process. In section 2.2 we develop conditions for which flux ropes can be expected to exhibit a fairly well ordered magnetic connection to either side of the initial current layer. The numerical method and simulation parameters are introduced in section 2.3. Section 2.4 presents the simulation results with different topologies in the magnetic

flux ropes. The result is applied to explain the observations of fossil FTEs in sections 2.5. The last section presents a discussion and conclusion with respect to the proposed mechanism.

2.2 Field line topology of magnetic flux ropes

A process for the formation of magnetic flux ropes is provided by multiple *X* line reconnection [*Lee and Fu* 1985]. Here the presence of two *X* lines generates a magnetic flux rope and each additional *X* line leads to a further flux rope. Fu et al. [1990] have presented a three-dimensional numerical study of multiple *X* line reconnection in the framework of incompressible resistive magnetohydrodynamics (MHD). The resulting magnetic topology of the lower ($z < 0$) magnetic flux tube is shown in Figure 2.1. It is seen that magnetic field lines at the ends of the flux tube are connected to both sides of the current sheet in an apparently random manner. However, individual field lines can be classified into distinct categories based on their topology. Sketches of magnetic flux ropes which illustrate these magnetic connections are shown in Figures 2.2*a* - *d*. The four different types of topology in terms of the magnetic connection to the magnetosphere (MSP) or the IMF are (1) MSP to MSP, (2) IMF to MSP, (3) IMF to IMF, and (4) MSP to IMF. Obviously, the four types of field line topology may coexist in one magnetic tube leading to a relatively complex mixed topology as illustrated in Figures 2.2*e* and 2.2*f*.

We now determine the conditions for which a certain topology may dominate in a tube such that a major amount of flux has the same magnetic connectivity. In order to formulate these conditions we make some fairly restrictive assumptions. However, we will illustrate with the results of numerical computations that these assumptions are

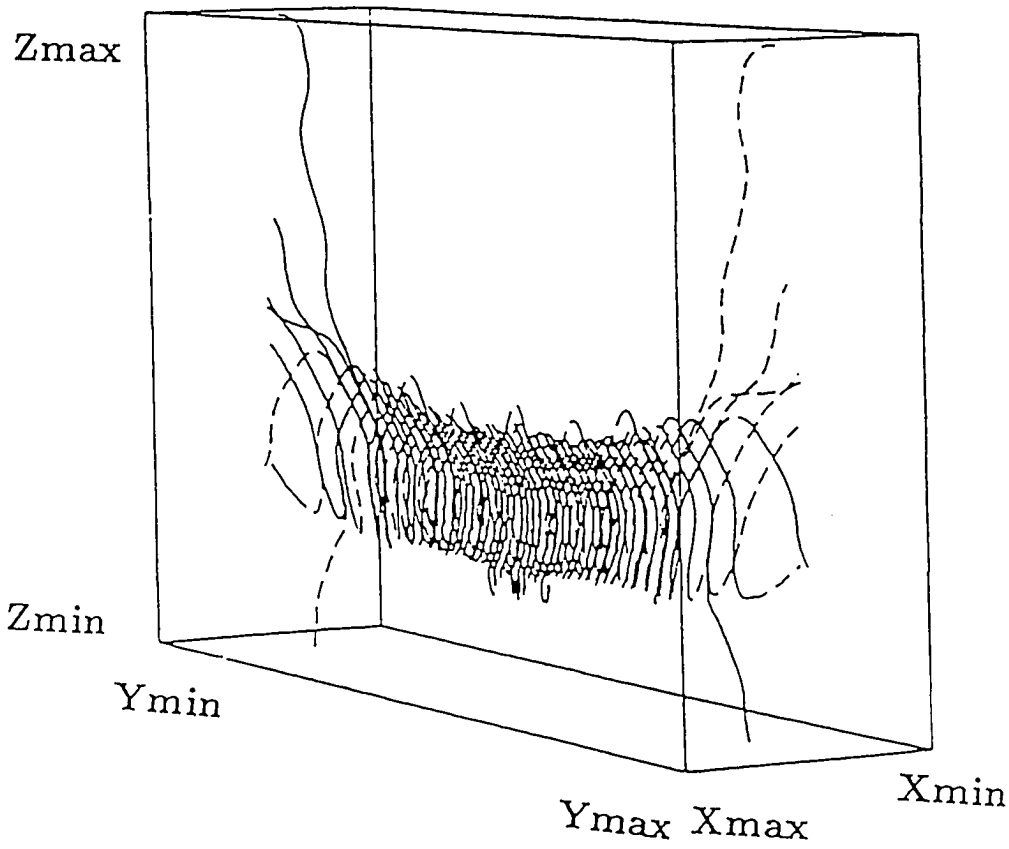

Figure 2.1 Magnetic field lines in a frayed magnetic rope formed in the 3D MXR reconnection. Solid (dashed) lines indicate sections of field lines on the magnetosphere (magnetosheath) side (*Fu et al.*, 1990).

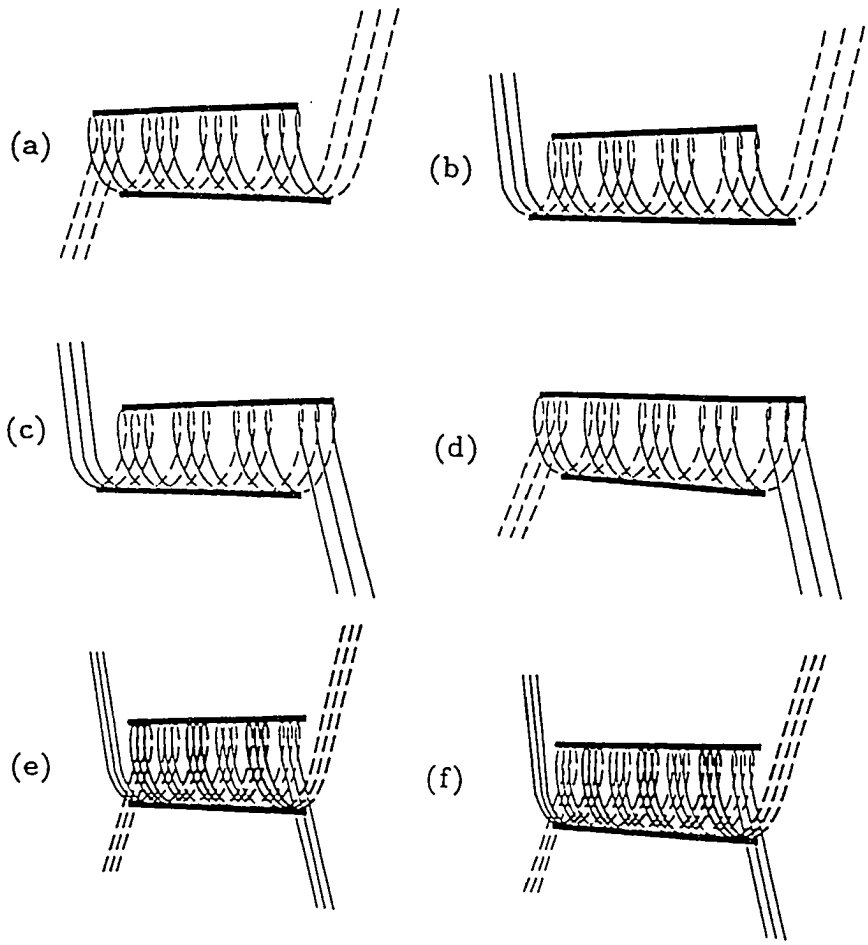

Figure 2.2 Six possible patterns of the field line topology of the magnetic flux rope. The heavy bars denote the reconnection X lines. The solid (dashed) lines indicate field lines on the magnetosheath (magnetospheric) side.

not as restrictive as they appear to be: 1. The onset of reconnection is assumed to occur at the same time for all X lines and the specific reconnection rate (i.e., the electric field component parallel to the magnetic field) is assumed to be the same everywhere on the X lines. 2. We suppose that the pitch angle Φ of all reconnected magnetic field lines with respect to the orientation of the corresponding X line is determined by either one of the asymptotic magnetic field directions. These assumptions neglect for instance a certain amount of magnetic flux which is present inside the current layer and also exclude dynamical effects which would alter the pitch angle of the magnetic field lines like three-dimensional flow patterns at the ends of the flux ropes. Using these assumptions the problem of the flux rope topology for a given pair of X lines becomes a pure geometrical problem as illustrated in Figure 2.3, which represents a sketch of a flux rope geometry in a projection onto the y-z plane. In this figure sections of field lines which originate from the MSP are indicated by dashed lines and solid lines represent IMF origin. The coordinate system is chosen as noted above such that the B_y component is the same for the interplanetary and magnetospheric magnetic fields while the corresponding z components point into opposite directions. This choice of the coordinate system is also motivated by the fact that the net current is flowing in the y direction, such that we can expect that the X lines (thick plotted solid lines) are located along the y direction at least for the nonlinear evolution of the reconnection process. A corresponding orientation of the parallel electric field is observed for the reconnection due to a patch of resistivity.

We remark that magnetic flux always enters the flux rope at the dawnside (i.e., left-hand side) for a positive B_y component and leaves the rope on the duskside (vice versa for negative B_y). In order that, at a certain instant of time, the magnetic flux enters only from MSP, it is required that the leftmost segment of magnetosheath flux which is

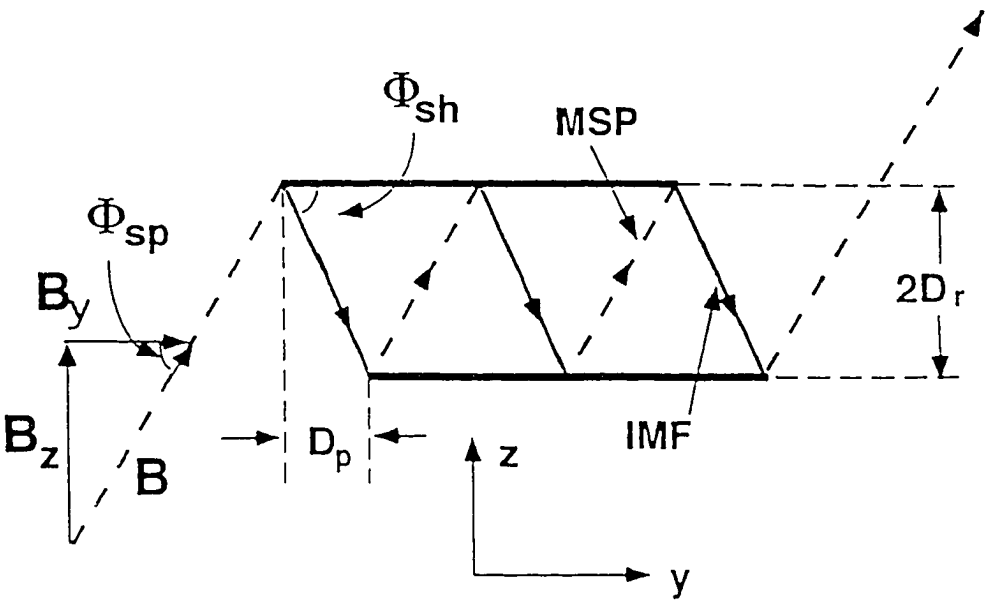

Figure 2.3 Simplified reconnection geometry for two X lines (thick plotted lines) in a projection onto the y-z plane. The chosen geometry refers to the sketch in Figure 2.2*a*.

newly reconnected at the lower X line ought to undergo reconnection at the upper X line as well. This requires that the end of the upper X line is shifted by at least the distance D_p in the negative y direction compared to the termination point of the lower X line. Here D_p is given by $D_p = D_r/tan\Phi_{sh}$ where D_r is the separation distance of the X lines and Φ_{sh} is the pitch angle of the magnetosheath field with respect to the X lines. If we define $\Delta y = y_u - y_l$, where y_u and y_l refer to the y coordinates of the left end points of the upper and lower X lines, respectively, the condition for magnetospheric connection is

$$\Delta y < D_r B_y / B_{sh\,z} \,. \tag{2.1}$$

Note that both $B_{sh\,z}$ and Δy are negative in (2.1) and $\Delta y < 0$ implies that the upper X line is shifted to the left with respect to the lower one. The lower indices sh and sp denote magnetosheath and magnetospheric origin, respectively. It is now straightforward to determine the corresponding condition for the entrance of magnetosheath flux:

$$\Delta y > D_r B_y / B_{sp\,z} \,. \tag{2.2}$$

Similarly magnetic flux leaves the flux rope only into the magnetosphere for $\Delta y < D_r B_y / B_{sh\,z}$ and only into the magnetosheath for $\Delta y > D_r B_y / B_{sp\,z}$, where Δy refers to the right endpoints of the X lines. Now any combination of the conditions for the entrance and exit of magnetic flux yields a certain topological connection for a major amount of the flux which is contained in the flux rope. For instance, if the whole upper X line is sufficiently shifted to the left we expect a pure MSP-MSP connection (Figure 2.2*a*) and a sufficient shift to the right yields an IMF-IMF magnetic connection (Figure 2.2*c*). Further, an IMF-MSP topology (Figure 2.2*b*) requires appropriate X line

locations and in addition that the lower X line is at least $2|D_p|$ longer than the upper one (vice versa for the MSP-IMF topology). It is also easy to see that a negative B_y component requires a shift of the upper X line in the opposite direction compared to the above considerations.

2.3 Simulation model

In order to support these considerations a number of three-dimensional resistive MHD computations have been carried out to study the dynamics and topological aspects of MXR. The simulation is based on the solution of the compressible MHD equations in a 3D simulation domain. The time evolution of systems under consideration is determined by the following set of MHD equations:

$$\frac{\partial \rho}{\partial t} = -\nabla \cdot (\rho \mathbf{v}) \tag{2.3}$$

$$\frac{\partial (\rho \mathbf{v})}{\partial t} = -\nabla \cdot \left[(\rho \mathbf{v}\mathbf{v}) + \left(p + \frac{B^2}{2\mu_0} \right) \mathbf{I} - \frac{1}{\mu_0} \mathbf{B}\mathbf{B} \right] \tag{2.4}$$

$$\frac{\partial \mathbf{B}}{\partial t} = \nabla \times (\mathbf{v} \times \mathbf{B}) - \nabla \times (\eta \mathbf{j}) \tag{2.5}$$

$$\frac{\partial \epsilon}{\partial t} = -\nabla \cdot \mathbf{S} \tag{2.6}$$

where ρ is the plasma mass density, $\mathbf{v}$ is the plasma velocity, p is the plasma pressure, $\mathbf{B}$ is the magnetic field, η is the electric resistivity, μ_0 is the magnetic permeability in free space, and $\mathbf{I}$ is the unit tensor. The current density $\mathbf{j}$ is given by the magnetic induction

equation

$$\mathbf{j} = \frac{1}{\mu_0}\nabla \times \mathbf{B} \tag{2.7}$$

The energy flux S and the energy density ϵ are defined as

$$\mathbf{S} = \left(\epsilon + p + \frac{B^2}{2\mu_0}\right)\mathbf{v} - \frac{1}{\mu_0}(\mathbf{B}\cdot\mathbf{v})\mathbf{B} + \frac{\eta}{\mu_0}\mathbf{j}\times\mathbf{B} \tag{2.8}$$

$$\epsilon = \frac{1}{2}\rho v^2 + \frac{B^2}{2\mu_0} + \frac{p}{\gamma - 1} \tag{2.9}$$

where γ is the adiabatic constant chosen to be $\gamma = 5/3$. For the actual simulation, the magnetic field strength, the plasma density, the plasma pressure, the length scales, the current density, the plasma velocity, the resistivity, and the timescale are normalized to typical values $B_0, \rho_0, L_0, V_0 = B_0/\sqrt{\mu_0\rho_0}, t_0 = L_0/V_0, P_0 = {B_0}^2/\mu_0, J_0 = B_0/a\mu_0$, and $\eta_0 = \mu_0 L_0 V_0$. Dimensionless quantities will be used throughout the remainder of the thesis. The normalized equations are solved simultaneously using a two-step Lax-Wendroff finite differencing scheme with a third-order artificial diffusion term [*Lapidius*, 1967].

The geometry and coordinate system of the simulation model are illustrated in Figure 2.4. The initial configuration consists of two regions with different magnetic field orientations which are separated by a one-dimensional current layer of half-width L_0 in normalized units. The x axis is oriented normal to this current layer, and the one-dimensional current layer is centered at the $x = 0$ plane. Since we are interested in basic properties for the magnetic field topology in this chapter, or the core field enhancement and the generation of FACs in next two chapters, we will not consider asymmetry in the density or the magnetic field across the current layer. The z axis is

aligned with the antiparallel magnetic field components, and the orientation of the y axis is chosen to complete the coordinate system.

The initial magnetic field is given in normalized units by

$$B_y(x) = \cos(\frac{\phi}{2})$$

and

$$B_z(x) = \sin(\frac{\phi}{2})tanh(x) \tag{2.10}$$

where ϕ is the angle between the magnetic fields on the two sides of the current sheet. The plasma pressure is chosen such that total pressure is balanced across the current layer. The plasma beta is set to $\beta = 1$ outside the current sheet and the initial plasma velocity is set to zero. We also assume a constant initial density of 1 for simplicity.

The simulation is carried out only in one half of the physical domain due to the symmetry condition. At the boundaries, $x = L_x$, $y = \pm L_y$, and $z = \pm L_z$, the normal derivatives of all physical quantities are assumed to be zero. The line symmetric boundary condition is imposed in the plane $x = 0$. To reduce the amplitude of waves reflected by the boundary, a damping term is applied at the outermost grid points.

In order to model magnetic connection under various conditions in a self consistent manner, we trigger reconnection at appropriate locations, by using a localized resistivity of the form

$$\eta = \eta_b + \eta_a(x, y, z) \tag{2.11}$$

where η_b is a small background resistivity and $\eta_a(x, y, z)$ is the locally enhanced resistivity which is used to prescribe the position and the size of a reconnection region. The detailed formulation of $\eta_a(x, y, z)$ in the simulation will be described the in next section.

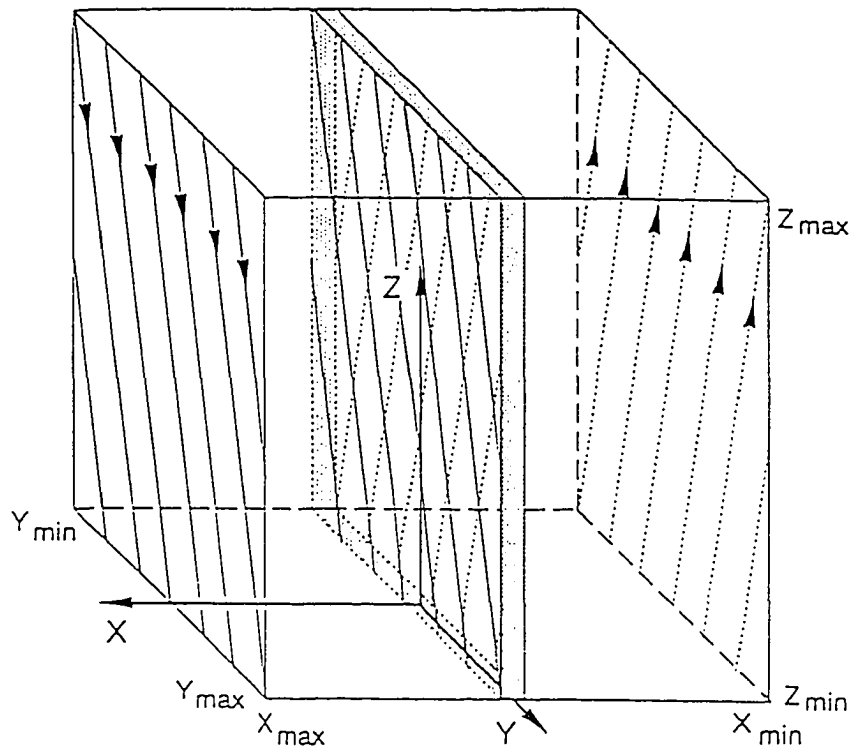

Figure 2.4 Illustration of the geometry of the initial configuration for the three-dimensional MHD simulations. The shaded area represents the current layer in the system. The orientations of magnetic fields are indicated on the boundary surfaces.

2.4 Simulation results

In this chapter, five simulation cases are conducted to examine the magnetic field topology in the MXR reconnection. In the first four cases, it is shown that all reconnected magnetic field lines appear to have well defined connections, which are similar to the field line topology in the schematic drawing shown in Figure 2.2a-d. In the last case, we show that all different magnetic connections are mixed in one magnetic flux rope. In the simulation, the magnetic field shear angle is chosen to be $B_y = 0.1$. In order to obtain a preferable magnetic field topology, the locally enhanced resistivity for these runs is chosen to be

$$\eta_a(x,y,z) = [\eta_1(y,z) + \eta_2(y,z)]exp\{-(x-x_0)^2\} \tag{2.12}$$

where η_1 and η_2 determine the positions and the lengths of two X lines. The detailed formulations of η_1 for the upper X line and η_2 for the lower X line are given as

$$\eta_1(y,z) = \begin{cases} \eta_e exp\{-(z-z_1)^2\}, & \text{if } |y-y_1| \le X_{L1}; \\ \eta_e exp\{-(|y-y_1| - X_{L1})^2\} exp\{-(z-z_1)^2\}, & \text{otherwise,} \end{cases} \tag{2.13a}$$

$$\eta_2(y,z) = \begin{cases} \eta_e exp\{-(z-z_2)^2\}, & \text{if } |y-y_2| \le X_{L2}; \\ \eta_e exp\{-(|y-y_2| - X_{L2})^2\} exp\{-(z-z_2)^2\}, & \text{otherwise,} \end{cases} \tag{2.13b}$$

where $\eta_e = 0.05$ is the localized enhanced resistivity. The upper and lower X lines are located at $(x_0, z_1) = (0, 25)$ and $(x_0, z_2) = (0, -25)$, respectively. The parameters X_{L1} and X_{L2} are the half-lengths of the upper and lower X lines, while y_1 and y_2 are set to determine the related shift between the two X lines. The background resistivity $\eta_b = 0.001$ corresponds to $R_m = 1000$. Other common parameters used in the simulation are $N_x = 51, L_x = 15, N_y = 65, L_y = 50, N_z = 101$, and $L_z = 50$.

2.4.1 MSP to MSP connection

In this case, the half-lengths X_{L1} and X_{L2} of the upper and lower resistive regions are chosen to be 30, while y_1 and y_2 are respectively 10 and -10, which implies that the upper resistive region is shifted to the right by 20 with respect to the lower resistive region such that the condition for the relative shift of the two X line termination positions is well satisfied in order to produce an MSP-MSP connection.

Figure 2.5 presents perspective views of magnetic field lines of flux ropes for this run. In Figure 2.5 we have traced seven field lines at $t = 100$, where dashed lines represent sections of magnetic field lines of preferably magnetospheric orientation (i.e., $B_z > 0$) and solid lines indicate magnetosheath orientation (i.e., $B_z < 0$). It is seen that in the plot the flux tubes appear to have well defined magnetic connections. All traced magnetic field lines start from the magnetosphere and finally still go to the magnetosphere with multiple entries to the magnetosheath side through multiple reconnections. In such a flux rope, we have rather smooth ends in which the topology is much simpler than one with frayed ends obtained by Fu et al. [1990]. We can expect that the central region in the magnetic flux rope contains the initial current sheet plasma and the magnetospheric and magnetosheath plasmas are mixed in the boundary region of the flux rope. In view of the quite restrictive assumptions for deriving these conditions one would expect the presence of a certain amount of flux with a different magnetic connection (e.g., magnetic flux that is present in the magnetopause layer itself initially). In order to obtain more detailed information about the topological structure of the flux rope in Figure 2.5, we consider a cross section of the flux rope and trace a large number of field lines through this cross section. Figure 2.6 shows the detailed topology of the magnetic flux in the cross section $y = 0$. Note that the four symbols indicate

the four different magnetic connections. The sign + indicates an MSP-MSP connection of the corresponding magnetic field lines while signs $*$, $\bullet$, and $\triangle$ stand for IMF-IMF, IMF-MSP, MSP-IMF connections, respectively. The result in Figure 2.6 illustrates that the major amount of flux in the magnetic flux rope has indeed MSP to MSP connection indicated in the previous figure. But there still is a certain amount of magnetic flux with complicated connections in the central region of the flux rope. We remark that it is not straightforward to define a proper boundary of the flux rope and the boundary indicated in Figure 2.6 is defined by magnetic flux which intersects the plane $x = 0$ at least twice.

Figure 2.7 shows (a) the plasma flow pattern in the plane $x = 0$ and (b) the x integrated value of the FACs obtained at $t = 100$. After the onset of magnetic reconnection, the reconnected magnetic flux moves toward the central region due to the magnetic tension force. The magnetic frozen-in condition still holds outside the reconnection or diffusion region. Therefore, plasmas that are a mixture of both the magnetosheath and magnetospheric components will move with the magnetic flux, which leads to the plasma pressure and magnetic pressure built up. The tube-aligned motion, which is shown in Figure 2.7a, reduces the enhanced pressure in the rope. The strong twist of the magnetic field as shown in Figure 2.5 indicates that the tube-aligned current is accumulated in the flux tube and simultaneously the guiding magnetic field is largely increased in this process (which is detail studied in the next chapter). Consequently, FACs in the magnetic flux tube will be significantly enhanced (see Figure 2.7b).

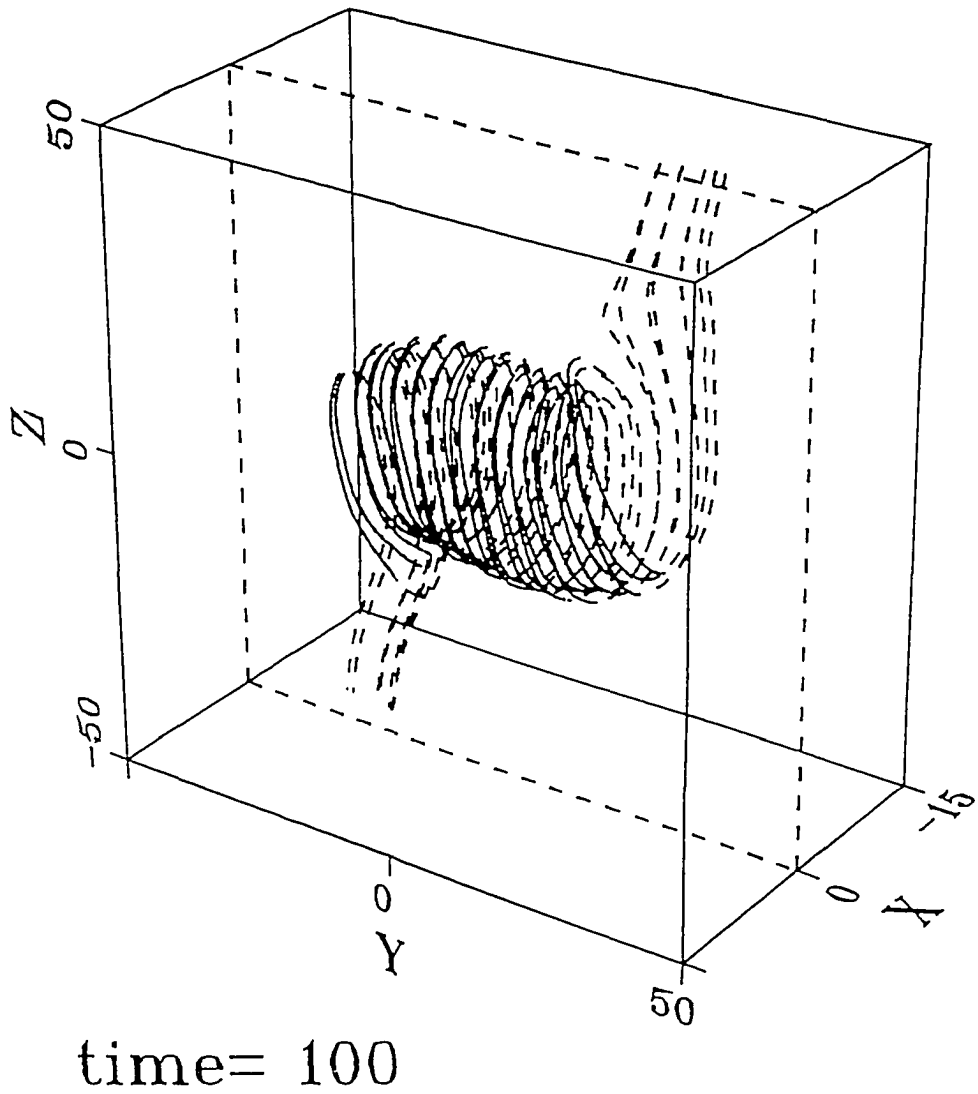

Figure 2.5 Perspective view of magnetic field lines in a magnetic flux ropes with an MSP-MSP connection formed in the 3D MXR reconnection.

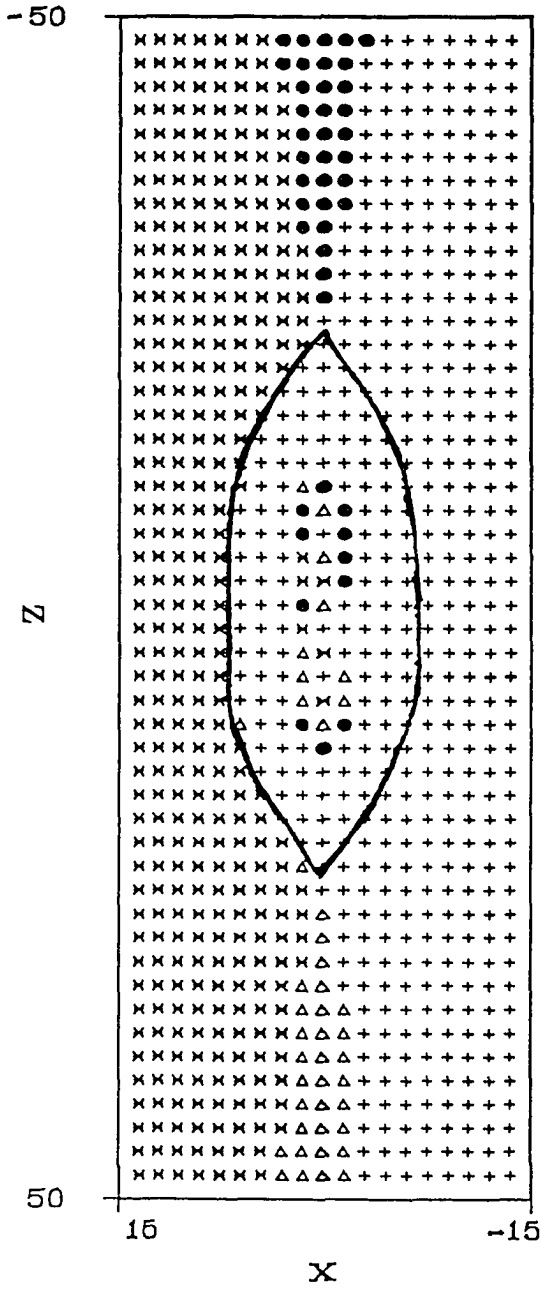

Figure 2.6 Illustration of the magnetic topology in a cross section of the flux rope bounded by thick solid lines for the configuration shown in Figure 2.5. The sign +, *, •, and △ stand for MSP-MSP IMF-IMF, IMF-MSP, MSP-IMF connections.

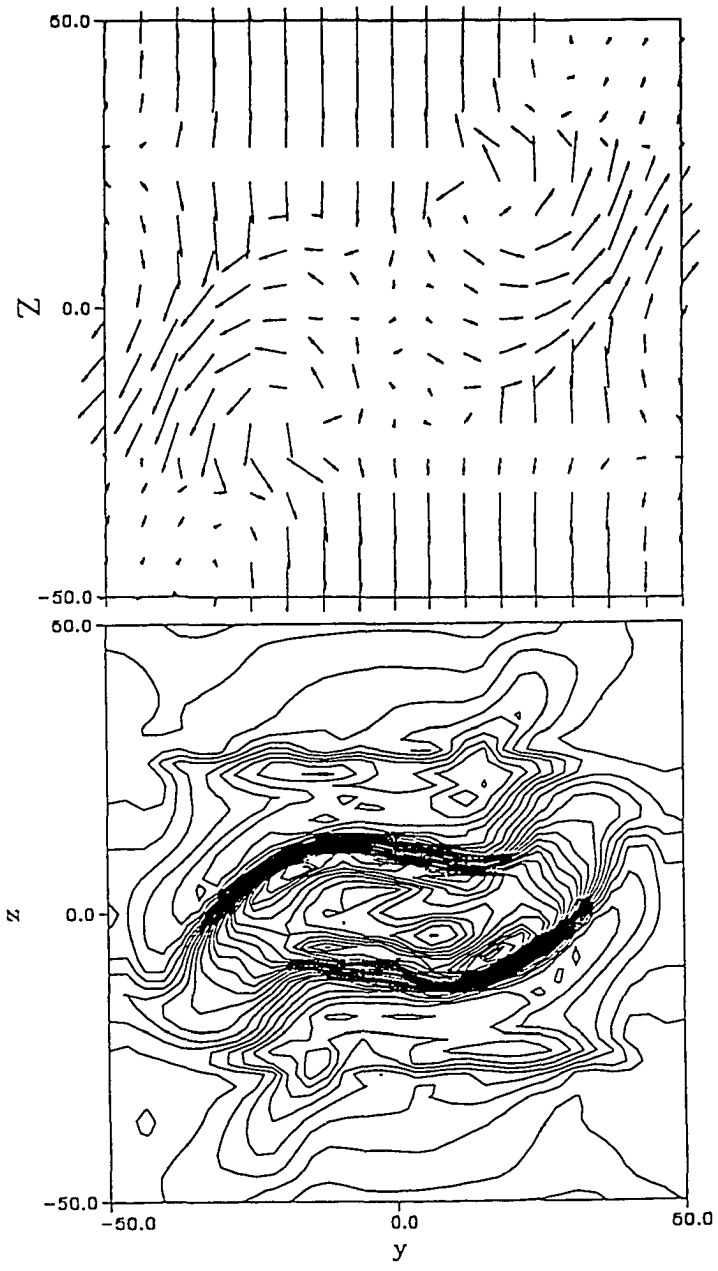

Figure 2.7 (a) The plasma flow pattern in the plane $x = 0$ and (b) the x integrated value of the FACs obtained at $t = 100$.

2.4.2 Other magnetic connections

When the length and the relative shift of the two locally enhanced resistivity regions are appropriately chosen, we can obtain different magnetic connections in the flux ropes. Figure 2.8 shows a perspective view of magnetic field lines for other four runs with (a) an IMF-MSP connection, (b) an IMF-IMF connection, (c) an MSP-IMF connection, and (d) a complex mixed connection. The detailed magnetic topologies of the corresponding cases through the plane $y = 0$ are shown in Figure 2.9. For the so-called smooth end cases (see Figure 2.8a-c and 2.9a-c), the results indicate that a major amount of the magnetic field lines has a well-defined magnetic connection except for only in the small central part of the magnetic flux tube where there are mixed connections. We note that the area of the central part with mixed connections reduces since the well-defined reconnected flux continuously convects into the flux rope and compresses the region of mixing connections with the evolution of the reconnection process. But the complicated structure of the magnetic topology still exists in the center region of the flux tube because the magnetic flux is not removed. For the last run, Figure 2.9d shows that all different connections of magnetic flux are present in the flux rope and mixed together in a random manner when the two X lines have the same length and no relative shift. None of the four magnetic connections is dominant. Generally, the magnetic flux topologies in the three-dimensional cases are much more complicated than that in the two-dimensional cases. In our simulation, it is impossible to identify the separatrices due to the mixture of the different topologies in the flux tube, which demonstrates that the concept of the separatrix and separator or X line can not be applied to three-dimensional cases. For convenience, we still use the term "X line" to refer the reconnection or locally enhanced resistivity region.

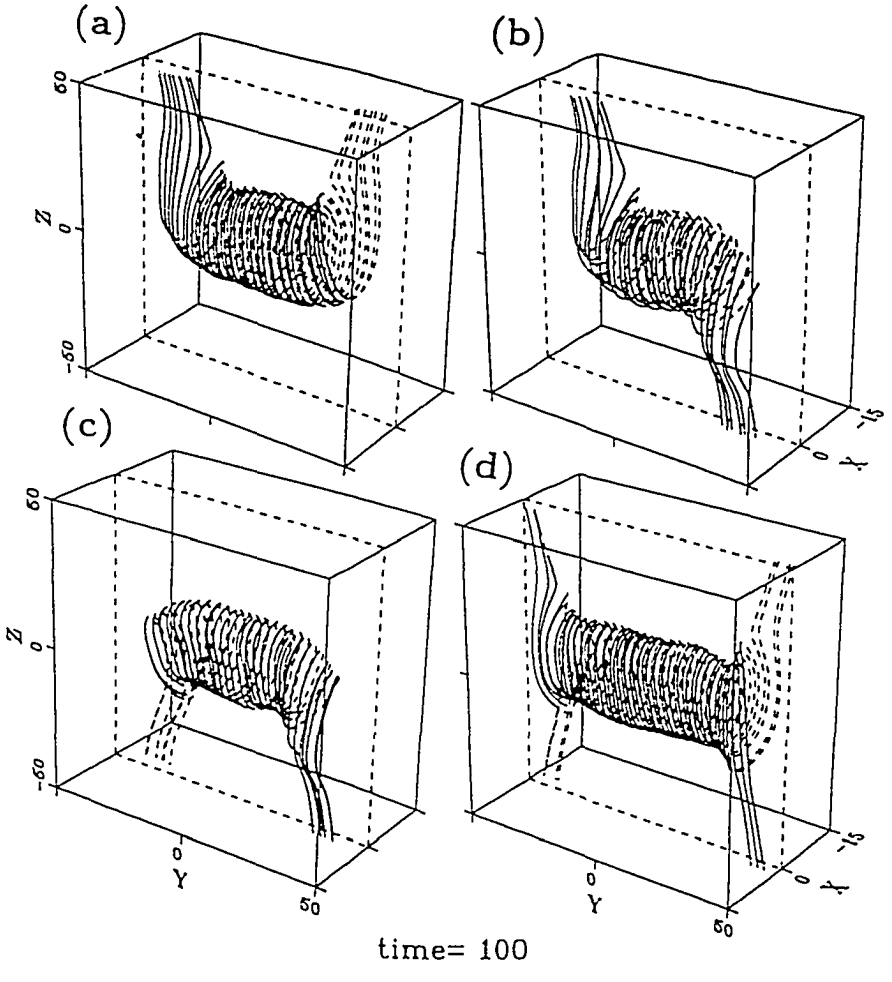

Figure 2.8 Perspective view of magnetic field lines with (a) an IMF-MSP connection, (b) an IMF-IMF connection, (c) an MSP-IMF connection, and (d) a complex mixed connection.

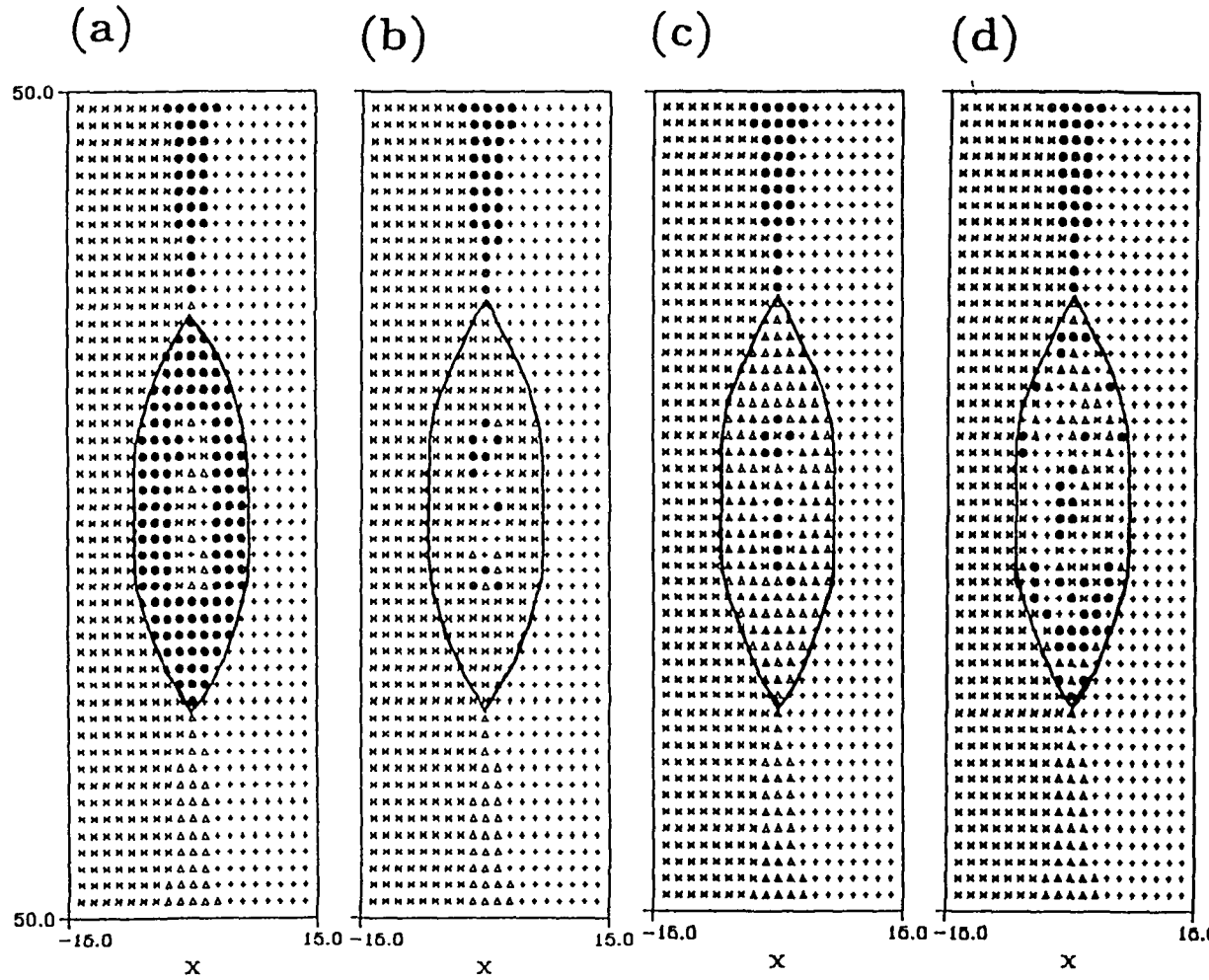

Figure 2.9 The detailed magnetic field topologies in the plane $x = 0$. The boundaries of magnetic flux ropes are indicated by thick solid lines. The sign $+$, $*$, $\bullet$, and $\triangle$ stand for MSP-MSP IMF-IMF, IMF-MSP, MSP-IMF connections.

2.5 Formation of fossil FTEs and the low-Latitude boundary layer

As mentioned in Section 2.1, *Klumpar and Fuselier* [1990] identified a new type of magnetic flux transfer events. Although these events obviously show the magnetic signatures of FTEs as mentioned above, they exhibit different and additional plasma signatures compared to previous observations. All of these magnetospheric FTEs are bordered by magnetospheric plasma and the authors offered three possible explanations for the absence of LLBL plasma at the FTE boundaries. One of these explanations suggests an intermittent disappearance of the LLBL. Another explanation proposes a flux tube which is located adjacent to the magnetopause but of sufficient cross section such that it is partly uncovered by the LLBL. A third interpretation which is favored by the authors assumes flux tubes which may be wholy detached from the magnetopause and consist of closed magnetospheric field lines. The last interpretation is supported by the plasma data which shows the presence of a core region which is bounded by a region with a distribution of hot trapped magnetospheric electrons and cold bidirectionally streaming electrons. In the core region the electron distribution seems to be quite similar to the distribution which is somewhat later seen in the LLBL. Here the term core is used only to indicate a layered and time-centered structure.

Provided that the interpretations of a deep penetration and a closed magnetic flux region for the observations is correct, it seems difficult to understand these properties for FTE formation without a further development of existing FTE models. For a multitude of reconnection patches, *Kan* [1988], *Nishida* [1989], and *Kan and Klumpar* [1993] have illustrated that re-reconnection can lead to flux tubes of closed magnetospheric field lines. However, it was also pointed out that the topological problems might require some further reconnection process. Penetration of a flux tube into the magnetosphere, which

often has a larger magnetic field strength than the magnetosheath, is another problem. It has recently been shown [*Ding et al.*, 1991] that flux ropes formed by multiple *X* line reconnection extend deeper into the region of larger magnetic field strength than a bulge of flux which is formed by single *X* line reconnection [*Scholer*, 1988a; *Southwood et al.*, 1988].

In Section 2.2, we have already illustrated that MXR is able to form flux ropes with a preferable magnetic topology. The result shown in Figure 2.5 illustrates properties of a flux rope with both ends connected to the magnetosphere. Thus this flux rope has the appropriate topological properties. The central region of the flux rope should consist of a mixture of magnetosheath and (previously present) boundary layer plasma and the size is determined by the width of the original boundary layer. If reconnection continues for a sufficiently long time there ought to be a boundary region with a magnetosheath/magnetospheric plasma composition. Because a previously present boundary layer is also composed of magnetosheath and magnetospheric plasma, our model implies that the core has more magnetosheath-like properties while the boundary region distributions ought to show more magnetospheric influence. A schematic sketch of a magnetic flux tube with closed magnetospheric field lines at the dayside magnetopause is shown in Figure 2.10. After reconnection ceases, the closed flux rope which is initially formed at the magnetopause will still be attached to this boundary. The twisted magnetic flux ropes found in the semiglobal simulations of *Ogino et al.* [1989] might be due to a similar process. Note that due to the magnetic connection to the magnetosphere an average force toward the magnetosphere is exerted on the flux rope. Whether or not a full penetration into the magnetosphere due to some interchange motion is possible cannot be answered in the framework of the present computations.

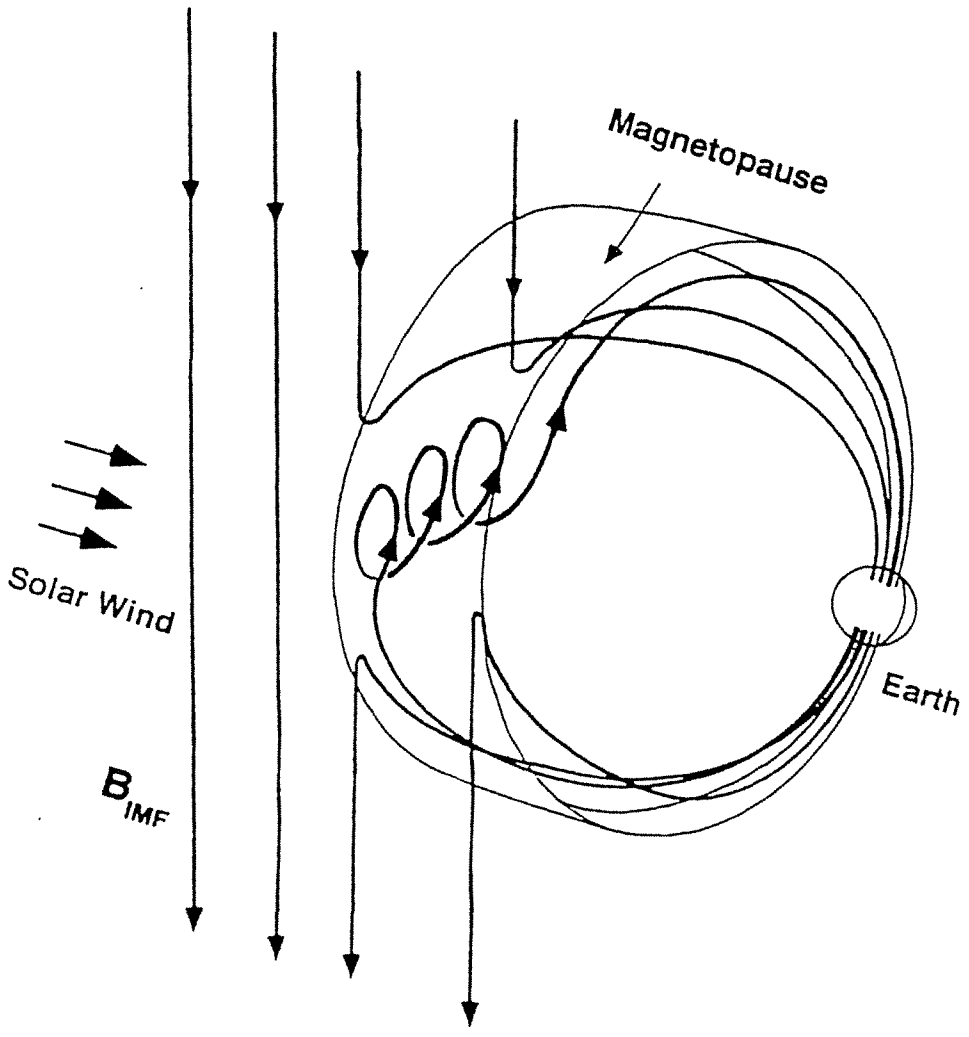

Figure 2.10 Perspective sketch of a flux rope on closed geomagnetic field lines.

2.6 Discussion and conclusion

The purpose of this chapter has been to examine the magnetic field line topology of magnetic flux ropes formed in MXR. Previous work has shown that MXR presents a model for the formation of magnetic flux ropes which often exhibit a relatively complex magnetic topology as shown in Figure 2.1. Here we have studied conditions for which the major amount of magnetic flux in a flux rope of finite extent has a simple magnetic topology, where the four possible connections of magnetic field lines are: IMF to MSP, MSP to IMF, IMF to IMF, and MSP to MSP. The magnetic connection of a flux rope determines whether there is a northward, southward, outward, or inward drag exerted on a flux rope such that the topology has an important impact on the dynamical evolution. The topology and the formation process are also important for the plasma composition, and last but not least, the topology of magnetic flux ropes contributes to the degree of opening of the magnetosphere and therefore has an influence on the global dynamics.

By assuming that the parallel electric field is the same everywhere along the reconnection lines, we reduce the question of a plain topology for the flux rope to a simple geometrical problem. We have illustrated that a sufficient relative shift of two reconnection lines associated with a suitable difference in the length of these lines can lead to the dominance of any of the four possible topological structures. This mechanism has been demonstrated by the results of three-dimensional resistive MHD computations. In order to avoid misunderstandings, we do not claim that every MXR process leads to a simple magnetic topology. In a real system the dynamical evolution will determine whether or not certain conditions apply. However, it should be pointed out that any topological structure that leads to a singular dynamical evolution in the framework of ideal MHD will eventually be removed by an appropriate dissipative process.

With respect to the formation of fossil FTEs, special emphasis has been given to the structures with an MSP-MSP magnetic connection. It has been illustrated that a flux rope with this connection can be expected to extend quite far into the magnetosphere. A sufficiently long reconnection process would also lead to a layered structure of the particle composition. Since boundary layer flux is reconnected first, one would expect a mixture of boundary layer and magnetosheath plasma in the core region. This again would be bounded by a region composed of magnetospheric and magnetosheath plasma. All of these features would fit quite well with the observation of fossil FTEs [*Klumpar and Fuselier*, 1990]. The final fate of these flux structures after the magnetic signatures have decayed will be to contribute to the low- and high-latitude boundary layers.

CHAPTER 3

Enhancements of core magnetic field in different reconnection processes

3.1 Introduction

An enhanced core magnetic field or guide field is often associated with the flux tubes or ropes in the Earth's magnetosphere. At the dayside magnetopause, the magnetic flux tubes associated with FTEs as shown in Figure 1.3 are often observed to have strong core fields [*Russell and Elphic*, 1978; *Paschmann et al.*, 1982; *Berchem and Russell*, 1982]. *Scholer* [1988b] interpreted the enhanced core fields in FTEs by a sweep-up mechanism based on the bursty reconnection model of FTEs [*Scholer*, 1988a, b; *Southwood et al.*, 1988]. In a numerical study, *Otto* [1990] illustrated that the core magnetic field strongly depends on the presence or absence of a corresponding B_y component in the magnetopause current layer. *Berchem and Russell* [1982] have shown that B_y (B_M) is often enhanced in the magnetopause current layer. A mechanism for generating an enhanced value of B_y is two-dimensional (2D) or three-dimensional (3D) stagnation point flow [*Shi*, 1989; *Ma et al.*, 1993]. If the outflow direction is in the y direction or includes the y direction (in the 3D case), it is possible to remove plasma from the stagnation region, but the magnetic flux in the y direction can accumulate over the ambient level.

In the magnetotail, observations show a significant B_y component within plasmoids [*Hones et al.*, 1982; *Sibeck et al.*, 1984; *Richardson and Cowley*, 1985; *Elphic et al.*, 1986; *Nishida et al.*, 1986]. Three-dimensional numerical computations have

investigated the influence of a preexisting B_y component on magnetotail reconnection [*Hesse and Birn*, 1990] and show local enhancements of B_y within 3D plasmoids [*Birn and Hesse*, 1991]. However, these are relatively small compared to the lobe magnetic field. Recent observations [*Moldwin and Hughes*, 1992a, b] confirm earlier results [*Elphic et al.*, 1986] that the value of B_y in magnetotail plasmoids can be comparable to or larger than the local lobe magnetic field strength. The structure of this class of plasmoids can be strikingly similar to the structure associated with flux transfer events at the dayside magnetopause. In particular, ISEE observations [*Elphic et al.*, 1986] of the magnetic field structures have been interpreted as magnetotail flux ropes with enhanced core magnetic fields.

In this chapter, we will discuss mechanisms which may explain the strong enhancements of the magnetic field B_y component which is sometimes found to be significantly larger than the magnetic field strength outside the flux tubes. This study will compare the core magnetic field increases in SXR, MXR, and patchy reconnection in the framework of 2D and 3D magnetohydrodynamic (MHD) simulations. According to these simulation results, we will determine and compare the increase of magnetic field in the center of the developing flux tubes for the various processes and analyze the mechanisms which are associated with the core magnetic field increase. The following section briefly describes the simulation model and parameters. Section 3.3 presents the simulation results for the 2D and 3D cases. We discuss the implications for the dayside magnetopause and the magnetotail and present a summary of our results in section 3.4.

3.2 Simulation model

The intermediate variance magnetic field component (B_y) is often observed to be enhanced in the current layer of the dayside magnetopause and the nightside magnetotail. Throughout this chapter, we refer to this component as the B_y component of the magnetic field and choose the x direction normal to the current layer. In a hodogram representation of the y and z components of the magnetic field, the B_y enhancement leads to a bulge in the rotation of the magnetic field through the current layer as shown in the graph (b) in Fig 3.1. The enhancement of B_y in current sheets can be explained by stagnation flow configurations which lead to a concentration of the parallel magnetic flux components and thus to an increase of the magnetic field B_y component [Ma et al., 1993].

For convenience, we use an angle ϕ which measures the magnetic shear across the current layer (i.e., $\phi = 180°$ corresponds to antiparallel magnetic fields). Thus the magnetic field for the initial configuration is given by

$$B_y(x) = (B_{y0}^2 + \alpha B_{z0}^2 cosh^{-2}(x))^{\frac{1}{2}} \tag{3.1}$$

$$B_z(x) = B_{z0} tanh(x), \tag{3.2}$$

where

$$B_{z0} = \sin(\frac{\phi}{2}),$$

$$B_{y0} = \cos(\frac{\phi}{2}) \tag{3.3}$$

where α is a parameter which determines the variation of B_y across the initial current sheet and $\alpha = 0$ implies that an initial state has a constant y component of the magnetic field across the current layer, while $\alpha = 1$ represents a force-free initial configuration. A sketch of the hodogram for the B_y and B_z components for a trajectory through the

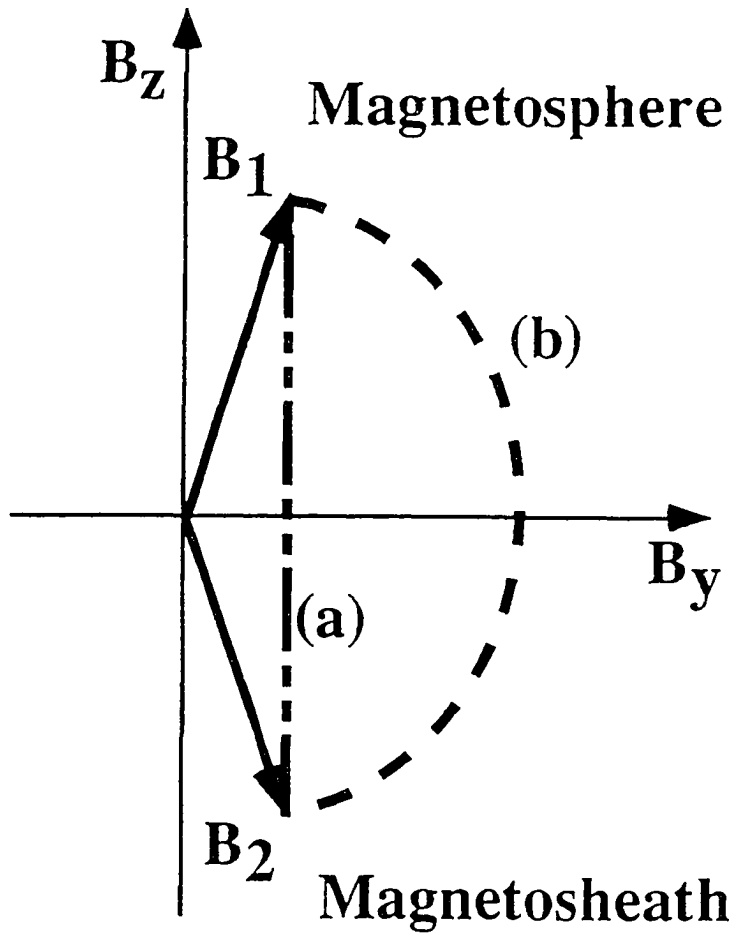

Figure 3.1 Schematic drawing of the initial configuration. Curve (a) is the constant B_y case, and curve (b) is the force-free state.

current layer is presented in Figure 3.1. We will employ both initial conditions for the various reconnection processes. The thermal pressure is chosen such that total pressure is balanced across the current layer:

$$\frac{B^2(x)}{2} + p(x) = const \tag{3.4}$$

and the plasma beta is 1 outside the current sheet. For the simulations we assume a constant density of 1 for simplicity. The initial plasma velocity is assumed to be zero.

The time evolution of the magnetic topology and plasma structures is calculated by solving the 2D and 3D normalized MHD equations as described in Chapter 2.3. For such normalization, typical parameters for the dayside magnetopause are $B_0 = 45$ nT, $n_0 = 10$ cm^{-3}, and $L_0 = 300$ km, which yield $v_0 = 300$ kms^{-1} and $t_0 = 1$ s. For the magnetotail the parameters are $B_0 = 20$ nT, $n_0 = 0.5$ cm^{-3}, and $L_0 = 1$ R_E, which yield $v_0 = 600$ kms^{-1} and $t_0 = 10$ s. The normalized equations are solved simultaneously using a two-step Lax-Wendroff finite differencing scheme with a third-order artificial diffusion term [*Lapidius*, 1967]. At the boundaries, $x = \pm X_L$ and $z = L_z$ for the 2D cases, and $x = \pm X_L$, $y = \pm L_y$, and $z = L_z$ for the 3D cases; the normal derivatives of all physical quantities are assumed to be zero. The mirror symmetric and line symmetric boundary conditions are imposed in the $z = 0$ plane for the 2D and the 3D simulations, respectively.

In order to simulate the various reconnection processes, a localized resistivity of the form is chosen to be the same as Equation (2.9). We remark that the small background resistivity used in the simulation gives rise to a slow diffusion process which tends to reduce the maximum of the B_y value in the current sheet. For the simulation timescales this reduction is about 7 % for the equilibrium current sheet and is approximately the same for all force-free cases.

3.3 Simulation results

In this chapter, we present 12 simulation cases to examine 2D single X line and multiple X line reconnection and the 3D generalization of these processes. Typical parameters of the simulation cases and the characteristic results are listed in Tables 3.1a and 3.1b. Since the concentration of B_y in the formed flux tubes is expected to depend on the initial B_y profile in the current sheet, we consider both a force-free initial state and an initial equilibrium with a constant value of B_y as illustrated in Figure 3.1. For all simulations the magnetic shear (i.e., the angle between the magnetic fields on either side of the current sheet) is chosen to be 150°, which gives a value of $B_y = 0.26B_0$ for the constant B_y cases.

3.3.1 Two-dimensional MXR and SXR processes

The parameters used in the 2D simulations of MXR and SXR processes are $N_x = 51$, $X_L = 15$, $N_z = 51$, and $L_z = 50$ for MXR in cases 1 and 7, while $N_z = 81$ and $L_z = 120$ for SXR in cases 2 and 8. To reduce the numerical error and save computer time, a nonuniform grid is employed, which provides a resolution of 0.05 in the x direction and 0.5 in the z direction near the reconnection region. The localized enhanced resistivity η_a in the simulation of the 2D reconnection processes is given by

$$\eta_a(x,z) = \eta_1 exp\{-(z-z_0)^2\} exp\{-(x-x_0)^2\} \tag{3.5}$$

where $\eta_1 = 0.05$. The resulting resistivity is enhanced in the vicinity of $(x_0, z_0) = (0, 25)$ for MXR and $(x_0, z_0) = (0, 0)$ for SXR. Note that the symmetry condition at $z = 0$ implies that for MXR a second resistive region exists at $z = -z_0$. We have

Table 3.1 Physical parameters and results for 12 simulation cases.

Table 3.1a. Initial B_y Profile: Force Free

Case	Type	$\frac{X_L}{a}$	$\frac{B_{ymax}}{B_0}$
1	MXR (2D)	infinite	1.3
2	SXR (2D)	infinite	1.1
3	MXR (3D)	20	2.7[a]
4	patchy (3D)	20	1.3
5	MXR (3D)	10	2.2[a]
6	patchy (3D)	10	1.3

Table 3.1b. Cases with an Initial Constant B_y: $B_{y0} = 0.26B_0$

Case	Type	$\frac{X_L}{a}$	$\frac{B_{ymax}}{B_0}$	$\frac{B_{ymax}}{B_{y0}}$
7	MXR (2D)	infinite	0.60	2.3
8	SXR (2D)	infinite	0.41	1.6
9	MXR (3D)	20	1.7[a]	6.5
10	patchy (3D)	20	0.89	3.4
11	MXR (3D)	10	1.4[a]	5.4
12	patchy (3D)	10	0.87	3.3

MXR, multiple X line reconnection; SXR, single X line reconnection; 2D, two-dimensional; 3D, three-dimensional.

[a]Maximum B_y value do not reach a saturated level during the simulation time from $t = 0$ to $t = 350$. Maximum B_y values are chosen as those at $t = 240$

chosen this value of the X line separation mainly because it yields a flux rope diameter of about 2 R_E, parallel to the current layer for the magnetopause applications in agreement with FTE observations. The background resistivity is chosen as $\eta_b = 0.001$, which corresponds to a magnetic Reynolds number of $R_m = 1000$. In the simulations we switch on the resistivity at time $t = 0$.

Case 1.

For the MXR case with an initial force-free magnetic field configuration, the appearance of the two resistive regions leads to the onset of magnetic reconnection in these regions and to the formation of a magnetic island which is centered at $z = 0$. Figure 3.2 shows the magnetic field lines, the B_y contour lines, and the plasma flow pattern in the x-z plane at $t = 150$. The magnetic island has grown to a large size as a result of continuous magnetic reconnections. In the initial force-free field as shown in Figure 3.1, B_y has a maximum value of 1 at the center of the current sheet ($x = 0$). Figure 3.2 shows that the initial large B_y in the current sheet is now either concentrated in the magnetic island or carried out of the simulation box at $z = \pm 50$. The B_y value in the magnetic island is larger than in the surrounding region. The initial large B_y flux in the current sheet is entirely removed from the reconnection regions. Note also that the enhanced plasma flow from the two X lines leads to a stagnation flow in the center of the magnetic island which expands in the x direction. We found that the maximum B_y value in the magnetic island at $t = 150$ is about 1.2, which is slightly larger than the initial peak value of 1, while B_y is reduced to 0.25 near the X line (at $z \sim 25$). This result illustrates that 2D magnetic reconnection does not lead to a significant enhancement of B_y. The major effect of the process seems to be a redistribution of the initial B_y flux.

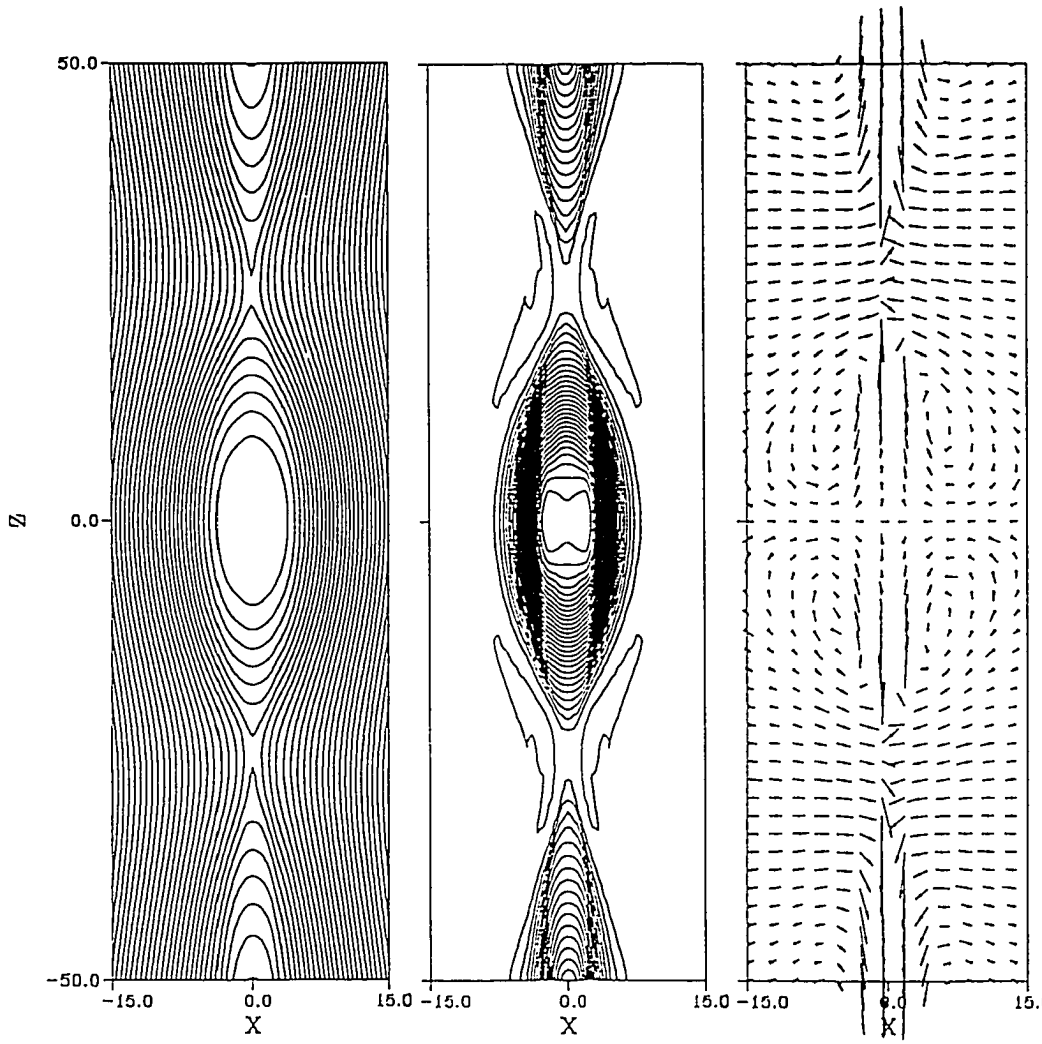

Figure 3.2 Contours of magnetic field lines (left), contours of the B_y component (middle), and the plasma flow pattern (right) for the two-dimensional multiple X line reconnection (MXR) simulation with initial force-free configuration (case 1) at $t = 150$.

Case 2.

For the SXR process, the reconnection takes place at $(x, z) = (0, 0)$, which leads to the formation of a bulge-shaped magnetic structure. Figure 3.3 shows the magnetic field lines, the B_y distribution, and plasma flow pattern in the x-z plane at $t = 180$ for case 2. Figure 3.3 shows that the B_y flux is removed from the neutral line located at $(x, z) = (0, 0)$ and pumped into the bulge-shaped magnetic field region. We see again that the major effect of the reconnection process is a redistribution of B_y. The maximum value of B_y in the enhanced region is ~ 1.08, which is close to the initial peak value of B_y in the current sheet. However, at the reconnection site (X line), B_y reduces to 0.25 from the initial $B_y = 1.0$ at the same position. The concentration of B_y also contributes to the increase of the total pressure at the center of the bulge region. The gradient of the total pressure accelerates the plasma at the leading edge ($z \approx 35$) of the magnetic bulge. This process may prevent further accumulation of B_y.

For all processes under consideration the maximum value of B_y is a function of time. We have therefore monitored the value of the maximum of B_y as a function of time as shown Figure 3.4a, in which the solid and dashed lines represent the MXR processes and the SXR process, respectively. We find for the SXR process that the evolution of B_y saturates at $t = 120$. At the early stage, the time evolution of B_y is the same for the MXR and SXR cases. For the MXR case, accumulated magnetic flux from each reconnection region collides with each other near the center of the magnetic island at about $t = 80$ and the magnetic flux B_y quickly increases afterward.

Figure 3.4b shows the maximum value of B_y as a function of time for cases 7 and 8, in which B_y has a constant initial profile. Without illustration we remark that the magnetic field and the plasma flow are similar to the corresponding force-free cases. Both the value of B_y and the thermal pressure are enhanced in the magnetic island.

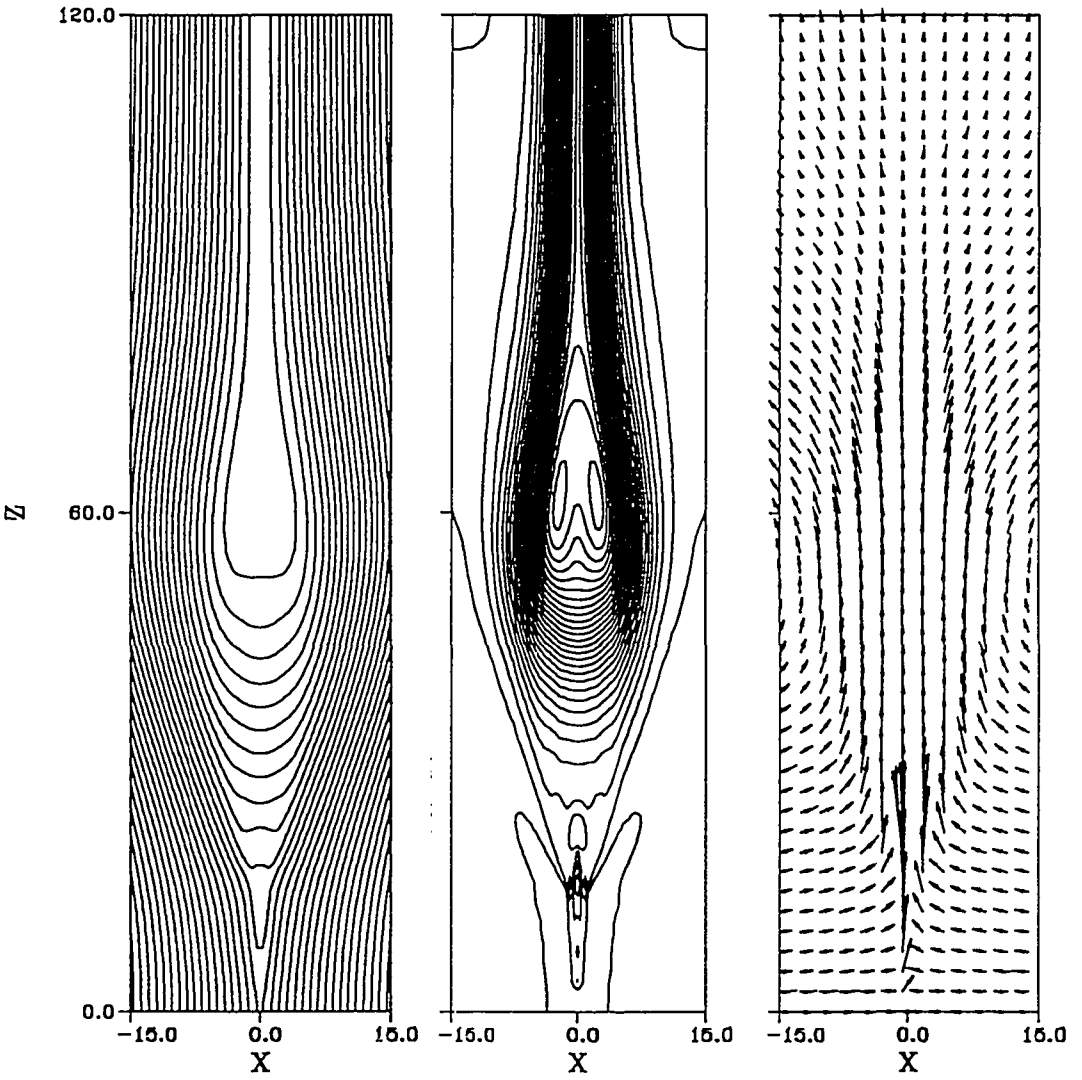

Figure 3.3 Contours of magnetic field lines (left), contours of the B_y component (middle), and the plasma flow pattern (right) for 2D single X line reconnection (SXR) simulation with initial force-free configuration (case 2) at $t = 180$.

The initial value of B_y is 0.26 and the maximum values at the final stage are 0.60 for MXR (Case 7) and 0.41 for SXR (Case 8). The amplifications of B_y for the MXR and SXR processes are respectively 2.3 and 1.6. However, the final B_y value is still small compared to the ambient field strength.

3.3.2 Three-dimensional MXR and patchy reconnection processes

For the 3D processes we use the same locations of the resistive regions as in the 2D cases in the x, z plane. We limit, however, the extent of these regions in the y direction. In particular, η_a is given by

$$\eta_a(x,y,z) = f(y)exp\{-(z-z_0)^2\}exp\{-(x-x_0)^2\}, \tag{3.6}$$

where

$$f(y) = \begin{cases} \eta_1, & \text{if } |y| \leq X_L; \\ \eta_1 exp\{-(|y|-X_L)^2\}, & \text{otherwise.} \end{cases} \tag{3.7}$$

The localized enhanced resistivity η_1 is chosen to be 0.05 in the simulation. The magnetic reconnection is triggered at $(x_0, z_0) = (0, 25)$ for MXR and $(x_0, z_0) = (0, 0)$ for patchy reconnection. The parameter X_L is the half-length of the X line and is chosen to be 20 and 10. The background resistivity $\eta_b = 0.001$ corresponds to $R_m = 1000$. Note that the larger enhanced resistivity is used to save computer time. Other parameters used in the 3D simulations of MXR and patchy reconnection processes are $N_x = 51, X_L = 15, N_y = 65, L_y = 40$, $N_z = 51$, and $L_z = 50$ for MXR, while $N_z = 81$ and $L_z = 120$ for patchy reconnection. The highest resolution near a reconnection region is the same as the 2D simulation in the x and z direction. In the y direction we have chosen a uniform grid mesh. The initial configuration is the same as the one chosen for the 2D simulations. The resistivity is again switched on at the time $t = 0$.

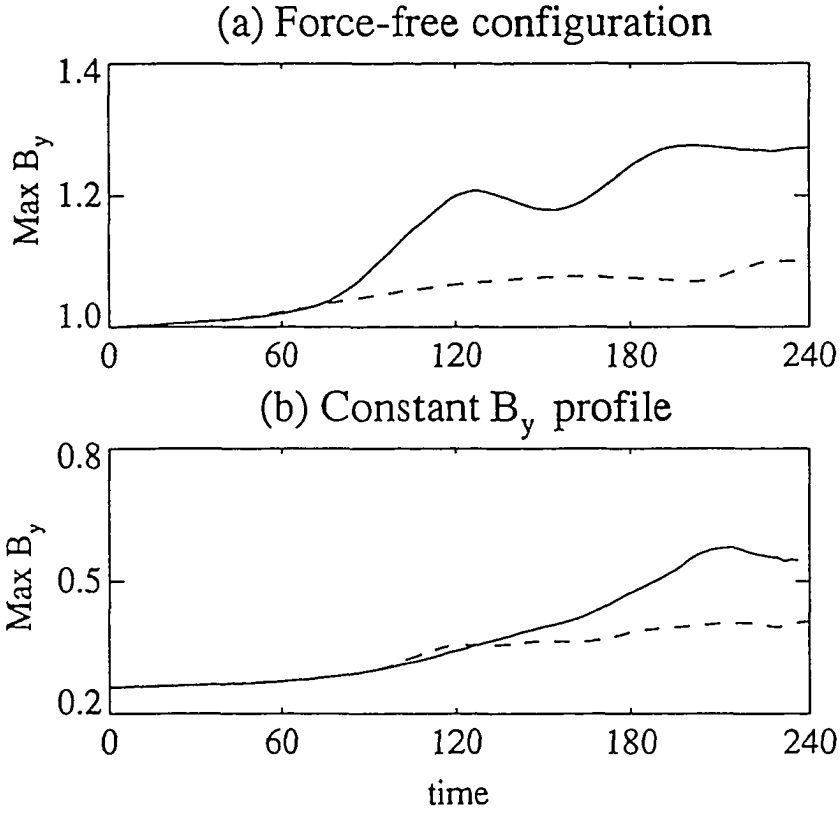

Figure 3.4 The maximum value of B_y as a function of time obtained in different reconnection processes. Solid and dashed lines represent results from 2D MXR and SXR simulations, respectively, for (a) the initial force-free configuration (cases 1 and 2) and (b) the initial constant B_y profile (cases 7 and 8).

Case 3.

For the MXR case, onset of magnetic reconnection along the resistive regions leads to the formation of a flux rope which is centered along the y axis. Figure 3.5 shows the magnetic field lines and the plasma flow pattern in the symmetry plane $y = 0$ at $t = 210$. The magnetic field plot indicates that the flux rope has grown to a similar size as shown for the 2D case in Figure 3.2. In the x-z plane, plasma flow patterns for 2D and 3D cases are different. It is seen from Figure 3.5 that the 3D case does not show the stagnation flow pattern around the origin of the system. The cause for this difference is the plasma transport along the y direction in the 3D case. Magnetic reconnection generates helical flux which compresses the interior of the magnetic flux rope through the magnetic tension force. This compression leads to an outward force along the flux rope axis. Figure 3.6 shows that the total force ($\mathbf{F}$) is equal to the thermal pressure gradient force ($\mathbf{F}_p$) along the flux rope axis. It is not surprising that the magnetic force ($\mathbf{J} \times \mathbf{B}$) vanishes at the flux rope axis, because the symmetric condition applied leads to the alignment of the magnetic field with the electric field current. Figure 3.6 shows that there is a significant pressure gradient force which accelerates the plasma out of the flux rope.

The corresponding plasma flow is illustrated in Figure 3.7a, which shows the ejection of plasma out of the flux rope. The two thick solid lines indicate the two X lines. The flux rope is located between the two X lines. This tube-aligned flow balances the inflow from the reconnection regions. *Fu et al.* [1990] also detected this type of tube-aligned flow in their 3D incompressible MHD simulation. Since this plasma flow cannot carry B_y flux out of the flux rope region, the B_y flux accumulates to a much higher value than in the corresponding 2D cases. This concentration of magnetic flux in the y direction is clearly seen in Figure 3.7b. The initial value or the maximum B_y is 1

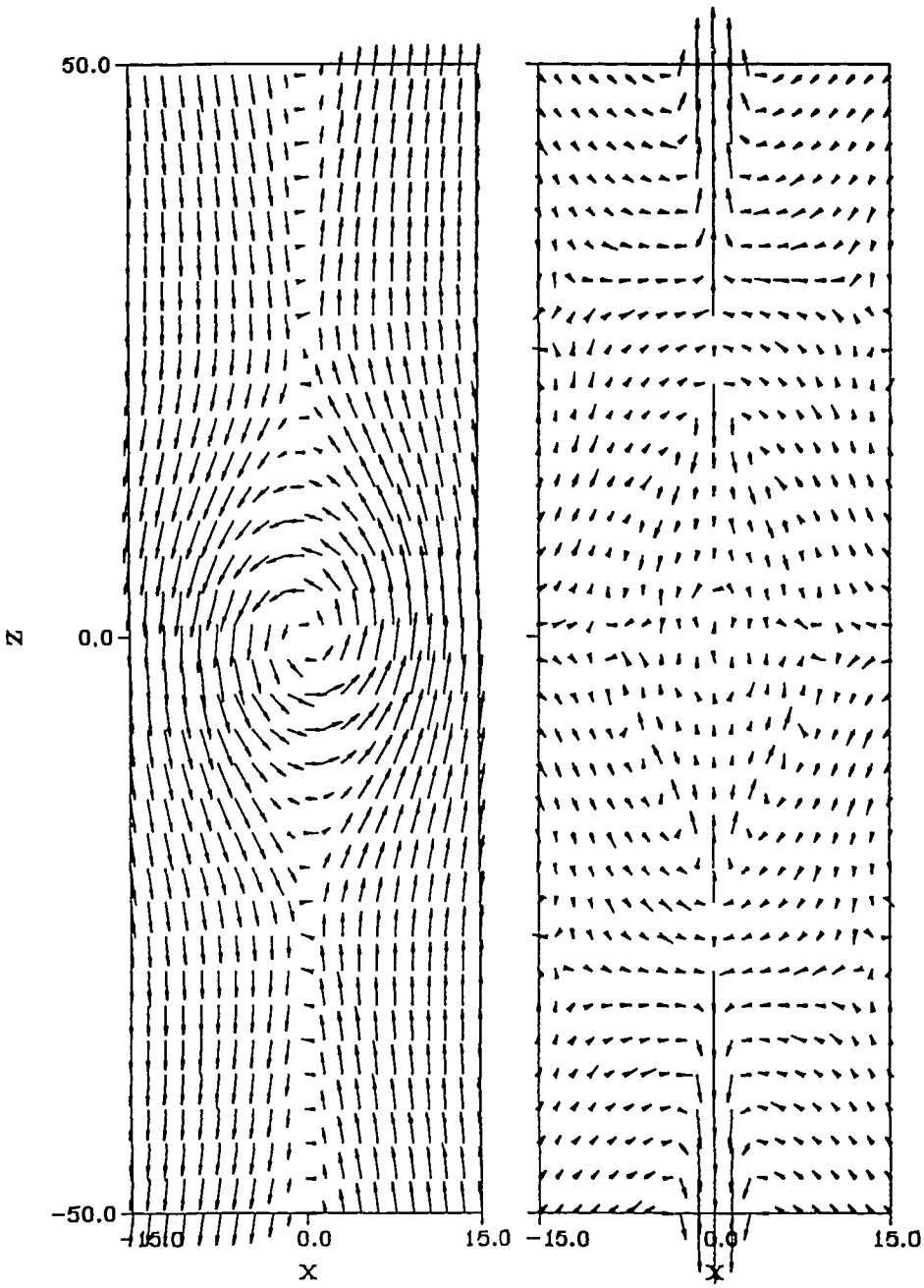

Figure 3.5 The magnetic field (left) and plasma flow pattern (right) in the $y = 0$ plane at $t = 210$ for case 3, which corresponds to 3D MXR with $X_L = 20$.

and the maximum at this instant of time is about 2.6, which is a significant increase of the magnetic field strength over the ambient field of 1.

Figure 3.8 provides a schematic sketch of the 3D MXR reconnection process, in which the presence of helical fields leads to the radially inward pinch of the rope as well as the enhancement of B_y and plasma pressure in the flux rope. The enhanced plasma pressure leads to the outward tube-aligned flow, which results in a further enhancement of B_y.

Case 4.

Figure 3.9 shows the magnetic field, the plasma flow, and the contour lines of B_y in the plane $y = 0$ at $t = 210$ for case 4 with localized reconnection. It is illustrated that the magnetic flux B_y is removed from the reconnection region around the y axis and is convected to the bulge-shaped magnetic field region. The accumulated magnetic flux is carried with the core region by the plasma flow in the z direction similar to the 2D case in Figure 3.3. However, the 3D effect becomes important; the maximum value of B_y in this case is 1.3. This maximum B_y value ($\sim$ 1.3) is above the ambient field but is considerably less than the maximum B_y value ($\sim$ 2.6) for the 3D MXR case. We also observe that the maximum value of B_y saturates during the evolution of the reconnection process.

For 3D cases with a constant initial B_y profile (cases 9, 10, 11, and 12) the maximum B_y values as shown in Table 3.1b are significantly larger than those for the corresponding 2D cases (cases 7 and 8). In particular, the maximum core magnetic field for MXR (cases 9 and 11) exceeds the surrounding magnetic field strength. Although the amplifications are large, the absolute B_y values are smaller for cases with the constant initial B_y than for cases with force-free fields shown in Tables 3.1a and 3.1b. Note that

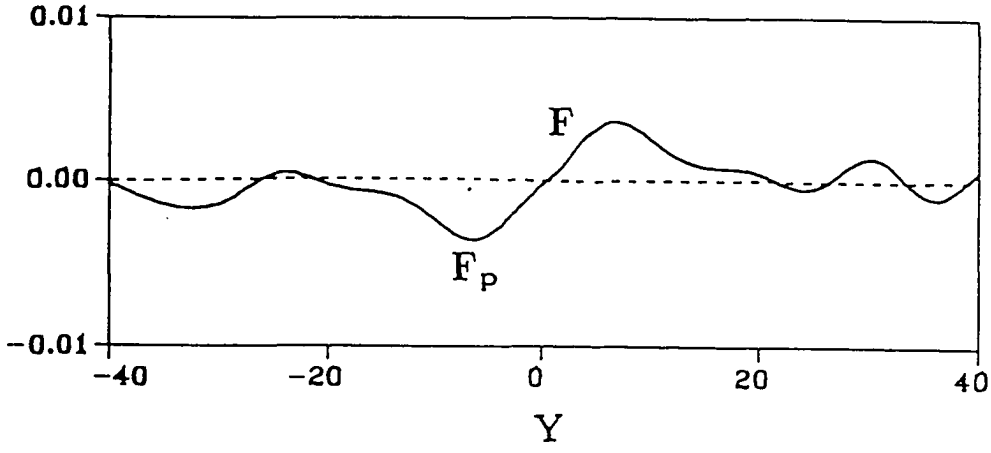

Figure 3.6 The total force ($\mathbf{F}$) and the thermal pressure gradient force ($\mathbf{F_p}$) along the flux rope axis at $t = 210$ for case 3.

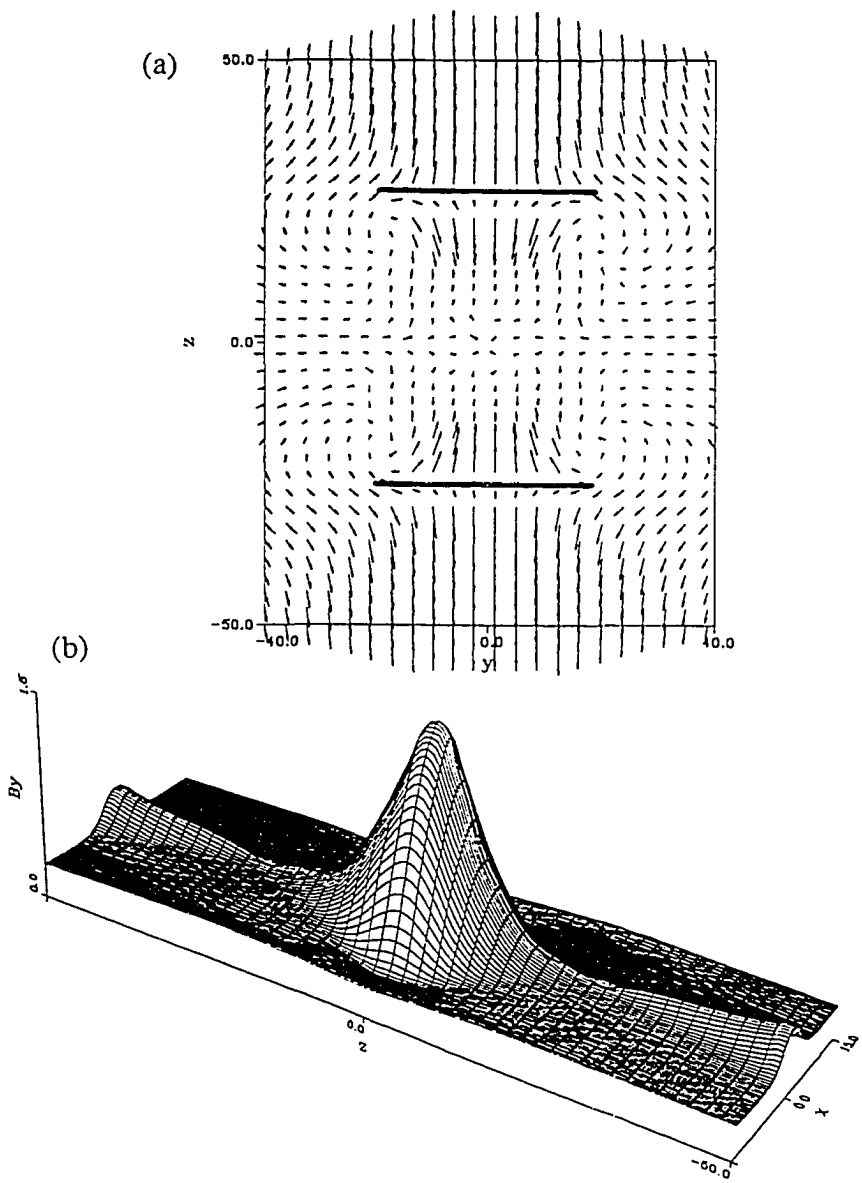

Figure 3.7 (a) The plasma flow pattern in the $x = 0$ plane and (b) the distribution of the B_y component in the $y = 0$ plane at $t = 210$ for case 3.

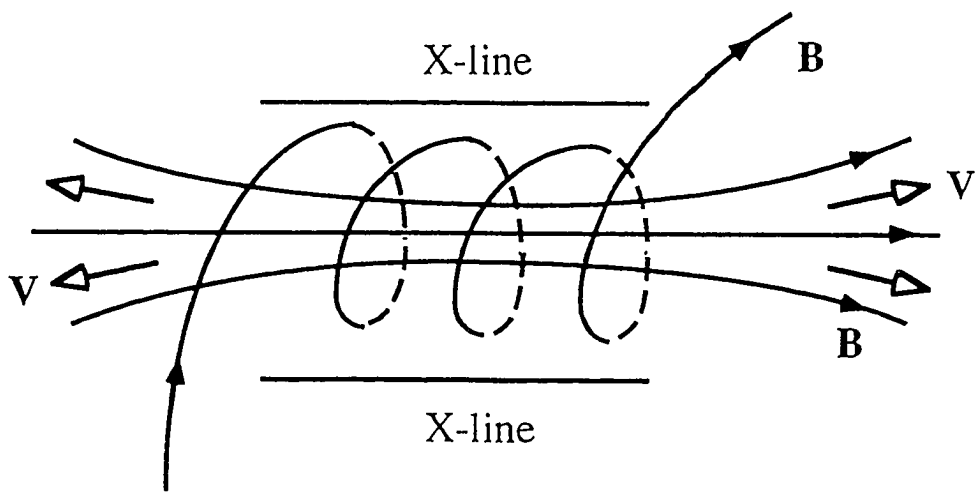

Figure 3.8 Schematic illustration of the core magnetic field and the tube-aligned flow in the magnetic flux tube. The magnetic tension force associated with the helical fields leads to the radially inward pinch of the rope as well as the enhancement of B_y and plasma pressure in the flux rope. The enhanced plasma pressure results in the outward tube-aligned flow.

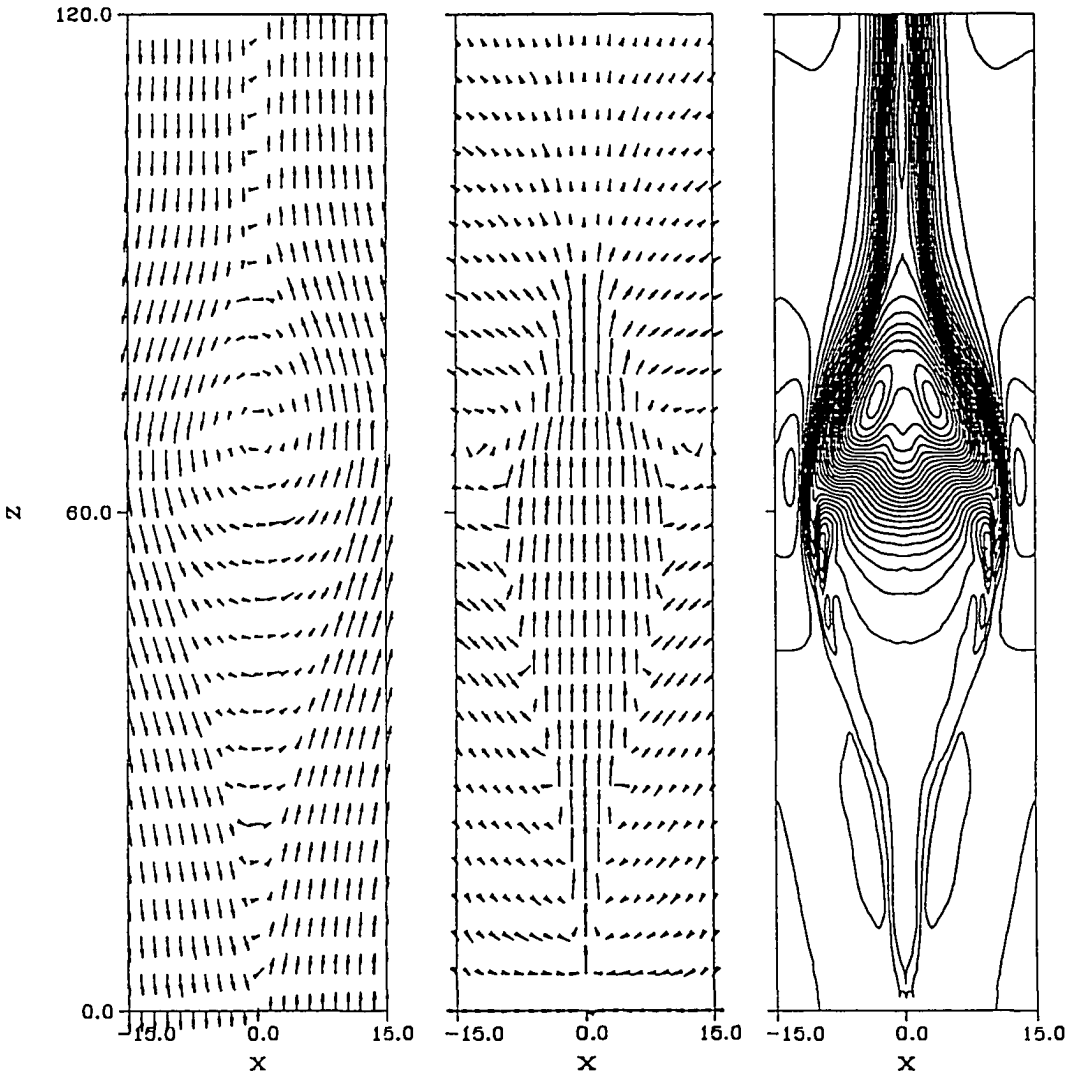

Figure 3.9 The magnetic field (left), plasma flow pattern (middle), and contours of B_y (right) in the $y = 0$ plane at $t = 210$ for case 4, which corresponds to the 3D patchy reconnection with $X_L = 20$.

the maximum B_y values for all cases in Tables 1a and 1b are chosen as those obtained at $t = 240$.

The maximum B_y values for the MXR cases with $X_L = 10$ are smaller than those with $X_L = 20$ as shown in Tables 1a and 1b. However, for very long line the 3D cases should approach the 2D result, which shows a smaller B_y amplification. In order to investigate the influence of the X line length on the evolution of the maximum B_y value, we simulate additional cases with different X line lengths ($X_L = 30, 40$, and 50). Figure 3.10 shows the maximum core field B_{ymax}, obtained at $t = 200$, as a function of the X line length. The peak value of B_{ymax} is located near $X_L = 30$. The value of B_{ymax} obtained in the 2D simulation (case 1) is also shown in Figure 3.10. Figure 3.11a shows the time evolution of the maximum B_y value for MXR with $X_L = 10, 30$, and 50 and the 2D case. The evolution for patchy reconnection with $X_L = 20$ (case 4) and 10 (case 6) is shown in Figure 3.11b. The saturated state is not observed up to $t = 350$ in the 3D MXR cases. The evolution of the maximum B_y component is weakly dependent on the X line length for patchy reconnection shown in Figure 3.11b.

3.4 Summary and discussion

The purpose of this chapter is to investigate the influence of various magnetic reconnection processes on the evolution of the core magnetic fields in magnetic flux ropes. We have compared the increase of the magnetic field in the flux tubes for 2D SXR and MXR processes and for the 3D generalization of these processes. For the presented simulations, a large increase in the magnetic field in the core of the flux tubes is mainly caused by the increase in the y component of the magnetic field B_y. For the application to the dayside magnetopause, this component corresponds approximately to

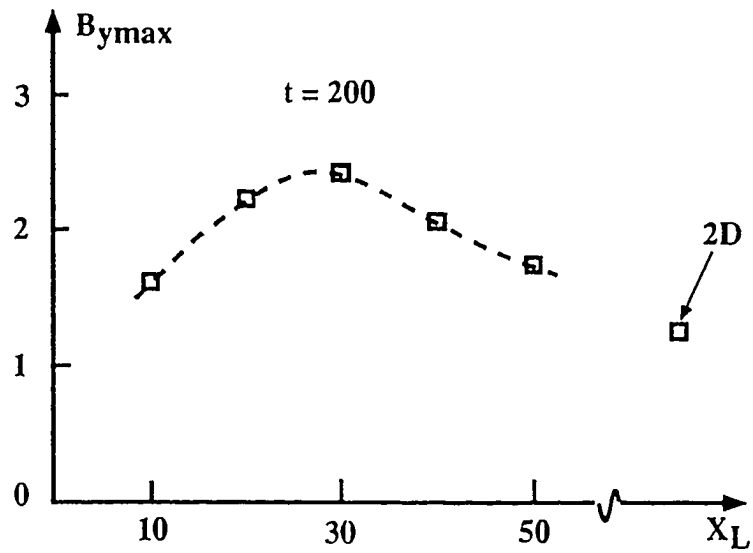

Figure 3.10 The maximum value of the B_y component obtained at $t = 200$ as a function of X line length X_L.

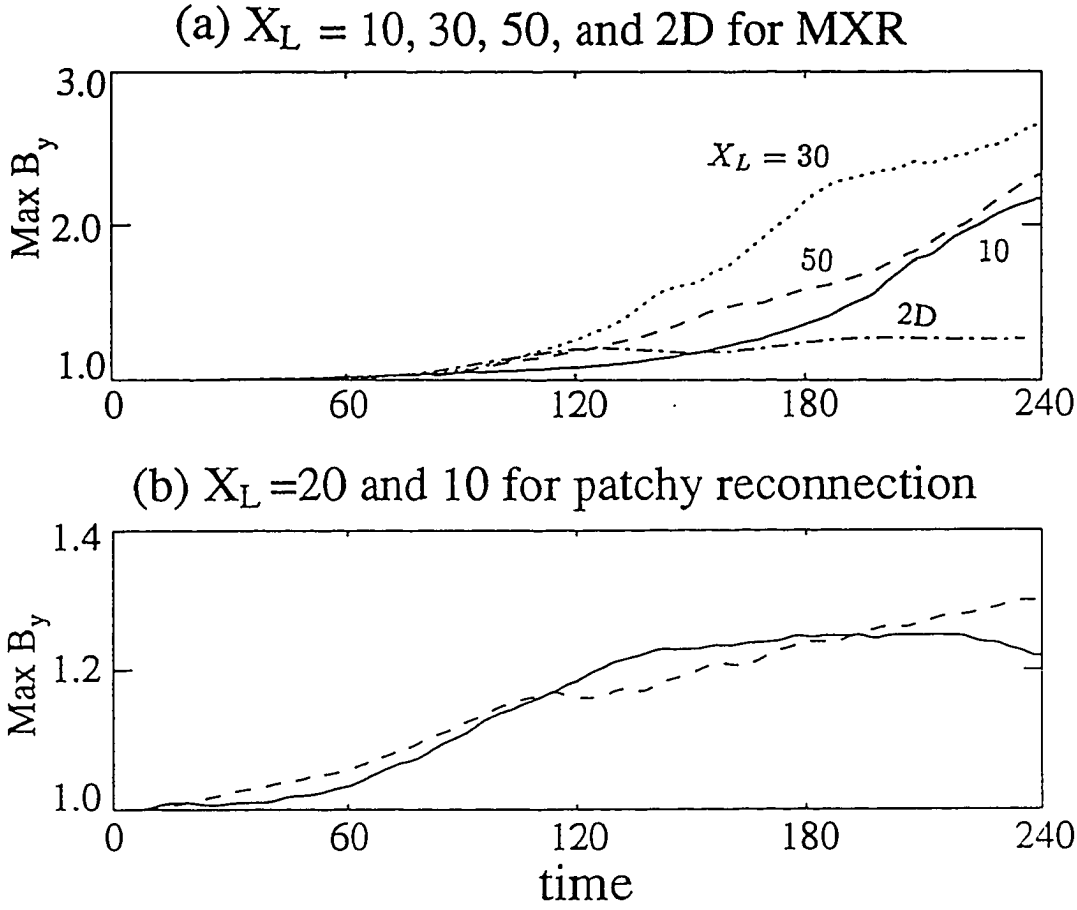

Figure 3.11 The maximum value of the B_y component as a function of time for (a) MXR with $X_L = 10$, 30, and 50 and the 2D case and (b) patchy reconnection with $X_L = 10$ and 20.

the M component in the boundary normal coordinates. Tables 1a and 1b summarize the amplification of the core magnetic field for different initial states and different reconnection processes. Our results can be summarized as follows: (1) The 3D MXR leads to a larger increase of the magnetic field for each set of initial states than the other reconnection processes. (2) The 3D processes always lead to a larger amplification than the corresponding 2D processes. A significant amplification of the core field above the ambient field is only found for the 3D processes. (3) For the same reconnection process the field amplification is larger for the constant initial B_y configuration than for the force-free initial state. However, the final core field in the constant initial B_y case is smaller than that in the force-free initial case. (4) A small core field is only found for cases where the preexisting B_y in the current sheet is significantly less than the field strength outside the current sheet. Two-dimensional reconnection with a single extended X line is favorable for a small core field in FTEs.

We interpret these results as follows: (1) For all cases the reconnection process leads to a redistribution of the magnetic flux in the y direction which is removed from the reconnection regions and accumulated in the reconnected flux tubes. This effect is clearly seen in Figures 3.2 and 3.3. (2) The MXR process leads to a larger magnetic tension than the corresponding patchy or single X line reconnection. The stronger compression of the flux tubes increases the core magnetic fields. (3) Obviously, 3D effects lead to a more substantial amplification of the magnetic field than the corresponding 2D processes. In the 3D cases the force imbalance in the y direction accelerates plasma out of the flux tube. This process reduces the amount of plasma and thermal pressure and allows a further compression of the flux rope. Since the axial transport does not apply to the magnetic flux in the y direction, this flux is accumulated in the core of the flux rope, leading to a significant amplification of the core magnetic field, as illustrated

in Figure 3.8. (4) Enhancement is larger for constant initial B_y configurations than for force-free initial states mainly because B_y is initially smaller in the constant initial B_y cases. However, the absolute value of the final magnetic field remains much smaller for the constant initial B_y.

Some caution should be applied to the numerical values of the magnetic field enhancement. These values are, in general, a function of time and location, and they depend on the particular properties of the system. Here, we emphasize the different behavior of different reconnection processes for two fixed sets of initial conditions. Thus we identify important aspects for the core field enhancement in magnetic flux ropes. For this study we have not explored factors which can be of importance for a particular configuration like a 2D or 3D magnetotail-like equilibrium or asymmetry across the current layer. Instead, we tried to concentrate on the major effects for various reconnection processes. The characteristic differences between the various processes should apply to any current sheet configuration.

Recently, *Lee et al.* [1993] found that different magnetic topologies (i.e., open, closed, and mixed flux ropes) can be formed depending on the position and size of the reconnection regions. Our results shown in this paper do not strongly depend on a particular magnetic flux topology.

The results of our simulations can explain the strong core magnetic field which has been observed [*Paschmann et at.*, 1982; *Berchem and Russell*, 1982] in FTE's at the dayside magnetopause. *Scholer* [1988b] suggested a mechanism to explain the origin of a strong core field, based on bursty reconnection [*Southwood et al.*, 1988; *Scholer*, 1988a]. This mechanism is based on a redistribution and an accumulation of the B_y flux in the vicinity of the tube axis. We have illustrated that this mechanism is indeed operating in both 2D and 3D cases. However, the limited compressibility of plasma

does not lead to a significant amplification of the magnetic field in 2D cases. For the concentration of the magnetic field in a flux tube above the level of the ambient magnetic field, we have shown that the 3D effects and, in particular, the acceleration of plasma along the y direction seem to be of major importance. As has been pointed out by *Otto* [1990], a small magnetic field in flux ropes [e.g., *Rijnbeek et al.*, 1984] is probably due to a small magnetic field in the current sheet at the onset of reconnection. In addition, a small field is indicative of largely 2D processes or single reconnection regions.

Our results can also be applied to the concentration of flux in magnetic flux ropes in the magnetotail. *Hughes and Sibeck* [1987] suggested that the presence of the B_y component in plasmoids may be due to the penetration of the IMF B_y component. To test this hypothesis, they compared the observed B_y within plasmoids with simultaneous upstream IMF B_y and concluded that the IMF B_y penetrates into plasmoids. It is also found that B_y has a maximum value inside plasmoids [*Elphic et al.*, 1986]. The enhancement of the B_y component in flux ropes may be a two-step process. *Ma et al.* [1993] have suggested a mechanism which is based on 3D stagnation flow which can accumulate and concentrate B_y flux in magnetospheric current sheets. The results of the present paper suggest this preexisting flux can be concentrated further by the onset of 3D magnetic reconnection. We remark that the suggested two-step mechanism conserves the sign of B_y, which seems to be a typical property for magnetospheric current sheets and magnetic flux ropes. The observed large core magnetic fields [*Elphic et al.*, 1986; *Moldwin and Hughes*, 1992a, b] with field amplitudes significantly above the lobe magnetic field are highly indicative of reconnection at several magnetic X lines.

CHAPTER 4

Generation of field-aligned currents and Alfven waves by magnetic reconnection

4.1 Introduction

Field-aligned currents were first proposed by Birkeland [1908] to explain the properties of the polar geomagnetic storms, e.g., the disturbance of the geomagnetic field and auroral phenomenon in the auroral zone. Later, Chapman [1927] developed a new current system to interpret the overall geomagnetic behavior. In Chapman's model, there is no place for field-aligned currents. In the following several decades, the Chapman's current system became dominant although Alfven [1939] argued that field-aligned currents are required to drive most of the ionospheric currents. After satellite Explorer 12 observed the transverse magnetic disturbances in the auroral zone [Zmuda et al., 1966, 1967], the importance of the field-aligned currents to magnetospheric physics became apparent. Now it is widely accepted that field-aligned currents play an important role in the coupling between the magnetosphere and ionosphere.

Zmuda and Armstrong [1974] used the TRIAD satellite magnetometer data to determine for the first time the flow directions of field-aligned currents at all magnetic local times in the northern auroral region. The spatial distribution and magnitudes of the field-aligned currents in this region was carried out by Iijima and Potemra [1976a] using the same TRIAD satellite magnetometer data. They found that field-aligned currents [see Figure 4.1] are concentrated in the so-called auroral oval which encircles the geomagnetic pole. The region 1 field-aligned current is located near the poleward

part of the field-aligned current region while the region 2 field-aligned current is near the equatorward part of the field-aligned current region. The flow directions of the region 1 and 2 field-aligned currents are opposite as shown in Figure 4.1.

Iijima and Potemra [1976b] further examined the data in the dayside high-latitude region. The satellites often observed an additional pair of field-aligned currents in the noon sector. The equatorward part of the field-aligned current pair merges with the dayside region 1 field-aligned currents. The poleward part of field-aligned current pair is highly confined around local noon, extending about 5 hours in local time and distributed between 78^o and 80^o invariant latitude. Furthermore, the senses of these field-aligned currents are opposite to those of the region 1 currents. From the spatial distributions, they suggested that these field-aligned currents are associated with magnetospheric cusp. Since the TRIAD satellite did not carry a charged particle detector, the statistical study did not examine the relationship between cusp field-aligned currents and cusp particles.

Later, Bythrow et al. [1988] and Erlandson et al. [1988] examined simultaneous measurements of the magnetic fields and charged particles near the noon sector. It was found that the cusp particle signature is coincident with the equatorward part of the observed pair of the field-aligned currents while the poleward part is characterized by the mantle particles, which are located poleward of the region of cusp particle precipitation. They concluded that the equatorward part of field-aligned currents flows along field lines that map to the dayside boundary layer, while the poleward part of field-aligned currents flow on those field lines that map tailward into the plasma mantle. Hence, they suggested that the poleward part of the field-aligned current pair should be called the "mantle" field-aligned currents. The equatorward part of the field-aligned current pair is called "region 1 field-aligned currents near noon". The distribution and the intensity of this additional FAC system are strongly dependent on the parameters of the IMF.

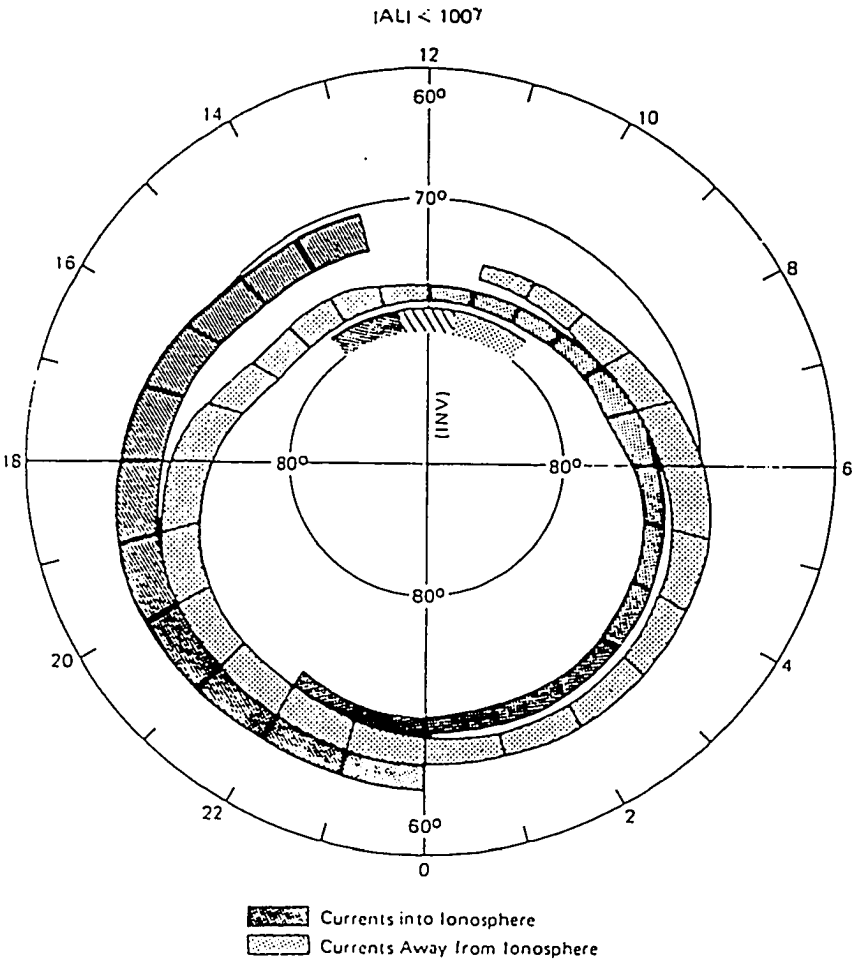

Figure 4.1 The distribution and flow directions of large-scale field-aligned currents in invariant latitude-MLT coordinates [Iijima and Potemra, 1976b].

The intensity of the FACs significantly increases with southward IMF. The distribution of the FACs are strongly modified by the IMF B_y. For IMF $B_y > 0$ ($B_y < 0$), the downward (upward) FAC dominates the Region 1 FAC at noon, while the upward (downward)FAC dominates the mantle FAC.

On the other hand, satellite observations of flux transfer events (FTEs) provided evidence for the time-dependent magnetic reconnection at the dayside magnetopause [Russell and Elphic, 1978; Paschmann et al., 1982]. Saunders et al. [1984] found that the field-aligned currents (FACs) along FTE flux tubes are carried away from the magnetopause by Alfven waves. Propagation of Alfven waves and the associated FACs to the polar ionosphere may lead to the formation of poleward-moving auroral forms (PMAFs)[e.g., Sandholt et al., 1986; Fasel et al., 1992; 1993a] and magnetic impulsive events [e.g., Lanzerotti et al., 1986; Mende et al, 1990].

Recently, Lockwood and Wild [1993] measured the time between the centers of successive FTE signatures. The distribution of inter-FTE intervals found by Lockwood and Wild [1993] peaks at $\sim$ 3 minutes, while the mean time for the inter-FTE intervals is $\sim$ 8 minutes. From ground-based optical observations, Fasel et al. [1993a] obtained the time distribution between successive PMAF intervals. The distribution peaks at $\sim$ 3 minutes, and the mean time between successive events is $\sim$ 6 minutes. There appears to be a good correlation between the time distribution for FTEs and for PMAFs.

Numerical simulations have been used to investigate the generation of FACs by magnetic reconnection in the nightside magnetotail [Sato et al., 1984; Birn and Hesse, 1991; Scholer and Otto, 1991; Scholer et al., 1991; Ugai, 1991]. Sato et al. [1984] obtained the Region 1 currents in their simulations. They argued that the cross tail current is diverted through the slow shocks due to magnetic reconnection. Birn and Hesse [1991] found that the Region 1 current is enhanced by the reconnection process

when their simulation starts from the equilibrium configuration already containing a Region 1 current. Employing solid wall boundary conditions in the earthward boundary, Scholer and Otto [1991] obtained both Region 1 and 2 FACs. Further, Scholer et al. [1991] examined the generation of the FACs in the region tailward of the reconnection site and observed the Region 1 like FACs. Ugai [1991] found that FACs with Region 1 sense can result from the velocity shear along the plasmoid boundary. However, in the above simulations, the effects of the B_y component are not taken into account and the generation of Alfven waves is not examined. Due to the finite B_y component at the dayside magnetopause, field-aligned currents will preexist in the current sheet. We can expect that the magnetic reconnection will give rise of different aspects for the generation of field-aligned currents at the dayside magnetopause and in the night magnetotail.

In this chapter we examine the generation of field-aligned currents and Alfven waves by 3D magnetic reconnection based on MHD simulations at the dayside magnetopause. In section 4.2, we briefly describe the numerical method and simulation parameters. The simulation results are present in section 4.3 and 4.4. The last section presents a discussion and conclusion.

4.2 Simulation model

In this chapter the three-dimensional simulation is based on the compressible MHD equations described in Section 2.3. A grid of $51 \times 64 \times 51$ is used in the simulation domain. The normalized equations are solved simultaneously using a two-step Lax-Wendroff finite differencing scheme with a third-order artificial diffusion term [*Lapidius*, 1967].

The geometry and coordinate system of the simulation model are illustrated in Figure 2.4. The initial configuration consists of two regions with different magnetic field orientations separated by a current layer of halfwidth a. In the following, we use a, ρ_0, B_0 and $V_{A0} = B_0/\sqrt{\mu_0\rho_0}$ as the fundamental quantities for normalization, where ρ_0 is the mass density and B_0 is the magnetic field magnitude in the region away from the initial current sheet. The x-axis is normal to the current layer which is centered at the $x = 0$ plane. The z-axis is aligned with the magnetic field components and the orientation of the y-axis is chosen to complete the coordinate system.

The initial magnetic field is given in normalized units by

$$B_y(x) = \cos(\frac{\phi}{2}) \tag{4.1}$$

$$B_z(x) = \sin(\frac{\phi}{2})tanh(x), \tag{4.2}$$

where an angle ϕ measures the magnetic shear across the current layer (i.e., $\phi = 180°$ corresponds to antiparallel magnetic fields). The plasma pressure is chosen such that total pressure is balanced across the current layer. The plasma beta β is set to 1 outside the current sheet and the initial plasma velocity is set to zero. We also assume a constant initial density of 1 for simplicity.

Considering the symmetries, the numerical simulations are only carried out in a quarter of the physical domain. At the boundaries $x = 15$, $y = \pm 50$ and $z = 90$, the normal derivatives of all physical quantities are set to zero. The line symmetric boundary conditions are imposed in both the $x = 0$ and $z = 0$ planes. To reduce the amplitude of waves reflected by the boundary, a damping term is applied at the outermost grid points.

Magnetic reconnection is triggered at appropriate locations by using a localized resistivity of the form

$$\eta(x,y,z) = \eta_b + f(y)exp\{-(z-z_0)^2\}exp\{-(x-x_0)^2\}, \tag{4.3}$$

where

$$f(y) = \begin{cases} \eta_1, & \text{if } |y| \leq X_L; \\ \eta_1 exp\{-(|y|-X_L)^2\}, & \text{otherwise.} \end{cases} \tag{4.4}$$

In the simulation, the small background resistivity η_b and the locally enhanced resistivity η_1 are chosen to be 0.005 and 0.05, respectively. In the magnetotail or at the dayside magnetopause, the magnetic reconnection would not take place on the entire line along the Earth but would be limited within a finite extent in the dawn-dusk direction. The parameter X_L controls the length of the X line. The results shown in this chapter use $X_L = 5$.

4.3 Simulation results: $B_y = 0$ case

After the onset of magnetic reconnection, a magnetic bulge region is formed that propagates away from the reconnection site as illustrated in Fig. 4.2. A quasi-steady trailing region of reconnection is formed behind the bulge front, with convergent flows in the x-y plane. The convergent flows give rise to a strong divergent flow in the z direction, which carries plasma and magnetic field into the leading bulge region. This process causes a large increase of the total pressure in the bulge region. Due to force imbalance in the x-y plane, the leading bulge structure expands outwards. The expansion causes divergent flows in the leading bulge region in the x-y plane. Fig. 4.2 shows the 3D perspective of six magnetic field lines at $t = 150$. The solid (dashed) lines is in the magnetosheath (magnetosphere) side with $x > 0$ ($x < 0$). It will be shown that

these convergent and divergent flows restructure the initial current system, leading to the generation of the FACs and Alfven waves.

Fig. 4.3 shows contours of FACs at $t = 180$ in the planes $x = -1.5$ and $y = 10$ for the $B_y = 0$ case. Solid (dashed) lines stand for positive (negative) values in the contour plots. Fig 4.3a shows that there exist two pairs of FACs in the $x = -1.5$ plane, which are respectively located in the leading bulge region ($z > 50$) and the trailing quasi-steady region ($z < 50$). The polarities of FACs in the bulge region are opposite to those in the quasi-steady region. The reversed polarity between the right and left side can also be seen in Fig. 4.3a. It should be mentioned that the FAC pair in the trailing quasi-steady region has not been identified in the previous studies.

Applying our coordinate system to the actual magnetopause, the $y < 0$ ($y > 0$) region corresponds to the prenoon (postnoon) sector. It is found that in the leading bulge region (upper part), the FAC flows into the ionosphere from the magnetosphere at the pre-noon side and the FAC is away from the ionosphere at the post-noon side. The sense of the FAC directions in the leading bulge region is the same as that of the observed Region 1 FAC at near noon.

It is worth noting that there exists an additional pair of FACs with the Region 2 sense in a small region near the point $(x, z) = (0, 90)$ in Fig. 4.3b. This pair of FACs has also been found in the simulation by Scholer and Otto [1991]. Due to the use of the solid wall boundary condition, the FAC pair in their simulation is strongly enhanced and reaches a large value which is comparable with the Region 1 FACs.

Figure 4.4 shows (a) contours of FAC, (b) contours of parallel vorticity, and (c) topology of magnetic field lines in the plane $z = 70$ at $t = 180$. In the plots, the position of the plane at each time is chosen such that the plane contains the maximum value of the total pressure, corresponding to the center of the bulge region. The solid thick lines

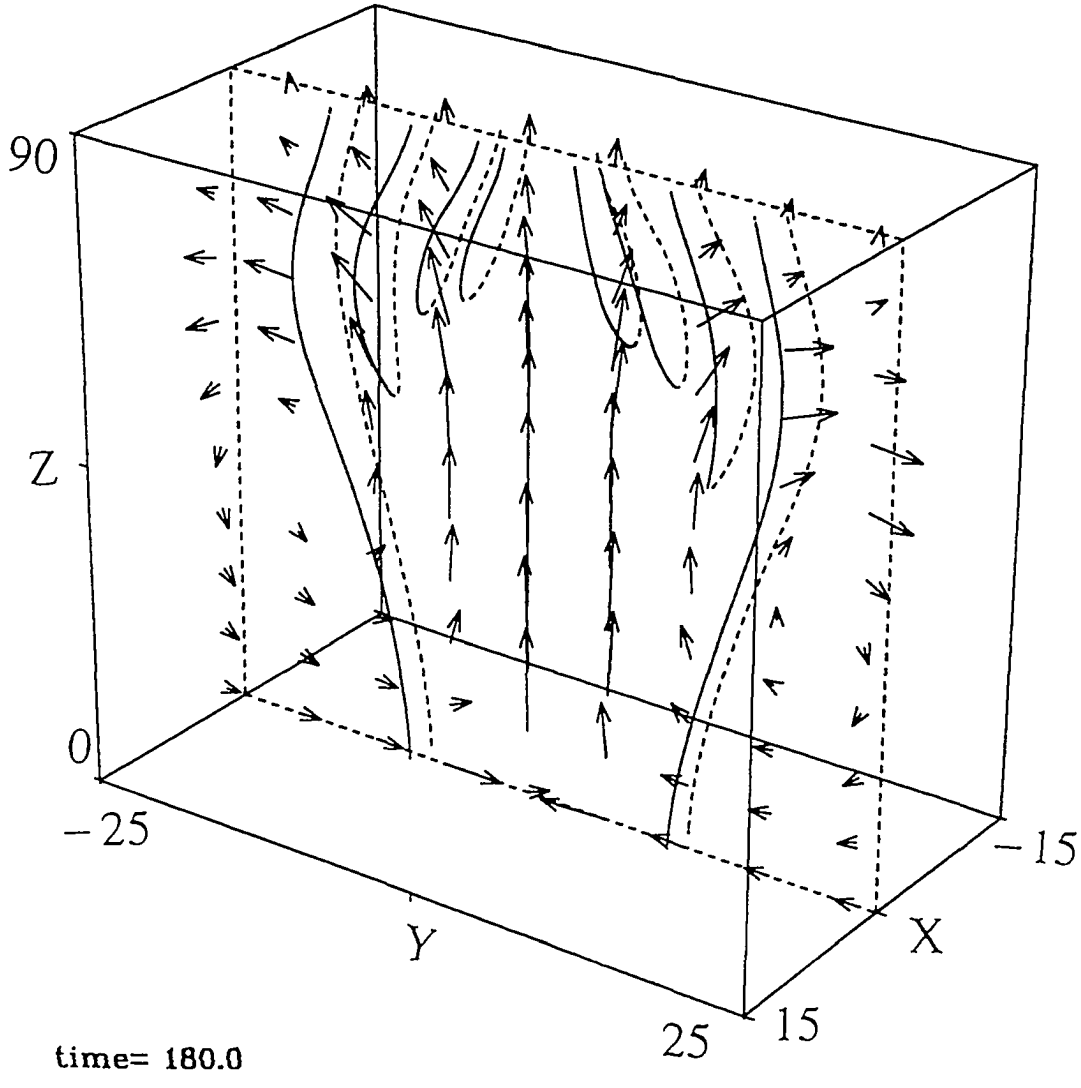

Figure 4.2 Perspective view of leading bulge structure formed in the 3D magnetic reconnection. The arrows indicate plasma flow directions.

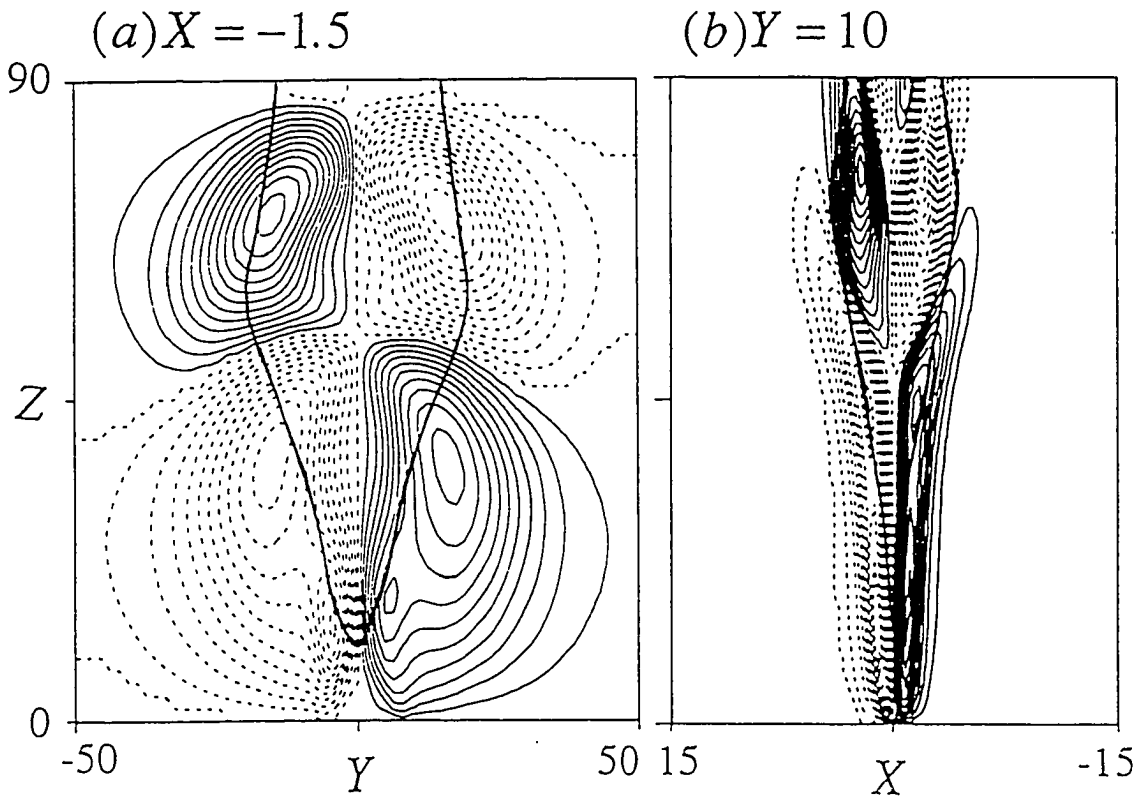

Figure 4.3 Contours of field-aligned currents ($J_{||}$) at $t = 180$ in the plane (a) $x = -1.5$ and (b) $y = 10$. Solid (dashed) lines stand for positive (negative) values. The thick solid lines indicate the boundary of the open and closed field line region.

indicate the boundary between the open and closed field line regions. The solid line cuts through the region where the density of the FACs has maximum values and hence a large percentage ($\sim$ 40%) of FACs is located in the closed field line region. The area of the generated FACs will increase with the expansion of the bulge structure. But the ratio of the FACs in the opened field line region and the closed field line region remains approximately constant. Note that the FACs in the closed field line region is due to the 3D effect. In two-dimensional simulations, the currents are located in the open field line region bounded by the separatrix [e.g., Shi and Lee, 1990].

When the bulge structure with high total pressure convects away from the reconnection site as mentioned above, the closed field line region is compressed due to the divergent flow in the x-y plane and the field lines are distorted (as shown in Fig. 4.2). The expansion of the leading bulge structure in the y direction gives rise to the y component of the magnetic field. This leads to the generation of the FACs ($J_{||} = \mathbf{J} \cdot \mathbf{B}/B$) because the initial current is in the y direction. In contrast, the magnetic field perturbation of the x component does not lead to the generation of FACs. The simulation results demonstrate that the FACs result predominantly from the terms $B_y \partial B_z/\partial x$ and $B_z \partial B_y/\partial x$ and are mainly elongated in the y direction as shown in Fig. 4.4a. Similarly, the convergent flow in the trailing region bends the field lines inward as shown in Fig. 4.2, leading to the generation of FACs with polarities opposite to those in the bulge region.

The bulge structure of high pressure plasma dragged by the open field lines would induce a dawn-dusk electric field ($v_z \times B_x$) near $x = 0$. The signs of the polarization charges associated with this convection electric field are positive in the prenoon sector and negative in the postnoon sector. It is well-known that the charge density is proportional to the parallel vorticity with a reversed sign. It is found that this part of the parallel vorticity indeed exists as shown Fig. 4.4b. The FACs would be generated by the

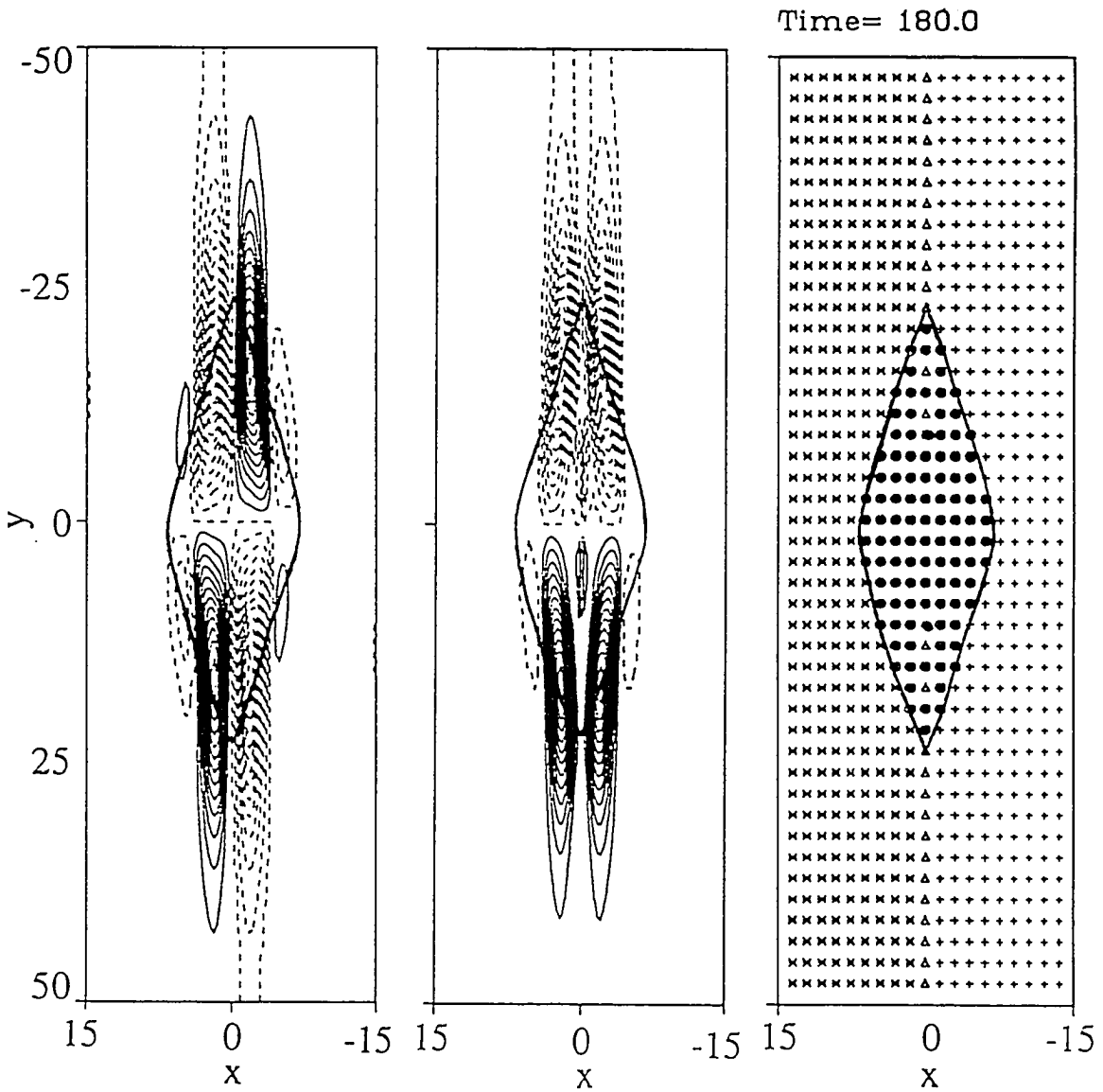

Figure 4.4 (a) Contours of FAC ($J_{||}$), (b) contours of parallel vorticity ($\Omega_{||}$), and (c) topology of magnetic field lines in the plane $z = 70$ obtained at $t = 180$. Solid (dashed) lines stand for positive (negative) values. The thick solid lines indicate the boundary of the open and closed field line region.

discharge of the polarization charges to the cusp ionosphere. But this special pattern of the FACs is not observed in Figure 4.4a. The reason may be that the ionospheric effect is not taken into account in our simulation.

As shown in Fig. 4.3 or 4.4, the average $J_{||}$ is ~ 0.04 in the normalized units of $B_0/a\mu_0$. For typical parameters at the dayside magnetopause, $B_0 = 50$ nT and $a = 300$ km, the average FAC density can be estimated as $J_{||} \sim 0.04 B_0/a\mu_0 \sim 4 \times 10^{-9}$ A/m^2. The FAC density at the ionosphere altitude can be estimated as the $J_{||i} \sim J_{||}(B_i/B_0)$, where $B_i \sim 5 \times 10^4$ nT is the magnetic field strength in the polar ionosphere. We then have $J_{||i} \sim 4 \times 10^{-6}$ A/m^2, which is consistent with the observations from satellites or ground stations [e.g., Iijima and Potemra, 1976a; Bythrow et al., 1988].

Recently, the time evolution of a localized magnetic flux tube was studied by Wei et al. [1991] using 2D MHD simulation with a cylindrical symmetry. They found that the localized magnetic flux tube tends to evolve into two separate magnetic flux tubes propagating in opposite directions. Based on the relation between the transverse components of the magnetic field and the flow velocity, it can be identified that the propagating velocity is the Alfven velocity. In general, any magnetic field perturbation associated with Alfven waves can be decomposed into two perturbations: one propagates parallel to the background magnetic field and another propagates antiparallel to the background magnetic field. The magnitudes of the magnetic field and the flow velocity for the two opposite propagating perturbations can be given by

$$\delta B_1 = (\delta B_0 - \delta V_0)/2, \qquad \delta V_1 = (\delta V_0 - \delta B_0)/2; \tag{4.5a}$$

$$\delta B_2 = (\delta B_0 + \delta V_0)/2, \qquad \delta V_2 = (\delta V_0 + \delta B_0)/2, \tag{4.5b}$$

where δB_0 and δV_0 are the initial magnitudes of the perturbed magnetic field and flow velocity, respectively.

From the above discussions, we draw a schematic sketch (Figure 4.5) to illustrate the evolution of the perturbation of the magnetic field and plasma flow velocity. Note that the heavy box indicates the simulation domain. The thick solid box stands for the magnetic field part of the perturbation while the height is the magnitude of the magnetic field and the width is the area of the perturbation. The thin solid (dashed) box stands for the positive (negative) flow velocity part of the perturbation while the height is the magnitude of the flow velocity and the width is the area of the perturbation. Both the background magnetic field B and the propagation Alfven velocity v_A is shown in the figure. Figure 4.5a shows the case with a very large perturbed area and the initial flow velocityequal to zero. From Equation (4.5), we can obtain that the magnitudes of the magnetic field and the flow velocity for the two decomposed perturbations are respectively $(\delta B_1, \delta V_1) = (\delta B_0/2, \delta B_0/2)$ and $(\delta B_2, \delta V_2) = (\delta B_0/2, -\delta B_0/2)$. For this case, the evolution of the pertubation in the simulation domain is not observed for a short running time since the area of the perturbation is much larger than the simulation domain. For the case with a small perturbation area compared to the case in Figure 4.5a, the pertubation gradually evolves into two separated perturbations propagating in opposite directions as shown in Figure 4.5b. In the $B_y = 0$ case, the perturbation comes from the magnetic reconnection in the localized region. We can predict that this perturbation will also evolve into the two separated perturbations carrying field-aligned currents and propagating in the opposite directions away from the reconnection region. Figure 4.5c shows a case with a nonzero initial flow velocity for the perturbation. In this case, the two decomposed perturbations should have different magnitudes of the magnetic field and the plasma flow velocity, but the propagation

velocities of the two perturbations are both equal to the Alfven velocity. The magnitudes of the magnetic field and the plasma flow velocity are given by Equation (4.5)

In order to check whether the opposite propagating Alfven waves associated with the FACs exist, we examine the Walen relation $\mathbf{v}_\perp = \pm(v_A/B)\mathbf{B}_\perp$, which must hold for Alfven waves [e.g., Papamastorakis et al., 1989]. Here $\mathbf{v}_\perp$ and $\mathbf{B}_\perp$ are the perpendicular components of the velocity and magnetic field, respectively. The Alfven waves are propagating antiparallel (parallel) to the background magnetic field when $\mathbf{v}_\perp$ and $\mathbf{B}_\perp$ are in phase (antiphase). In our 3D simulation, the magnetic field is nonuniform in space and it is not easy to identify $\mathbf{B}_\perp$. By taking the curl of the Walen relation, we have

$$J_{||} \approx \pm\frac{v_A}{B}\Omega_{||} \approx \pm\Omega_{||}, \tag{4.6}$$

where $v_A/B \approx 1$ in normalized units. It is demonstrated in Figure 4.4 that Equation (4.6) is valid in the simulation and the results are consistent with the generation of Alfven waves. Figure 4.6 plots the relation between FACs and parallel vorticities in the plane $z = 70$ obtained at t=180. All chosen points are in the magnetosphere side. Most points are located near the line with slope $l_p = -1$, which implies that the Walen relation is well satisfied. The negative slope ($l_p = -1$) indicates that the Alfven waves propagate parallel to the local magnetic field. Therefore, the FACs generated by the 3D reconnection process are associated with Alfven waves, which propagate away from the reconnection site. Saunders et al. [1984] also reported that during FTEs the FACs are carried away from the magnetopause by Alfven waves.

In general, we consider that the generation or redistribution of FACs is associated with both the pressure gradient force and inertia force. We use the momentum equation

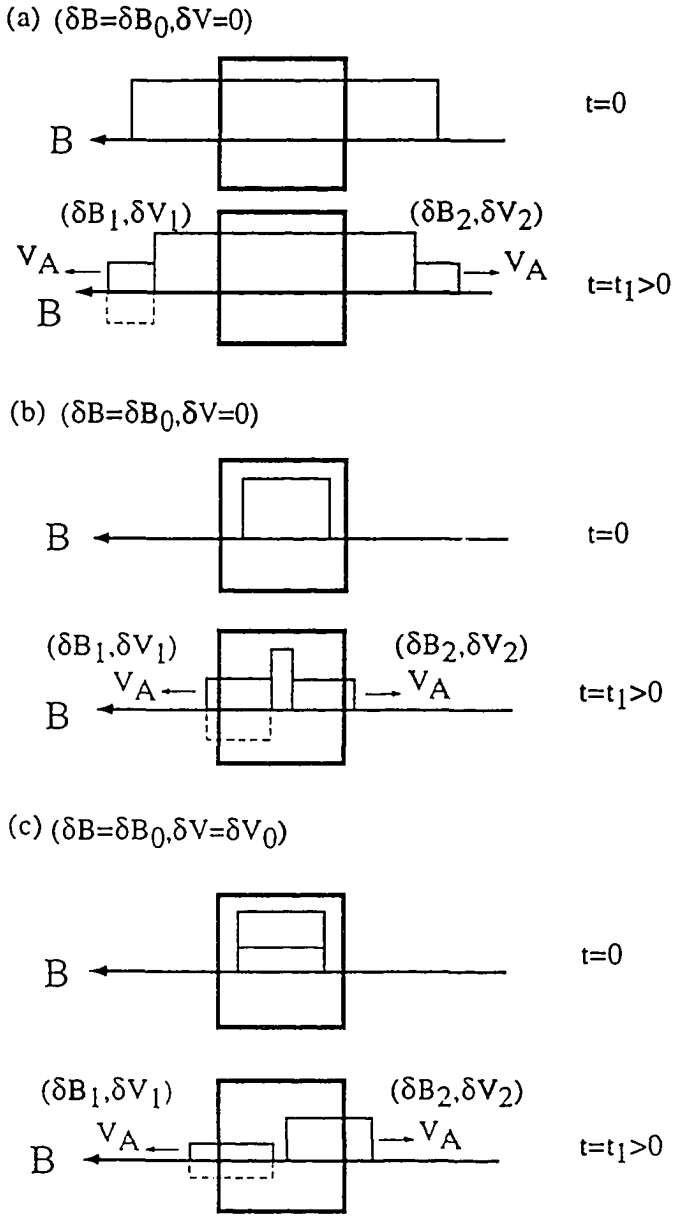

Figure 4.5 A schematic illustration of the evolution of the pertubations of the magnetic field and plasma flow associated with Alfven waves.

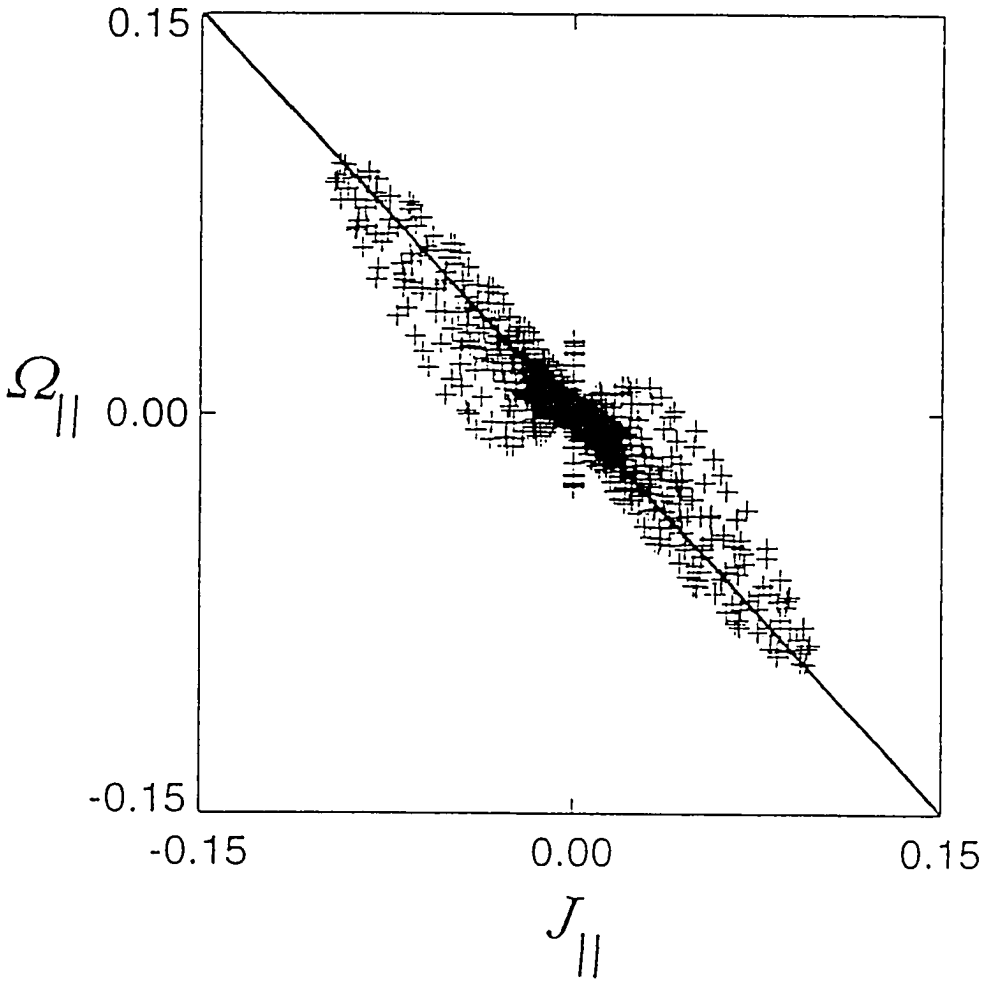

Figure 4.6 Scatter plot of field-aligned current ($J_{||}$) and parallel vorticity ($\Omega_{||}$) in the plane $z = 70$ obtained at $t = 180$.

and the continuity of the current density to determine which term is dominant in this reconnection process. Form the momentum equation, we have

$$\mathbf{J}_{\perp} = \frac{\mathbf{B}}{B^2} \times (\nabla p + \rho \frac{d\mathbf{v}}{dt}). \tag{4.7}$$

Employing $\nabla \cdot \mathbf{J} = 0$, we obtain

$$\nabla \cdot \mathbf{J}_{||} = B \frac{\partial}{\partial s}(\frac{J_{||}}{B})$$

$$= \nabla \cdot [\nabla p \times \frac{\mathbf{B}}{B^2} + \rho \frac{d\mathbf{v}}{dt} \times \frac{\mathbf{B}}{B^2}]. \tag{4.8}$$

For convenience, we refer to the two terms on the right side as the pressure term and inertia term, respectively. Figure 4.7 shows the distributions of each term of the above equation in the plane $x = 1.5$ obtained at $t = 180$. It is found that the distributions of the pressure term and the divergence of FAC are quite similar in the trailing region, which implies that the pressure term is dominant in this region. It is not surprising that the contribution of the inertia term can be neglected because we have a nearly steady state in this region. But in the bulge leading region, both the pressure term and the inertia term are responsible for the generation of FACs.

4.4 Simulation results: $B_y \neq 0$ cases

As mentioned earlier, if the B_y component is non-zero at the dayside magnetopause, an initial field-aligned current is present. The magnetic reconnection process may lead to redistribution of the FAC. It is therefore worth simulating cases with different values of B_y to investigate the influence of the solar wind B_y on the generation of FACs.

After the onset of magnetic reconnection, the tension force of the reconnected field lines would strongly accelerate the plasma to a high speed in z. This strong flow has a

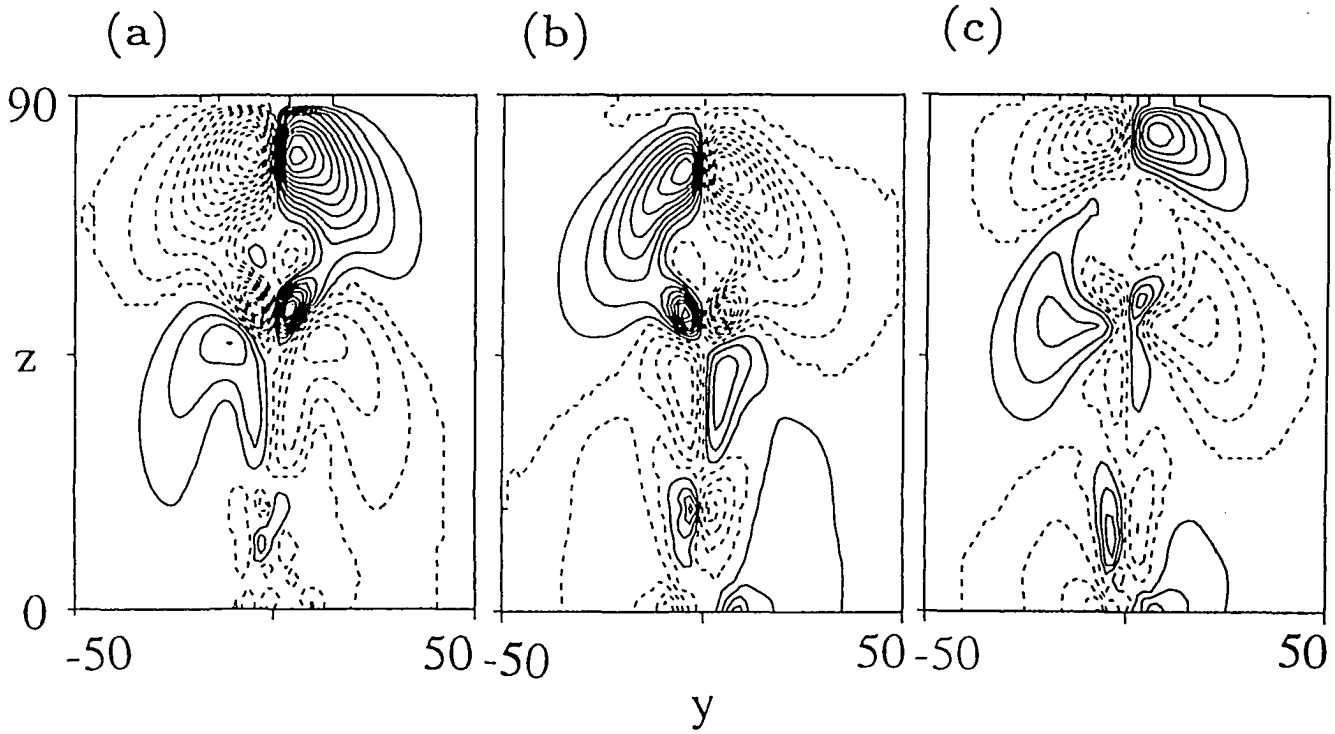

Figure 4.7 Contour plots of (a) the inertia term, (b) the pressure term, and (c) the divergence of field-aligned currents in the plane $x = 1.5$ at $t = 180$.

large gradient in x. This velocity shear component $\partial v_z/\partial x$ makes the major contribution to the parallel vorticity due to the initial finite B_y. Also, this component of the velocity shear causes a strong twist of the magnetic field and changes the current system since this flow does not align with the initial magnetic field. The velocity shear associated with $\partial v_y/\partial x$ is small due to the small value of v_y, which leads to a small contribution of the parallel vorticity. This is in contrast to the $B_y = 0$ case, in which the velocity shear component $\partial v_y/\partial x$ is dominant. The FACs are mainly contributed by $B_y(\partial B_z/\partial x)$, but the term $B_z(\partial B_y/\partial x)$ will modify the distribution of the FACs. Fig. 4.8 shows the 3D perspective view of eight magnetic field lines at $t = 210$. The portion with solid (dashed) lines is in the magnetosheath (magnetosphere) side with $x > 0$ ($x < 0$). It is found from Fig. 4.8 that the structure of the magnetic field lines is a more complicated than one in the $B_y = 0$ case.

Fig 4.9 shows (a) contours of FAC, (b) contours of parallel vorticity, and (c) topology of magnetic field lines in the plane $z = 70$ at t=240 for the case $B_y = -0.3$. Note that the open magnetic field line region is bounded by thick solid lines. It is found that the distribution of FACs is strongly modified by magnetic reconnection. However, only one sense of FACs is observed due to the large initial FAC. Fig 4.9a shows that the modification of FACs is mainly located in the open field line region since the reconnected magnetic flux is strongly twisted in this region. As mentioned earlier, the reconnected magnetic flux carries and accelerates heated plasma to cause the enhancement of the plasma pressure in the open flux region. The gradient force of the plasma pressure results in the flux rope expansion, which in turn disturbs magnetic fields in the closed field region. This is why the distribution of FAC is slightly changed in the closed field lines.

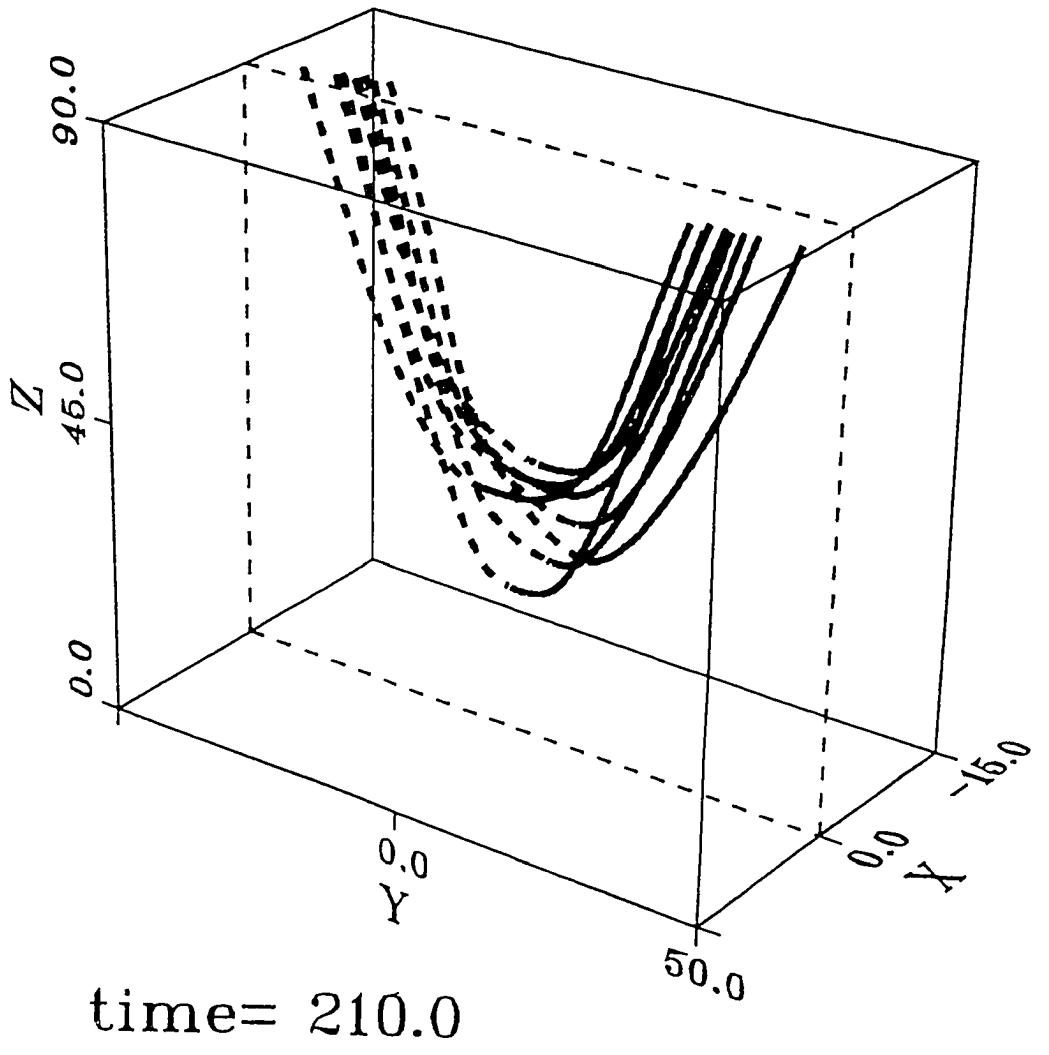

Figure 4.8 Perspective view of magnetic flux rope-like structure formed in the 3D magnetic reconnection.

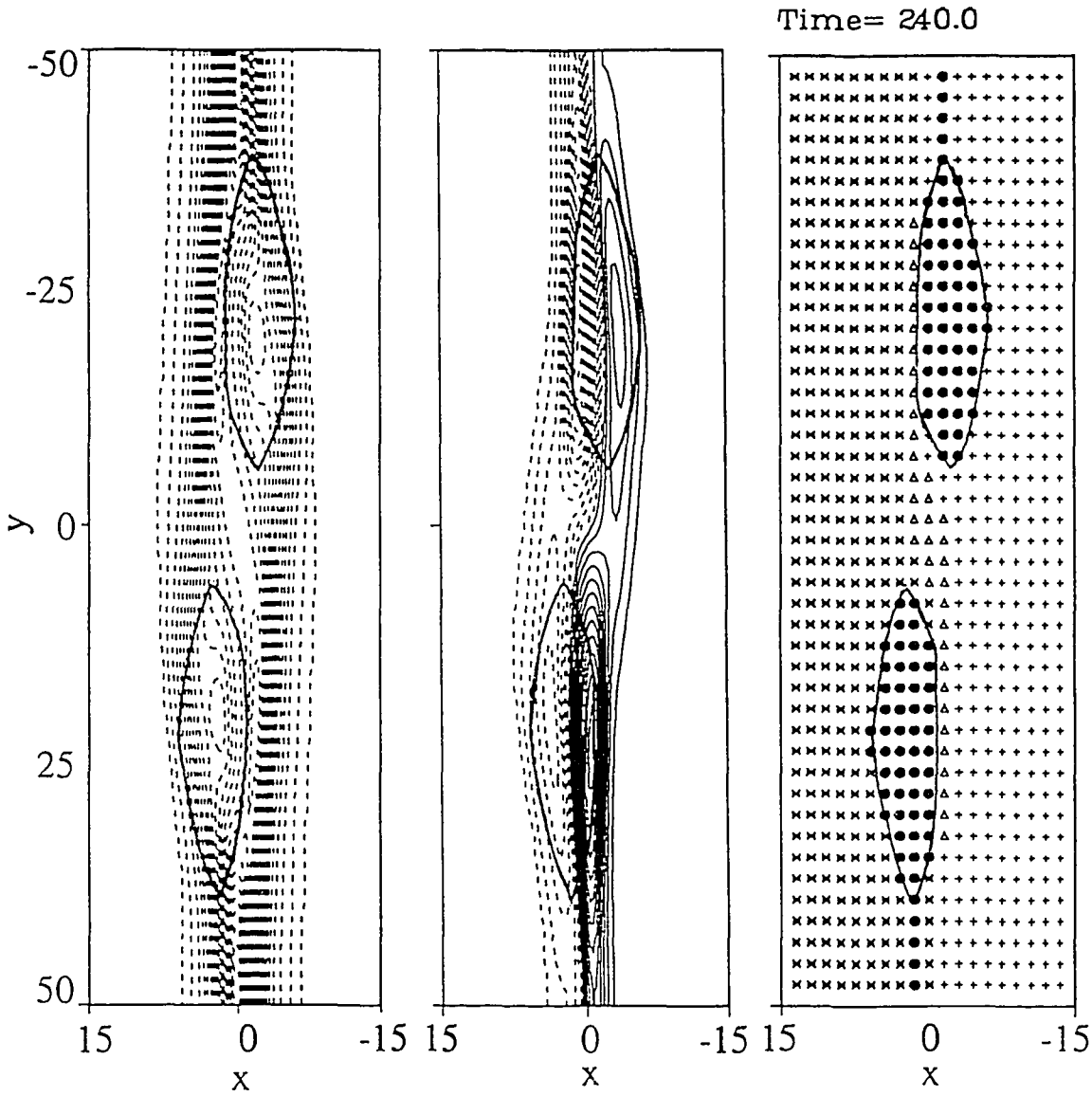

Figure 4.9 (a) Contours of FAC ($J_{||}$), (b) contours of parallel vorticity ($\Omega_{||}$), and (c) topology of magnetic field lines in the plane $z = 70$ obtained at $t = 240$. Solid (dashed) lines stand for positive (negative) values. The thick solid lines indicate the boundary of the open and closed field line region.

It seems hard to identify Alfven waves from the contour plots of total FACs and parallel vorticities in Fig 4.9a and b. Based on our earlier discussion of the evolution of perturbations, the magnetic field perturbation produced by the reconnection process should propagate away from the reconnection region. In addition, the perturbation propagating parallel to the background magnetic field is present in the magnetospheric side and the perturbation propagating antiparallel to the background magnetic field is observed in the magnetosheath side. We can expect that the parallel propagating perturbation in the prenoon sector ($y < 0$) of the magnetospheric side will be added to the initial parallel propagating one, while the antiparallel propagating perturbation in the postnoon sector ($y > 0$) of the magnetosheath side will be superimposed on the initial antiparallel propagating one. In order to check this prediction, we decompose the total FACs into two parts which propagate in the opposite directions based on Equation (4.5) and (4.6). Each part contains the initial component and the perturbed component caused by the magnetic reconnection. Figure 4.10 shows (a) contours of FAC associated with the perturbation propagating antiparallel to the background magnetic field and (b) contours of FAC associated with the perturbation propagating parallel to the background magnetic field. It is seen that the patterns of the two FAC contour plots are virtually identical except for the different locations of the perturbations. The antiparallel propagating FAC is nearly unperturbed on the dawn side ($y < 0$), while the nearly unperturbed region is located on the dusk side ($y > 0$) for the parallel propagating FAC.

Figure 4.11 shows (a) contours of the inertia term, (b) contours of the pressure term, and (c) the sum of the two terms in the plane $x = 1.5$ at $t = 240$. It is seen that the inertia term is mainly responsible for the redistribution of the FACs in the whole simulation domain. The pressure gradient effect can be neglected in this case. In the magnetic reconnection process, the z component of the plasma flow results mainly from

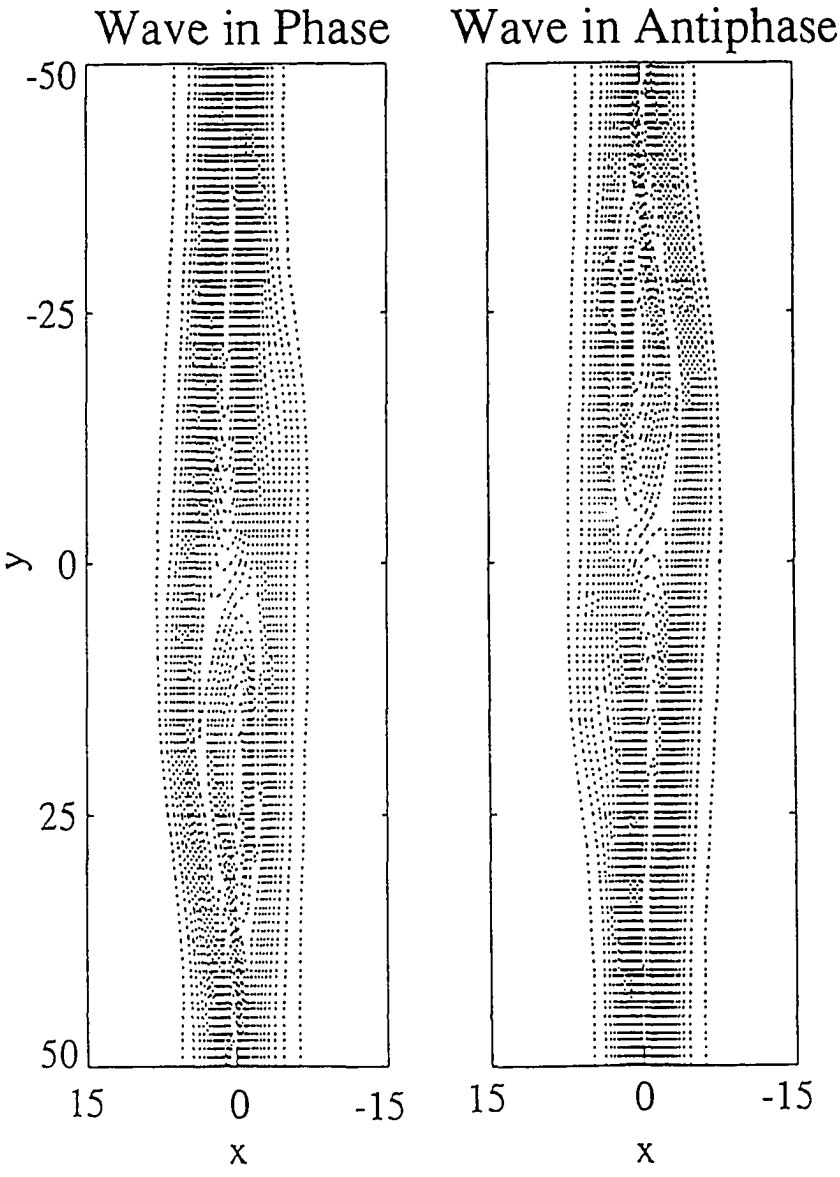

Figure 4.10 Contours of field-aligned currents associated with Alfven waves propagating (a) antiparallel and (b) parallel to the ambient magnetic field.

the magnetic tension force of reconnected field lines. The x and y components of the plasma flow are due to the imbalance of the total pressure. Hence we can expect that the z component is much larger than the other two components of the plasma flow. In the $B_y = 0$ case, $\mathbf{v} \times \mathbf{B}$ is small so that the inertia term is not the dominant component in the generation of the FACs. However, the presence of the B_y component leads to the large increase of the quantity $\mathbf{v} \times \mathbf{B}$. Consequently, the inertia term plays a major role in the redistribution of the FACs for the $B_y \neq 0$ cases.

Figure 4.12 shows the influence of the initial B_y on the generation or the redistribution of the FACs. The value of $J_{||max}$ plotted in Figure 4.12 corresponds to the maximum magnitude of FACs in the plane $z = 70$ at $t = 180$. Note that the solid (dashed) line is for the upward (downward) FAC. The results show that the FACs are strongly dependent on the initial B_y component. One sense of FACs drops to near zero when the initial B_y only increases to 10% of the total field strength. At the same time, another sense of FACs strongly increases to 0.3, which is about three times the value in the $B_y = 0$ case.

Figure 4.13 shows a schematic sketch of the global view of magnetic reconnection and the pattern of field-aligned currents in the northern hemisphere for different B_y components of the IMF. When IMF with $B_y = 0$ impinges on the dayside magnetopause, the antiparallel magnetic fields across the dayside magnetopause can be found in the equatorial plane. However, such antiparallel magnetic fields are only found at the magnetic local noon away from the equatorial plane as shown in Figure 4.13a. Hence, the reversal site of the downward and upward Region 1 field-aligned currents is located at the magnetic local noon. For $B_y > 0$ ($B_y < 0$), it is found that the location where the geomagnetic field and IMF are antiparallel shifts to the dusk (dawn) side as shown in left panel of Figure 4.13. Consequently, the reversal site of the downward and upward

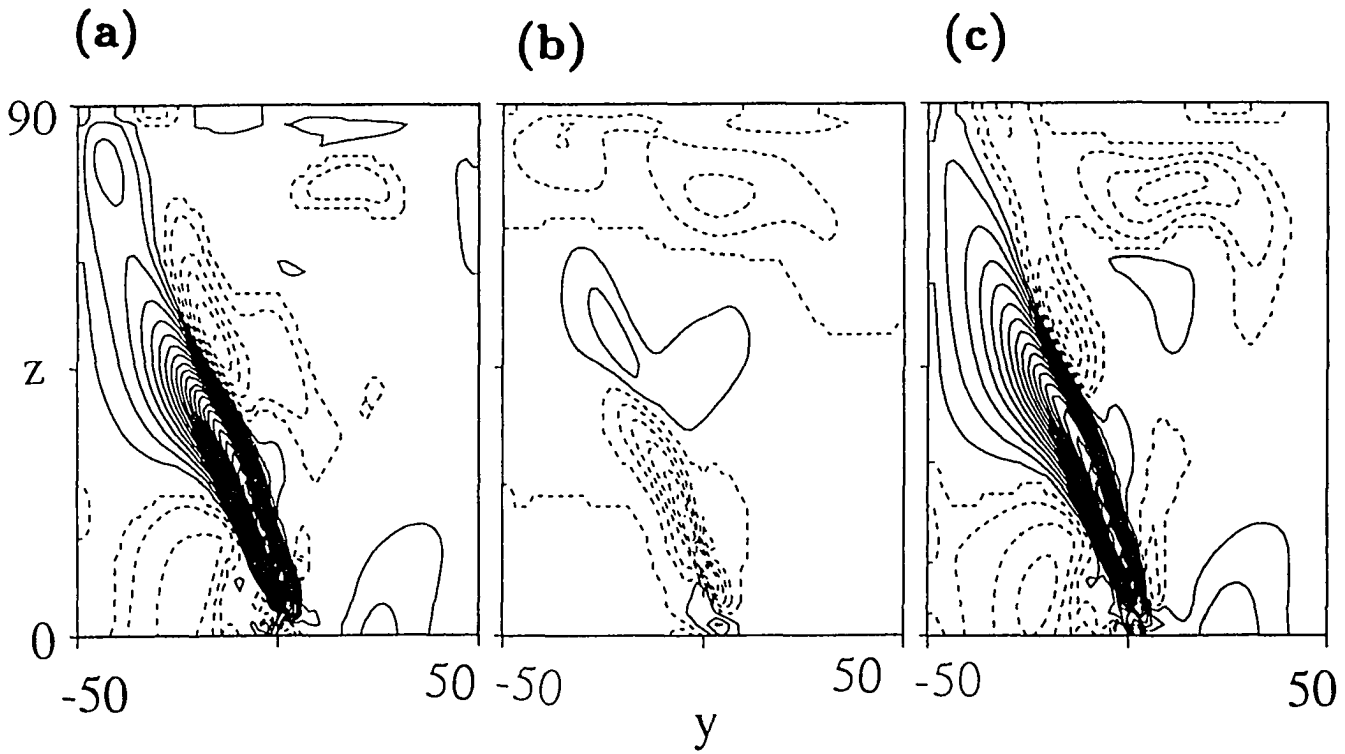

Figure 4.11 Contour plots of (a) the inertia term, (b) the pressure term, and (c) the divergence of field-aligned currents in the plane $x = 1.5$ at $t = 240$.

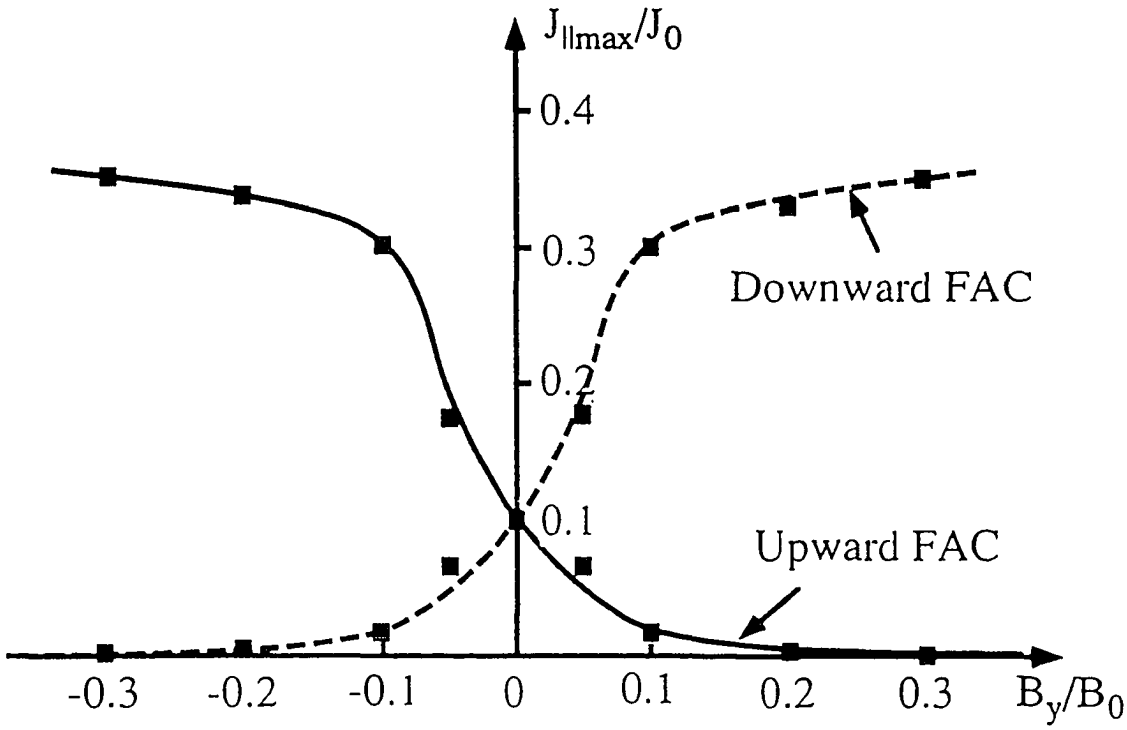

Figure 4.12 The maximum magnitudes of field-aligned currents in the plane $z = 70$ at $t = 180$ as a function of the initial value of B_y.

Region 1 field-aligned currents moves to the postnoon sector for $B_y > 0$, and to the prenoon sector for $B_y < 0$ as shown in left panel. The result is consistent with the observed pattern of the Region 1 field-aligned currents [e.g., Doyle et al., 1981 and Erlandson et al., 1988].

4.5 Discussion and summary

In this chapter, plasma dynamics at the dayside magnetopause are studied based on three-dimensional MHD simulations. Magnetic reconnection leads to the change of magnetic field topology and the conversion of magnetic energy into kinetic and thermal energy. It is found that the FACs and Alfven waves are also generated by magnetic reconnection. The relation between the FACs and the B_y component of the IMF is also investigated in this study. The results are summarized as follows:

1. The Alfven waves and field-aligned currents are generated in our simulation of magnetic reconnection. The Alfven waves carrying field-aligned currents propagate away from the reconnection region towards the polar ionosphere and solar wind.

2. For the $B_y = 0$ case, two pairs of field-aligned currents are generated on each side of the current sheet. The resulting polarities of the field-aligned currents in the leading bulge region are opposite to those in the trailing quasi-steady region.

3. It is found that the field-aligned currents are generated in both the open and closed field line region for the $B_y = 0$ case. The magnitude and flow direction of the resulting field-aligned currents are consistent with the observed Region 1 field-aligned currents at noon [e.g., Iijima and Potemra, 1976a; Bythrow et al., 1988].

4. For the $B_y \neq 0$ cases, the field-aligned currents are totally regulated due to the presence of B_y. Only one sense of the field-aligned currents is left when the B_y

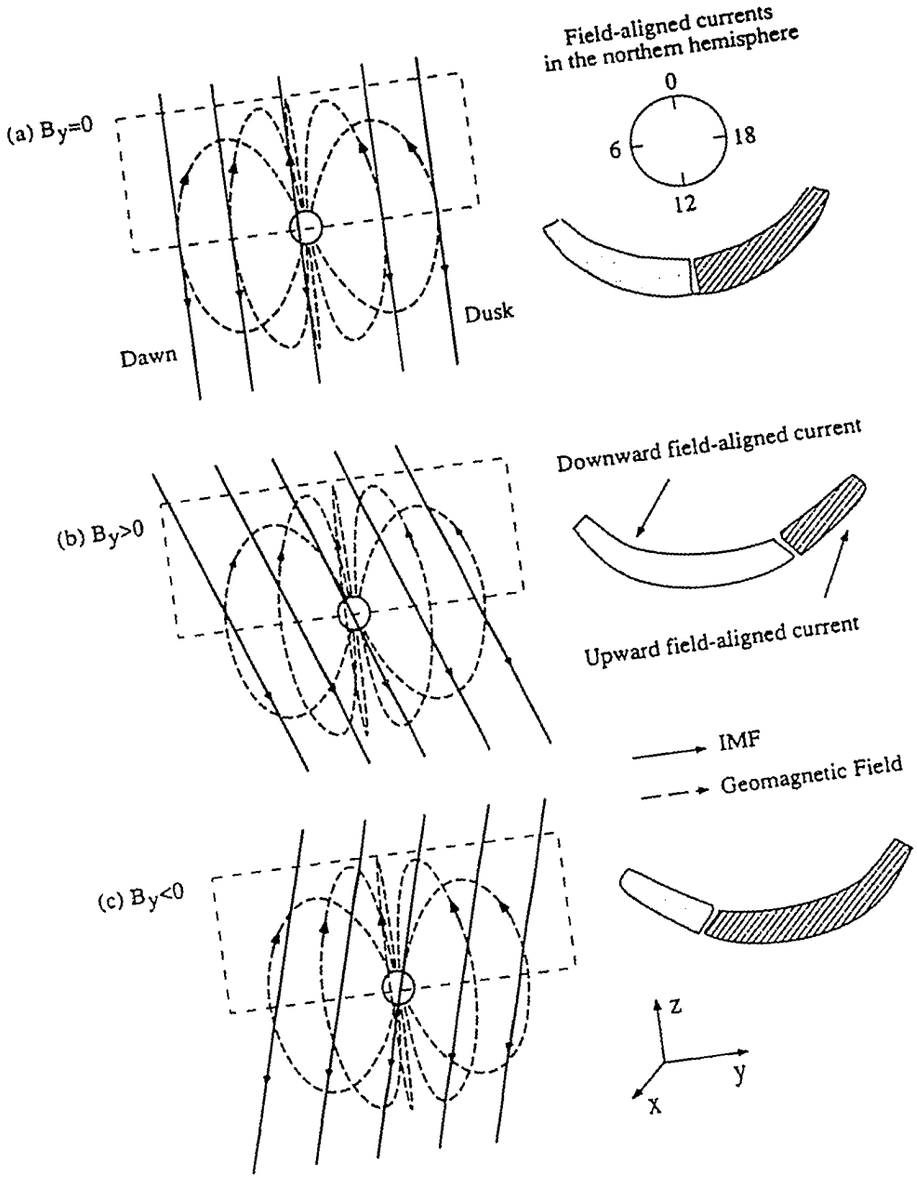

Figure 4.13 A schematic drawing of the global view of mangetic field and the resulting pattern of field-aligned currents due to magnetic reconnection.

component is greater that 0.3 of the total field. The meridian that separates the dawnside and duskside Region 1 field-aligned currents shifts to the prenoon (postnoon) sector when the initial B_y is positive (negative). This result is consistent with observations.

5. The generation of field-aligned currents results from both the inertia term and the pressure gradient term for the $B_y = 0$ case. For the $B_y \neq 0$ cases, the inertia term is mainly responsible for the redistribution of the field-aligned currents.

The Alfven waves with the associated FACs in both the open and closed field line regions will propagate towards the polar ionosphere, which may lead to the impulsive variation in the geomagnetic field [e.g., Lanzerotti et al., 1986] and the brightening of auroral arcs often observed from the ground [e.g., Sandholt et al., 1986; Fasel et al., 1992]. The Alfven waves with the associated FACs in the closed field line region will bounce back and forth between hemispheres due to the reflections at the ionosphere. This part of the FACs will evolve into damped standing Alfven waves [e.g., Lee et al., 1988]. Ground observations also indicate that magnetic impulsive events are often accompanied by damped oscillations [e.g., Lanzerotti et al., 1986].

CHAPTER 5

Discussion and summary

It is widely accepted that magnetic reconnection plays a crucial role in the interaction between the solar wind and the magnetosphere. The magnetic reconnection process leads to the transfer of energy, momentum, mass, and magnetic flux from the solar wind into the magnetosphere. The dayside and nightside magnetopauses are the interface regions between the solar wind and the magnetosphere, where this transfer take place. The transfer of energy into the magnetosphere provides the power for various magnetospheric and ionospheric processes. It is important to note that the magnetosphere and the ionosphere are coupled through the field-aligned currents.

The satellite observations of FTEs and accelerated plasma flow provide evidence that magnetic reconnection does indeed take place at the dayside magnetopause during southward IMF. Magnetic reconnection is also regarded as a possible source of impulsive magnetic variations [e.g., Lanzerotti et al., 1986; Fukunishi and Lanzerotti, 1989] and poleward moving auroral forms [e.g., Mende et al., 1990; Lockwood, 1991; Fasel et al., 1992] observed by the ground stations. Both observations of FTEs from satellites and poleward moving auroral arcs from the ground-based optical instruments indicate that the dayside magnetic reconnection can take place intermittently. Due to the finite size of magnetopause, magnetic reconnection at the dayside magnetopause should be studied as a three-dimensional process. Due to the limitation of the numerical resolution, global simulations are not able to resolve the fine structure and processes which involve small length scales. Thus, it is important to conduct three-dimensional simulation of magnetic reconnection to study the properties associated with the reconnection processes.

In Chapter 2, we examined the magnetic field line topology of magnetic flux ropes associated with the MXR reconnection process. In this process, the presence of at least two parallel X lines leads to the formation of a magnetic flux rope with each additional X line giving another flux rope. For a finite extent of these X lines, each magnetic field line in the flux rope is connected to the external magnetic field on one or the other side of the current layer. In general, the flux rope resulting from MXR has frayed ends as shown in Figure 2.1. However, it is found that for an appropriate extent and location of two neighboring *X* lines, a simple magnetic topology can be obtained, in which the major amount of magnetic flux in the rope is connected at each end to only one side of the current sheet. For a sufficient relative shift of the *X* lines, magnetic flux may enter a flux rope from the magnetosphere and return the magnetosphere. In order to support these considerations, we have carried out three-dimensional MHD simulations of MXR to study the magnetic field topology of the formed flux rope. The simulation results show that the majority of magnetic field lines in the flux rope has a simple magnetic topology for a certain relative shift of the two X lines. Smooth magnetic connections in the resulting flux rope are found in numerical simulations.

With respect to the formation of fossil FTEs, we concentrated on the structures with an MSP-MSP magnetic connection. Due to the magnetic connection to the magnetosphere, an average force toward the magnetosphere is exerted on the flux rope, which may lead to the penetration of the flux rope into the magnetosphere. A sufficiently long reconnection process would also result in a layered structure with a mixture of magnetospheric and magnetosheath plasma. All of these features would fit quite well to the observation of fossil FTEs [*Klumpar and Fuselier*, 1990]. It is expected that the final fate of these flux structures after the magnetic signatures have decayed will be to contribute to the low- and high-latitude boundary layers.

In Chapter 3, the evolution of the core magnetic fields in magnetic flux ropes was studied for various magnetic reconnection processes. We also compared the increase of core magnetic field in the flux tubes for 2D SXR and MXR processes and for the 3D generalization of these processes. Our simulation results show: (1) The 3D MXR always leads to a larger increase of the magnetic field for each set of initial states than the other reconnection processes. (2) The 3D processes always lead to a larger enhancement than the corresponding 2D processes. (3) For the same reconnection process, the field amplification is larger for the constant initial B_y configuration than for the force-free initial state. However, the final core field in the constant initial B_y case is smaller than that in the initial force-free case. (4) A small core field is only found for cases where the preexisting B_y in the current sheet is significantly less than the field strength outside the current sheet. Two-dimensional SXR reconnection leads to a small core field in FTEs.

The results of our simulations can explain the strong core magnetic field which has been observed [*Paschmann et at.*, 1982; *Berchem and Russell*, 1982] in some FTEs at the dayside magnetopause and the concentration of flux in magnetic flux ropes in the magnetotail. For FTE observations with the strong enhancement of the core magnetic field, we suggest that these FTEs are closely related to the 3D MXR reconnection process. A small magnetic field in FTEs is probably due to a small magnetic field in the current sheet at the onset of reconnection. In addition, a small field is indicative of largely 2D processes or single X line reconnection. The suggested two-step mechanism can explain the enhancement of the B_y component in magnetotail flux ropes.

In Chapter 4, the generation of the FACs and Alfven waves is studied based on the three-dimensional MHD simulation. It is the first 3D MHD simulation that investigates the relation between the FACs and the B_y component of the IMF. The results indicate that both FACs and Alfven waves are generated by the 3D reconnection process.

For $B_y = 0$, two pairs of FACs are generated on each side of current sheet. The polarities of the resulting FAC pair in the leading bulge region are opposite to those of FAC pair in the trailing quasi-steady region. It is further found that a large portion of the FACs ($\sim$ 40%) is located in the closed field line region. The magnitude and the sense of the FACs in the leading bulge region are consistent with the observed Region 1 FACs at noon. We examine the Walen relation between FAC and parallel vorticity and find that Alfven waves are generated and propagate away from the reconnection site. In addition, both the inertia term and the pressure gradient term contribute to the generation of FACs.

For the nonzero B_y cases, the initial FAC is redistributed by the magnetic reconnection process. The inertia term is mainly responsible for this redistribution in these cases. The results indicate that the presence of IMF B_y leads to the shift of the reversal site between the downward and upward Region 1 field-aligned currents. The resulting shift due to the influence of the B_y component is consistent with the statistical result of the satellite observations. Furthermore, the inertia term is mainly responsible for the redistribution of the field-aligned currents.

We suggest that the Alfven waves with the associated FACs in both the open and closed field line regions will propagate towards the polar ionosphere, which may lead to the impulsive variation in the geomagnetic field and the brightening of aurora arcs. The Alfven waves that bounce back and forth between hemispheres due to the reflections at the ionosphere will gradually evolve into damped standing Alfven waves in the closed field line region.

In the future, we will continue our study of the generation of FACs with consideration of the shear flow and the feed-back effects of the ionosphere. The shear flow may modify the distribution of B_y after the onset of reconnection, which in turn causes

additional field-aligned currents. The field-aligned currents generated by magnetic reconnection at the dayside magnetopause will propagate along geomagnetic field lines to the ionosphere. Part of field-aligned current can return to the reconnection site due to the reflection at the ionosphere. The reflected field-aligned currents may change the reconnection rate and the field-aligned currents. In addition, we plan to study the topology of magnetic flux rope formed by reconnections at multiple sites, which may lead to multiple enhancements of the field-aligned currents and Alfven waves and hence multiple brightenings in PMAFs

In summary, we have carried out MHD simulations to study the magnetic field topology, the enhancement of core magnetic field and the generation of field-aligned currents associated with 3D magnetic reconnection. In our simulation, magnetic flux ropes with either smooth or frayed ends can be obtained through the MXR process. The simulation of the core magnetic field indicates that the 3D processes always lead to a larger enhancement than the corresponding 2D cases, while the MXR process causes a larger increase of the core magnetic field than the patchy reconnection and SXR due to larger magnetic tensions in the MXR process. The results indicate that Alfven waves and field-aligned currents generated by 3D magnetic reconnection propagate away from the reconnection site. For cases with $B_y = 0$, two pairs of field-aligned currents are obtained on each side of the current sheet. It is found that a large portion of the field-aligned currents ($\sim 40\%$) is located in the closed field line region. For $B_y \neq 0$ cases, one sense of field-aligned currents is dominant due to the presence of the initial field-aligned current. The influence of the initial B_y on the longitudinal shift of the current reversal site, which separates the downward and upward field-aligned currents, is found to be consistent with observations

REFERENCES

Akasofu, S.-I., The magnetospheric currents: an introduction, in *Magnetospheric currents*, ed. T. A. Potemra, p. 29, Geophysical Monograph 28, AGU, Washington, D.C., 1984.

Alfven, H., A theory of magnetic storms and of the aurorae, *Proceedings of the Royal Swedish Academy of Sciences*, vol. 18, No. 3, 1939.

Axford, W. I., Magnetic field reconnection, in *Magnetic reconnection in Space and Laboratory Plasmas*, ed. by E. W. Hones, Jr., p. 1, Geophysical Monograph 30, AGU, Washington, D.C., 1984.

Baum, P. J., and A. Bratenahl, Magnetic reconnection experiments, *Adv. Electronics and Electron Physics, 54*, 1, 1980.

Berchem, J., and C. T. Russell, Magnetic field rotation through the magnetopause: ISEE-1 and -2 observations, *J. Geophys. Res., 87*, 8139, 1982.

Berchem, J. and C.T. Russell, Flux transfer evnts on the magnetopause: Spatial distribution and controlling factors, *J. Geophys. Res., 89*, 6689, 1984.

Biernat, H., M. F. Heyn, and V. S. Semenov, Unsteady Petschek reconnection, *J. Geophys. Res., 92*, 3392, 1987.

Birkeland, K., *The Norwegian Aurora Polaris Expedition 1902-3*, vol. 1, *On the Cause of Magnetic Storms and the Origin of Terrestrial Magnetism*, H. Aschehoug, Christiania, Norway, 1908.

Birn, J. and E. W. Hones, Three-dimensional computer modeling of dynamic reconnection in the geomagnetic tail, *J. Geophys. Res., 86*, 6802, 1981.

Birn, J., and M. Hesse, MHD simulations of magnetic reconnection in a skewed three-dimensional tail configuration, *J. Geophys. Res., 96*, 23, 1991.

Bythrow, P. F., T. A. Potemra, R. E. Erlandson, L. J. Zanetti, and D. M. Klumpar, Birkeland currents and charged particles in the high-latitude prenoon region: a new interpretation, *J. Geophys. Res., 93*, 9791, 1988.

Chapman, S., On certain average characteristics of world wide magnetic disturbance, *Proceedings of the Royal Society, A*, Vol. 115, p. 242, 1927.

Cowley, S. W. H., Comments on the merging of non antiparallel fields, *J. Geophys. Res., 81*, 3455, 1976.

Cowley, S. W. H., The causes of convection in the Earth's magnetosphere: A review of developments during the IMS, *Rev., Geophys., 20*, 531, 1982.

Daly, P. W., D. J. Williams, C. T. Russell, E. Keppler, Particle signature of magnetic transfer events at the magnetopause, *J. Geophys. Res., 86*, 1628, 1981.

Daly, P. W., M. A. Saunders, R. P. Rijnbeek, N. Sckopke, and C. T. Russell, The distribution of reconnection geometry in flux transfer events using energetic ions, plasma, and magnetic data, *J. Geophys. Res., 89*, 3843, 1984.

Ding, D. Q., L. C. Lee, and Z. F. Fu, Multipe X line reconnection, 3. A particle simulation of flux transfer events, *J. Geophys. Res., 91*, 13384, 1986.

Ding, D. Q., L. C. Lee, and Z. W. Ma, Different FTE signatures generated by the bursty single *X* line reconnection and the multiple *X* line reconnection at the dayside magnetopause, *J. Geophys. Res., 96*, 57, 1991.

Dungey, J. W., Interplanetary magnetic field and the auroral zones, *Phys. Rev. Lett., 6*, 47, 1961.

Elphic, R. C., Observations of flux transfer events: Are FTEs flux ropes, islands, or surface waves?, in *Physics of Magnetic Flux Ropes*, ed. by C. T. Russell, E. R. Priest, and L. C. Lee, p. 455, Geophysical Monograph 58, AGU, Washington, D. C., 1990.

Elphic, R. C., C. A. Cattell, K. Takahashi, S. J. Bame, and C. T. Russell, ISEE-1 and 2 observation of magnetic flux ropes in the magnetotail: FTE's in the plasma sheet?, *Geophys. Res. Lett., 13*, 648, 1986.

Erlandson, R. E., L. J. Zanetti, T. A. Potemra, P. F., Bythrow, and R. Lundin, IMF B_y dependence of region 1 Birkeland currents near noon, *J. Geophys. Res., 93*, 9804, 1988.

Farrugia, C. J., et al., Field and flow perturbations outside the reconnected field line region in flux transfer events: Theory, *Planet. Space Sci., 35*, 227, 1987.

Farrugia, C. J., et al., A multi-instrument study of flux transfer event structure, *J. Geophys. Res., 93*, 14465, 1988.

Fasel, G. J., J. Minow, R. W. Smith, C. S. Deehr, and L. C. Lee, Multiple brightenings of transient dayside auroral forms during oval expansion, *Geophys. Res. Lett., 19*, 2429, 1992.

Fasel, J. G., J. Minow, R. W. Smith, C. S. Deehr, and L. C. Lee, Ionospheric signatures of solar wind-magnetospheric interaction in dayside aurora, in *Airglow and Aurora, SPIE Proceedings, 2050*, S. Leontiev, ed., SPIE, Berlin, Germany, in press, 1993a.

Fasel, G. J., L. C. Lee, and R. W. Smith, A mechanism for the multiple brightenings of dayside poleward moving auroral forms, *Geophys. Res. Lett.*, in press, 1993b.

Fedder, J. A., C. M. Mobarry, and J. G. Lyon, Reconnection voltage as a function of IMF clock angle, *Geophys. Res. Lett., 18*, 1047, 1991.

Fu, Z. F., 2-D and 3-D simulation study of multiple *X* line reconnection, in *Magnetic Reconnection in Space Plasma*, ESA SP-285, edited by A. Galeev, p. 275, ESA Publications Division, ESTEC, Noordwijk, Netherlands, 1989.

Fu, Z. F., and L. C. Lee, Simulation of multiple X line reconnection at the dayside magnetopause, *Geophys. Res. Lett., 12*, 291, 1985.

Fu, Z. F., and L. C. Lee, Multiple X line reconnection, 2. The dynamics, *J. Geophys. Res., 91*, 13373, 1986.

Fu, Z. F., L. C. Lee, and Y. Shi, A three-dimensional simulation of the multiple X line reconnection process, in *Physics of Magnetic Flux Ropes, Geophys. Monogr. Ser.*, vol. 58, edited by C. T. Russel, E. R. Priest, and L. C. Lee, p. 515, AGU, Washington, D. C., 1990.

Fukunishi, H., and L. J. Lanzerotti, Hydromagnetic waves in the dayside cusp region and ground signatures of flux transfer envents, in *Plasma Waves and Instabilities at Comets and in Magnetopheres*, ed. by B. T. Tsurutani and H. Oya p. 1, Geophysical Monograph 53, AGU, Washington, D.C., 1989.

Galeev, A. A., M. M. Kuznetsova, and L. M. Zelenyi, Magnetopause stability threshold for patchy reconnection, *Space Sci. Rev., 44*, 1, 1986.

Giovanelli, R. G., Mangetic and electric phenomena in the Sun's atomsphere associated with sunspots, *Mon. Not. Roy. Ast. Soc., 107*, 338, 1947.

Gosling, J. T., M. F. Thomsen, S. J. Bame, and C. T. Russell, Accelerated plasma flows at the near-tail magnetopause, *J. Geophys. Res., 91*, 3029, 1986.

Gosling, J. T., M. F. Thomsen, S. J. Bame, R. C. Elphic, and C. T. Russell, Plasma flow reversals at the dayside magnetopause and the origin of asymmetric polar cap convection, *J. Geophys. Res., 95*, 8073, 1990.

Gosling, J. T., M. F. Thomsen, S. J. Bame, R. C. Elphic, and C. T. Russell, Observations of reconnection of interplanetary and lobe magnetic field lines at the high-latitude magnetopause, *J. Geophys. Res., 96*, 14097, 1991.

Greene, J. M., Geometrical properties of three-dimensional reconnecting magnetic fields with null, *J. Geophys. Res., 93*, 8583, 1988.

Haerendel, G., and G. Paschmann, Interaction of the solar wind with the dayside magnetopause, in *Magnetospheric Plasma Physics*, ed. by A. Nishida, p. 49, D. Reidel Publ. Co., Dordrecht, Holland, 1982.

Haerendel, G., G. Paschmann, N. Sckopke, H. Rosenbauer, and P.C. Hedgecock, The frontside boundary layer of the magnetosphere and the problem of reconnection, *J. Geophys. Res., 83*, 3195, 1978

Hesse, M., and K. Schindler, A theoretical foundation of general magnetic reconnection, *J. Geophys. Res., 93*, 5559, 1988.

Hesse, M., and J. Birn, Magnetic reconnection in the magnetotail current sheet for varying cross-tail magnetic field, *Geophys. Res. Lett., 17*, 2019, 1990.

Hesse, M., and J. Birn, Magnetosphere-ionosphere coupling during plasmoid evolution: First result. *J. Geophys. Res., 96*, 11513, 1991.

Hones, E. W., Jr., J. Birn, S. J. Bame, G. Paschmann, and C. T. Russell, On the three-dimensional magnetic structure of the plasmoid created in the magnetotail at substorm onset, *Geophys. Res. Lett., 9*, 203, 1982.

Hoyle, F., Magnetic storms and aurorae, in *Some Recent Researches in Solar Physics*, p. 102, Cambridge University Press, London, 1949.

Hughes, W. J., and D. G. Sibeck, On the 3-dimensional structure of plasmoids, *Geophys. Res. Lett., 14*, 636, 1987.

Iijima, T. and Potemra, The amplitude distribution of field-aligned currents at northern high latitudes observed bt Triad, *J. Geophys. Res., 81*, 2165, 1976a.

Iijima, T. and Potemra, Field-aligned currents in the dayside cusp observed by Triad, *J. Geophys. Res., 81*, 5971, 1976b.

Iijima, T., R. Fujii, T. A. Potemra, and N. A. Saflekos, Field-aligned currents in the south polar cusp and their relationship to the interplanetary magnetic field, *J. Geophys. Res., 83*, 5595, 1978.

Kan, J. R., A theory of patchy and intermittent reconnections for magnetospheric flux transfer events, *J. Geophys. Res., 93*, 5613, 1988.

Kan, J. R., and D. M. Klumpar, Patchy reconnection inferred from flux transfer events observed earthward of the magnetopause, submitted to *J. Geophys. Res.*, 1994.

Klumpar, D. M., and S. A. Fuselier, A series of flux transfer events in the dayside magnetosphere, in *Physics of Space Plasma, SPI Conf. Proc. Reprint Ser.*, Vol. 10, pp. 301-313, Cambridge, Mass. 1990.

Klumpar, D. M., S. A. Fuselier, and E. G. Shelley, Ion composition measurements within magnetospheric flux transfer events, *Geophys. Res. Lett., 17*, 2305, 1990.

Lapidius, A., Detached shock calculation by second-order finite differences, *J. Comput. Phys.*, 2, 154, 1967.

Lanzerotti, L. J., L. C. Lee, C, G, Maclennan, A. Wolfe, and L. V. Medford, Possible evidence of flux transfer events in the polar ionosphere, *Geophys. Res. Lett., 13*, 1089, 1986.

Lanzerotti, L. J., R. M. Konik, A. Wolfe, D. Venkatesan, and C, G, Maclennan, Cusp latitude magnetic impulsive events 1. Occurrence statistics, *J. Geophys. Res. 96*, 14,009, 1991.

Lee, L. C., and Z. F. Fu, A theory of magnetic flux transfer at the Earth's magnetopause, *Geophys. Res. Lett., 12*, 105, 1985.

Lee, L. C., Y. Shi, and L. J. Lanzerotti, A mechanism for generation of cusp region hydromagnetic waves, *J. Geophys. Res., 93*, 7578, 1988.

Lee, L. C., Time dependent magnetic reconnection: Two- and three-dimensional MHD simulation, *Comput. Phys. Commun., 59*, 163, 1990.

Lee, L. C., Z. W. Ma, Z. F. Fu, and A. Otto, Topology of magnetic flux ropes and formation of fossil flux transfer events and boundary layer plasmas, *J. Geophys. Res.*, *98*, 3943, 1993.

Lockwood, M., Flux transfer events at the dayside magnetopause: Transient reconnection or magnetosheath pressure pulse? *J. Geophys. Res.*, *96*, 1991.

Lockwood, M. and M.F. Smith, Low-altitude signatures of the cusp and flux transfer events, *Geophys. Res. Lett.*, *16*, 879, 1989.

Lockwood, M. and M. N. Wild, On the quasi-periodic nature of magnetopause flux transfer events, *J. Geophys. Res.*, *98*, 5935, 1993.

Lundin, R., On the magnetospheric boundary layer and solar wind energy transfer into the magnetosphere, *Space Sci. Rev.*, *48*, 263, 1988.

Ma, Z. W., L. C. Lee, A. Otto, and Y. Shi, B_y enhancements in magnetospheric current sheets and magnetic flux tubes, in *Physics of Space Plasma (1992), SPI Conference Proceeding Reprint Series*, ed. by T. Chang and J. R. Jasperse, Vol. 12, p. 575, Scientific Publishers, Inc., Cambridge, Mass., 1993.

Ma, Z. W., A. Otto, and L. C. Lee, Core magnetic field enhancement in single X line, multiple X line and patchy reconnection, *J. Geophys. Res.*, in press, 1994.

Mende, S. B., R. L. Rairden, L. J. Lanzerotti, and C. G. Maclennan, Magnetic impulses and associated optical signatures in the dayside aurora, *Geophys. Res. Lett.*, *17*, 131, 1990.

Moldwin, M. B., and W. J. Hughes, Multi-satellite observations of plasmoids: IMP 8 and ISEE 3, *Geophys. Res. Lett.*, *19*, 1081, 1992a.

Moldwin, M. B., and W. J. Hughes, On the formation and evolution of plasmoids: A survey of ISEE 3 geotail data, *J. Geophys. Res.*, *97*, 19259, 1992b.

Nishida, A., Can random reconnection on the magnetopause produce the low latitude boundary layer, *Geophys. Res. Lett.*, *16*, 1227, 1989.

Nishida, A., M. Scholer, T. Terasawa, S. J. Bame, G. Gloeckler, E. J. Smith, and R. D. Zwickl, Quasi-stagnant plasmoid in the middle tail: A new preexpansion phase phenomenon, *J. Geophys. Res.*, *91*, 4245, 1986.

Ogino, T., R. J., Walker, and Ashour-Abdalla, A magnetohydrodynamic simulation of the formation of magnetic flux tubes at the Earth's dayside magnetopause, *Geophys. Res. Lett., 16,* 155, 1989.

Otto, A., 3-D resistive MHD computation of magnetospheric physics, *Comput. Phys. Commun., 59,* 1985, 1990.

Otto, A., Three-dimensional magnetohydrodynamic simulations of processes at the Earth's magnetopause, *Geophys. Astrophys. Fluid Dyn., 62,* 69, 1991.

Otto, A., M. Hesse and K. Schindler, General magnetic reconnection in 3D systems, in *Topological Fluid Mechanics*, edited by H. K. Moffatt and A. Tsinober, p. 225, Cambridge University Press, New York, 1990.

Papamastorakis, I., G. Paschmann, W. Baumjohann, B. U. O. Sonnerup, and H. Luhr, Orientation, Motion, and other properties of flux transfer event sturctures on September 4, 1984, *J. Geophys. Res., 94,* 8854, 1989.

Parker, E. N., Sweet's mechanism for merging magnetic fields in conducting fluids, *J. Geophys. Res., 62,* 509, 1957.

Paschmann, G., G. Haerendel, I. Papamastorakis, N. Sckopke, S. J. Bame, J. T. Gosling, and C. T. Russell, Plasma and magnetic field characteristics of magnetic flux transfer events, *J. Geophys. Res., 87,* 2159, 1982.

Paschmann, G., I. Papamasrtorakis, W. Baumjohann, N. Sckopke, C. W. Carlson, B. U. O. Sonnerup, and H. Luhr, The magnetopause for larger magnetic shear: AMPTE/IRM observations, *J. Geophys. Res., 91,* 11,099, 1986.

Paschmann, G., G. Haerenddel, N. Sckopke, E. Mobius, H. Luhr, and C. W. Carlson, Three-dimensional plasma structures with anomalous flow directions near the earth's bow shock, *J. Geophys. Res., 93,* 11,279, 1988.

Petschek, H. G. Magnetic Annihilation, in *AAS-NASA Symposium on the Physics of Solar Flares,* ed. by W. N. Hess, p. 425, NASA Spec. Publ. SP-50, 1964.

Priest, E. R., and T. G. Forbes, New models for fast steady state magnetic reconnection, *J. Geophys. Res., 91,* 5579, 1986.

Priest, E. R., and L. C. Lee, Nonlinear magnetic reconnection models with separatrix jets, *J. Plasma Phys., 44,* 337, 1991.

Richardson, I. G., and S. W. H. Cowley, Plasmoid-associated energetic ion bursts in the deep geomagnetic tail: Properties of the boundary layer, *J. Geophys. Res.*, *90*, 12,133, 1985.

Rijnbeek, R. P., and S. W. H. Cowley, Magnetopause flux erosion events are flux transfer events, *Nature, 309*, 135, 1984.

Rijnbeek, R. P., S. W. H. Cowley, D. J. Southwood, and C. T. Russell, Observations of reverse polarity flux transfer events at the Earth's magnetopause, *Nature, 300*, 23, 1982.

Rijnbeek, R. P., S. W. H. Cowley, D. J. Southwood, and C. T. Russell, A survey of dayside flux transfer events observed by ISEE 1 and 2 magnetometers, *J. Geophys. Res.*, *89*, 786, 1984.

Rijnbeek, R. P., C. J. Farrugia, D. J. Southwood, M. W. Dunlop, W. A. C. Mierjedrzejowicz, C. P. Chaloner, D. S. Hall, and M. F. Smith, A magnetic boundary signature within flux transfer events, *Planet. Space Sci., 35*, 871, 1987.

Russell, C. T., and R. C. Elphic, Initial ISEE magnetometer results: Magnetopause observations, *Space Sci. Rev., 22*, 691, 1978.

Russell, C. T., and R. C. Elphic, ISEE observations of flux transfer events at the dayside magnetopause, *Geophys. Res. Lett., 6*, 33, 1979.

Sandholt, P. E., C. S. Deehr, A. Egeland, B. Lybekk, R. Viereck, and G. J. Romick, Signatures in the dayside aurora of plasma transfer from the magnetosheath, *J. Geophys. Res.*, *91*, 10063, 1986.

Sato, T., R. J. Walker, and M. Ashour-Abdalla, Driven magnetic reconnection in three dimensions: Energy conversion and field-aligned currents, *J. Geophys. Res., 89*, 9761, 1984.

Sato, T., T. Shimada, M. Tanaka, T. Hayashi, and K. Watanabe, Formation of field-twisting flux tubes on the magnetopause and solar wind particle entry into the magnetosphere, *Geophys. Res. Lett., 13*, 801, 1986.

Saunders, M. A., C. T. Russell, and N. Sckopke, Flux transfer events: Scale and interior structure, *Geophys. Res. Lett., 11*, 131, 1984.

Schindler, K, and A. Otto, Resistive instability, in *Physics of Magnetic Flux Ropes, Geophys. Monogr. Ser.*, vol. 58, edited by. C. T. Russel, E. R. Priest, and L .C. Lee, p. 51, AGU, Washington, D. C., 1990.

Schindler, K., M. Hesse, and J. Birn, General magnetic reconnection: Parallel electric field and helicity, *J. Geophys. Res., 93*, 5574, 1988.

Scholer, M., Magnetic flux transfer at the magnetopause based on single X line bursty reconnection, *Geophys. Res. Lett., 15*, 291, 1988a.

Scholer, M., Strong core fields in magnetopause flux transfer events, *Geophys. Res. Lett., 8*, 748, 1988b.

Scholer, M. and A. Otto, Magnetotail reconnection: Current diversion and field-aligned current, *Geophys. Res. Lett. 18*, 733, 1991.

Scholer, M., D. Hovestadt, F. M. Ipavich, and G. Gloeckler, Energetic protons, alpha particles, and electrons in magnetic flux transfer events, *J. Geophys. Res., 87*, 2169, 1982.

Scholer, M., F. M. Ipavich, G. Gloeckler, D. Hovestadt, and B. Klecker, Leackage of magnetosheric ions into the magnetosheath along reconnected field lines at the dayside magnetopause, *J. Geophys. Res., 86*, 1299, 1981.

Scholer, M., A. Otto, and G. J. Gadbois, Three-dimensional numerical simulations of magnetotail reconnection, in *Magnetospheric Substorms, Geophys. Monogr. Ser., 64*, ed. by J. R. Kan, T. A. Potemra, S. Kokubun, and T. Iijima, 171, AGU, Washington, D.C., 1991.

Sckopke, N., G. Paschmann, G. Haerendel, B. U. O Sonnerup, S. J. Bame, T. G. Forbes, E. W. Hones, Jr., and C. T. Russell, Structure of the low-latitude boundary layer, *J. Geophys. Res., 86*, 2099, 1981.

Semenov, V. S., I. V. Kubyshkin, M. F. Heyn, and H. K. Biernat, Temporal evolution of the convective plasma flow during a reconnection process, *Adv. Space Rev., 4*, 471, 1984.

Shi, Y. A simulation study of magnetic reconnection process at the dayside magnetopause, *Thesis*, 1989.

Shi, Y., and L. C. Lee, Structure of the reconnection layer at the dayside magnetopause, *Planet. Space Sci., 38*, 437, 1990.

Shi, Y., C. C. Wu, and L. C. Lee, A study of multiple X line reconnection at the dayside magnetopause, *Geophys. Res. Lett., 15*, 295, 1988.

Sibeck, D. G., A model for the transient magnetospheric response to sudden solar wind dynamic pressure variations, *J. Geophys. Res., 95*, 3755, 1990.

Sibeck, D. G., Transient events in the outer magnetosphere: Boundary waves or flux transfer events? *J. Geophys. Res., 97*, 4009, 1992.

Sibeck, D. G., G. L. Siscoe, J. A. Slavin, E. J. Smith, S. J. Bame, and F. L. Scarf, Magnetotail flux ropes, *Geophys. Res. Lett., 11*, 1090, 1984.

Song, Y., and R. L. Lysak, Current dynamo effect of 3D time-dependent reconnection in the dayside magnetopause, *Geophys. Res. Lett., 16*, 911, 1989.

Sonnerup, B. U. O., Magnetic reconnection ina highly conducting incompressible fluid, *J. Plasma Phys., 4*, 161, 1970.

Sonnerup, B. U. O., The reconnecting magnetosphere, in *Magnetospheric Physics*, edited by B. M. McCormac, p. 23, D. Reidel, Hingham, Mass., 1974.

Sonnerup, B. U. O., Magnetic field reconnection, in *Solar System Plasma Physics, Vol. 3*, ed. by L. T. Lanzerotti, C. F. Kennel, and E. N. Parker, p. 45, North-Holland, Amsterdam, 1979.

Sonnerup, B. U. O., Magnetic reconnection at the magnetopause: An overview, in *Magnetic reconnection in Space and Laboratory Plasmas*, ed. by E. W. Hones, Jr., p. 92, Geophysical Monograph 30, AGU, Washington, D.C., 1984.

Sonnerup, B. U. O., On the stress balance in flux transfer events, *J. Geophys. Res., 92*, 8613, 1987.

Sonnerup, B. U. O., G. Paschmann, I. Papamastorakis, N. Sckopke, G. Haerendel, S. J. Bame, J. R. Asbridge, J. T. Gosling, and C. T. Russell, Evidence for magnetic field reconnection at the Earth's magnetopause, *J. Geophys. Res., 86*, 10,049, 1981.

Southwood, D. J., C. J. Farrugia, and M. A. Saunders, What are flux transfer events?, *Planet. Space Sci., 36*, 503, 1988.

Sweet, P. A., The neutral point theory of solar flares, in *Electromagnetic Phenomena in Cosmical Physics,* ed. by B. Lehnert, p. 123, Cambridge University Press, London, 1958.

Ugai, M., Computer simulations of field-aligned currents generated by fast magnetic reconnection in three dimensions, *J. Geophys. Res., 96,* 21173, 1991.

Vasyliunas, V. M., Theoretical models of magnetic field line merging, 1, *Rev. Geophys., 13,* 303, 1975.

Vasyliunas, V. M., Steady state aspects of magnetic field line merging, in *Magnetic reconnection in Space and Laboratory Plasmas*, ed. by E. W. Hones, Jr., p. 25, Geophysical Monograph 30, AGU, Washington, D.C., 1984.

Wei, C. Q., L. C. Lee, S. Wang, and S.-I. Akasofu, Evolution of magnetic flux ropes associated with flux transfer events and interplanetary magnetic clouds, *J. Geophys. Res., 96,* 1619, 1991.

Wright, A. N., The evolution of an isolated reconnected flux tube, *Planet. Space Sci., 35,* 813, 1987.

Wright, A. N., and M. A. Berger, The effect of reconnection upon the linkage and interior structure of magnetic flux tubes, *J. Geophys. Res., 94,* 1295, 1989.

Yeh, T., and W. I. Axford, On the reconnection of magnetic field lines in conducting fluids, *J. Plasma Phys., 4,* 207, 1970.

Zmuda, A. J., and J. C. Armstrong, The diurnal flow pattern of field-aligned currents, *J. Geophys. Res., 79,* 4611, 1974.

Zmuda, A. J., J. H. Martin, and F. T. Heuring, Transverse magnetic disturbances at 1100 km in the auroral region, *J. Geophys. Res., 71,* 5033, 1966.

Zmuda, A. J., F. T. Heuring, and J. H. Martin, Dayside magnetic disturbances at 1100 km in the auroral oval, *J. Geophys. Res., 72,* 1115, 1967.